Antagonistic activities of Vegfr3/Flt4 and Notch1b fine-tune mechanosensitive signaling during zebrafish cardiac valvulogenesis

---

Federica Fontana

Univ.-Diss.

zur Erlangung des akademischen Grades
"doctor rerum naturalium"
(Dr. rer. nat.)
in der Wissenschaftsdisziplin "Biologie"

eingereicht an der
Mathematisch-Naturwissenschaftlichen Fakultät
Institut für Biochemie und Biologie
der Universität Potsdam

Ort und Tag der Disputation: Potsdam, 13.11.2020

Hauptbetreuer:	Prof. Dr. Salim Seyfried
Betreuerinnen:	Prof. Dr. Petra Knaus
Gutachter*innen:	Prof. Dr. Salim Seyfried
	Prof. Dr. Ralph Gräf
	Prof. Dr. Taija Mäkinen

Published online on the
Publication Server of the University of Potsdam:
https://doi.org/10.25932/publishup-48751
https://nbn-resolving.org/urn:nbn:de:kobv:517-opus4-487517

Table of Content

Abstract

Cardiac valves are essential for the continuous and unidirectional flow of blood throughout the body. During embryonic development, their formation is strictly connected to the mechanical forces exerted by blood flow. The endocardium that lines the interior of the heart is a specialized endothelial tissue and is highly sensitive to fluid shear stress. Endocardial cells harbor a signal transduction machinery required for the translation of these forces into biochemical signaling, which strongly impacts cardiac morphogenesis and physiology. To date, we lack a solid understanding on the mechanisms by which endocardial cells sense the dynamic mechanical stimuli and how they trigger different cellular responses. In the zebrafish embryo, endocardial cells at the atrioventricular canal respond to blood flow by rearranging from a monolayer to a double-layer, composed of a luminal cell population subjected to blood flow and an abluminal one that is not exposed to it. These early morphological changes lead to the formation of an immature valve leaflet. While previous studies mainly focused on genes that are positively regulated by shear stress, the mechanisms regulating cell behaviors and fates in cells that lack the stimulus of blood flow are largely unknown. One key discovery of my work is that the flow-sensitive Notch receptor and Krüppel-like factor (Klf) 2, one of the best characterized flow-regulated transcriptional factors, are activated by shear stress but that they function in two parallel signal transduction pathways. Each of these two pathways is essential for the rearrangement of atrioventricular cells into an immature double-layered valve leaflets. A second key discovery of my study is the finding that both Notch and Klf2 signaling negatively regulate the expression of the angiogenesis receptor Vegfr3/Flt4, which becomes restricted to abluminal endocardial cells of the valve leaflet. Within these cells, Flt4 downregulates the expressions of the cell adhesion proteins Alcam and VE-cadherin. A loss of Flt4 causes abluminal endocardial cells to ectopically express Notch, which is normally restricted to luminal cells, and impairs valve morphology. My study suggests that abluminal endocardial cells that do not experience mechanical stimuli loose Notch expression and this triggers expression of Flt4. In turn, Flt4 negatively regulates Notch on the abluminal side of the valve leaflet. These antagonistic signaling activities and fine-tuned gene regulatory mechanisms ultimately shape cardiac valve leaflets by inducing unique differences in the fates of endocardial cells.

Zusammenfassung

Herzklappen sind essentiell für den kontinuierlichen und gerichteten Blutfluss durch den Körper. Während der Embryonalentwicklung ist die Bildung der Herzklappen stark von vom Blutfluss generierten, mechanischen Kräften abhängig. Das Endokard, ein endotheliales Gewebe, das das Herz im Inneren auskleidet, reagiert sehr sensibel auf biomechanische Einwirkungen. Endokardzellen weisen eine Signaltransduktionsmaschinerie auf, welche die Umwandlung dieser Kräfte in biochemische und elektrische Signale ermöglicht und somit unverzichtbar für die Herzmorphogenese und -physiologie ist. Allerdings fehlt uns noch immer das Verständnis der Mechanismen, mit denen Endokardzellen dynamische, biomechanische Signale wahrnehmen und wie verschiedene zelluläre Antworten ausgelöst werden können. Im Zebrafischembryo reagieren Endokardzellen im atrioventrikulärem Kanal auf Blutfluss induzierte Schubspannung mit einer Umorganisation, wobei sich aus einer Einzelschicht an Zellen eine Doppelschicht bildet. Letztere besteht aus einer luminalen Zellpopulation, die dem Blutstrom ausgesetzt ist und einer abluminalen Population, der der Kontakt zum Blut fehlt. Diese initialen morphologischen Veränderungen führen zur Ausbildung des frühen Herzklappensegels. Bisherige Studien berichteten im Besonderen über Gene die positiv von einer veränderten Schubspannung in Endokardzellen reguliert werden. Allerdings sind die Mechanismen, die das Verhalten und die Spezifizierung von den Zellen regulieren, die nicht in Kontakt mit dem Blutfluss sind, weitgehend unbekannt. Eine meiner Schlüsselentdeckungen in dieser Arbeit ist, dass zwei der am besten charakterisierten, durch Blutfluss transkriptional regulierten Faktoren, der Notch Rezeptor und der Krüppel-like factor (Klf) 2, durch Schubspannung aktiviert werden. Dies funktioniert auf zwei parallelen mechanosensitiven Signaltransduktionswegen und beide Kaskaden sind essentiell für die Umorganisation der atrioventrikulären Zellen während der Bildung der frühen zweischichtigen Klappensegeln. Eine zweite wichtige Entdeckung meiner Studien ist, dass die Expression des angiogenen Faktors Vegfr3/Flt4, die auf abluminale Endokardzellen im frühen Klappensegel beschränk ist, von beiden Signalwegen, Notch und KLf2, negativ reguliert wird. Außerdem veringert Flt4 die Expression der Zelladhäsionsproteine Alcam und VE-cadherin in abluminalen Zellen und führt die Herzklappenmorphogenese herbei. Der Verlust von Flt4 wiederum führt zu einer ektopischen Expression von Notch in abluminalen Endokardzellen, welche sonst nur in luminalen Zellen auftritt. Daher zeigt meine Arbeit, dass abluminale Endokardzellen, die keinem mechanischem Reiz ausgesetzt sind, Notch herunterregulieren und damit die Expression von Flt4 auslösen. Flt4 wiederum blockiert dann zusätzlich den

Notch Signalweg in dieser Zellpopulation. Diese antagonistischen Signalaktivitäten und fein abgestimmte Genregulationsmechanismen sorgen für Unterschiede in der Spezifizierung der Endokardzellen und formen so schließlich die Segelklappen im Herz.

1. Introduction

During vertebrate embryogenesis, the heart is the first organ to function and blood flow is established while the cardiovascular system is still developing. Hence, cardiovascular development of heart and vessels is interconnected with the biomechanical forces exerted by blood flow. The inner endothelial lining of the heart is comprised of endocardial cells (EdC) that are sensitive to these stimuli and respond by activating complex signaling, which are essential for proper heart morphogenesis. In particular, the formation of cardiac valves is dependent on fine-tuned mechanosensitive signaling and most heart valve malformations originate during embryogenesis. Currently, we still lack a precise understanding of how these processes are regulated. In this study, I analyzed the impact of blood flow on valve EdCs in zebrafish (*Danio rerio*) embryos. Zebrafish are particularly suitable for studies requiring manipulation of blood flow, since embryos can survive without a beating heart until 7 days post fertilization (Sehnert et al., 2002). Well-established genetic and pharmacological tools, high numbers of offspring, and transparent embryos are additional features that make zebrafish a powerful model to study embryonic heart development (Bakkers, 2011).

1.1. Mechanical forces in cardiovascular development

During embryonic development, biomechanical forces are important regulators of morphogenesis. Examples include the epithelial spreading over the yolk during zebrafish gastrulation, which is driven by circumferential contractions and flow-frictional mechanisms (Behrndt et al., 2012). Compression and stretching of the apical surface of cells are required respectively for cell apoptosis and proliferation, necessary for *Drosophila* wing formation (Diaz de la Loza and Thompson, 2017). Mechanical forces are especially crucial during cardiac development, since blood flow and cardiac contractility produce biophysical inputs while heart formation is ongoing (Haack and Abdelilah-Seyfried, 2016). The embryonic heart rate increases as development progresses, to accommodate the need of blood supply. At the same time, this triggers the growth of the endocardium, a specialized endothelial tissue that is lining the interior of the heart (Lindsey and Butcher, 2011). Hence, fluid forces guide cardiac morphogenesis, by promoting growth and tissue remodeling through regulation of changes in gene expression (Groenendijk et al., 2005; Sidhwani and Yelon, 2019). Understanding how

physical forces influence tissues morphogenesis and remodeling is crucial for human health, since pathologies such as atherosclerosis, cardiac hypertrophy, and aortic dissection can be considered as disorders due to defective mechanobiology (Givens and Tzima, 2016). The endocardium is of particular importance in these pathologies, due to its direct contact with blood flow. The molecular mechanisms of mechanosensation and of biochemical and electrical signal transduction are likely to be similar between endocardium and other endothelial tissues. The cardiovascular system is subjected to two main biomechanical forces due to blood flow (Figure 1.1). Blood pressure causes a circumferential stretching of endothelial cells (ECs), which results from a hydrostatic pressure that is caused by the natural pulsatility of blood flow (Givens and Tzima, 2016). A second force component of blood flow is fluid shear stress, which is the frictional force due to tangential stress generated by blood flow. This force induces changes in proliferation, differentiation, cell shape, and permeability within ECs and EdCs (Haack and Abdelilah-Seyfried, 2016; Hahn and Schwartz, 2009). Shear stress is directly proportional to velocity and viscosity of the blood and inversely proportional to the vessel diameter. Typical magnitudes in human blood vessels range (5-50 dyn/cm^2) (Lipowsky et al., 1978) and approximately 10 times lower in lymphatic vessels (Dixon et al., 2006), while circumferential stretch of the vessel wall during the cardiac cycle can be >1000 Pa (Baeyens and Schwartz, 2016; Haga et al., 2007). In the adult mature cardiovascular system, most ECs are subjected to laminar blood flow. In a few regions, including large artery branch points, or within pathological tissues, such as stenotic arteries or heart valves, and aneurysms, the flow pattern becomes turbulent and disturbed (Baratchi et al., 2017). Turbulent flow is chaotic and the flow variables (as velocity, pressure, and temperature) change in a random manner. In regions of disturbed flow, endothelial morphology can change, without a preferred orientation relative to the direction of flow. Tension forces generated by cell growth, cell division, and cell and tissue migration (partially also induced by blood flow) have also an influence on the formation of the cardiovascular system (Bornhorst et al., 2019; Dietrich et al., 2014; Helker et al., 2013). In addition to these forces, EdCs are exposed to unique forms of mechanical stress, including stretching during the diastole and contraction during the systole of each cardiac contractile cycle (Mickoleit et al., 2014). During cardiac development, the highest shear forces occur in the inner curvature region of the heart tube and in regions with lumen constrictions, corresponding to the atrioventricular canal (AVC) and the outflow tract (OFT), where endocardial cushions form and develop into functional valves (Hierck et al., 2008a).

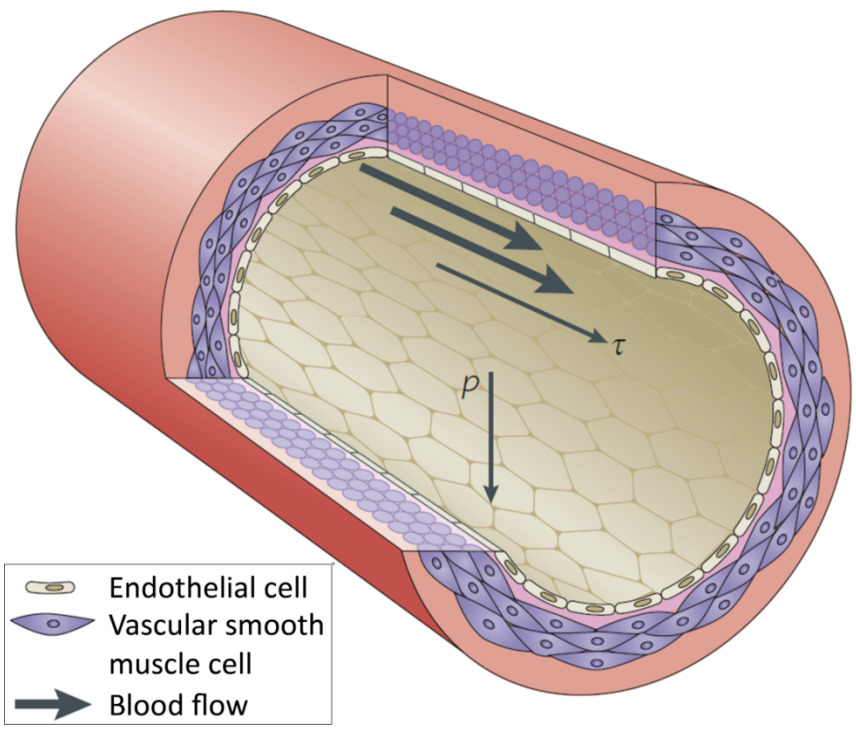

Figure 1.1. Schematic representation of an artery wall section. The inner endothelial cells align longitudinally, while the outer vascular smooth muscle cells align circumferentially. Circumferential stretching of the vessel wall results from pressure (p), perpendicular to the vessel wall. Blood flow-induced shear stress (τ) is parallel to the vessel wall and is exerted longitudinally. Adapted from Hahn and Schwartz, 2009.

1.2. Mechanotransduction in the cardiovascular system

In order to shape tissues during morphogenesis and regulate homeostasis, the mechanical forces impacting ECs and EdCs need to be converted into biochemical signals. This process, referred to as mechanotransduction, requires that ECs express specific molecular sensors which enable these cells to detect such stimuli and to initiate the molecular cascades required to regulate gene expression and cell behavior (Figure 1.2). Laminar shear stress induces an elongation of ECs (Levesque and Nerem, 1985) due to changes in cytoskeletal organization, focal adhesions and re-positioning of junctional complexes (Noria et al., 1999; Seebach et al., 2007). Mechanical forces are transferred to the junctions through the cytoskeleton by modulating myosin-dependent cytoskeletal remodeling (Conway et al., 2013). Hence, the cytoskeletal tension within the cell is important for mechanotransduction. Cell-cell tension is also associated with deformation of the ECM, which is sensed by fibroblasts through the

YAP signaling pathway (Steed et al., 2016a). On a molecular level, mechanical forces also promotes the expression of transcription factors, such as Krüppel-like factor 2 (KLF2) and Nuclear factor-E2-related factor-2 (NRF2/Nrf2), which influence endothelial survival, proliferation and differentiation by controlling gene expression regulation (Baratchi et al., 2017). The activation of KLF2 involves signaling via the MEK5/ERK5/MEF2 signaling pathway (Dekker et al., 2002; Ohnesorge et al., 2010). KLF2 reduces vessel permeability and thrombosis by inducing the expression of endothelial nitric oxide synthase (eNOS) and caveolin. In addition, KLF2 enhances EC metabolism and represses inflammatory responses that are induced by IL-1b or TNF-a (Novodvorsky and Chico, 2014). ECs experiencing disturbed flow exhibit activation of nuclear factor kappa B (NF-kB) and expression of proinflammatory genes, including vascular cell adhesion molecule (VCAM)-1, E-selectin and interleukin (IL)-8. The Yes-associated protein (YAP) and the transcriptional co-activator with a PDZ-binding motif (TAZ) mediate the increases in ICAM-1 and VCAM-1 expression. These complex cellular responses require both mechanosensors and mechanoadaptors to coordinate rapid changes and physiological adaptations. Mechanosensors are the initial responders to changes in biomechanical stimuli (Givens and Tzima, 2016). Because flow is in direct touch with apical surfaces of ECs, structures on the apical side have been studied as direct mechanosensors. These include primary cilia and ion channels (Goetz et al., 2014; Heckel et al., 2015; Hierck et al., 2008b; Li et al., 2014). Within the ion channels, Polycystic kidney disease 2 (Pkd2; also known as Trpp2) and transient receptor potential cation channel, subfamily V, member 4 (Trpv4) were reported as sensor for oscillatory flows within the AVC region in the zebrafish endocardium (Heckel et al., 2015). Piezo proteins are another recently identified class of mechanically activated ion channels, which act as mediators of flow responses within the endothelium (Li et al., 2014; Ranade et al., 2014). In particular, PIEZO1 is activated by shear stress within ECs and is essential for murine vascular development (Ranade et al., 2014). In the mouse and zebrafish endocardium, *Piezo1* is expressed with highest levels in the AVC and OFT regions (Faucherre et al., 2020; Ranade et al., 2014). Functional studies in zebrafish revealed an involvement of Piezo1 in OFT valve development (Duchemin et al., 2019; Faucherre et al., 2020). Primary cilia have been reported as sensors for low fluid shear forces during vascular morphogenesis (Goetz et al., 2014; Iomini et al., 2004). In tune with this model, primary cilia progressively disappear from endocardial high shear stress regions (at the cardiac cushions) in chick embryos, but remain in regions where flow is low or disturbed (Egorova et al., 2011). This shear stress-mediated differential

distribution of cilia within the developing endocardium appears to be one of the factors that biases EdC responses to blood flow (Koefoed et al., 2014).

In addition to cilia and ion channels, other cellular structures have been implicated in endothelial mechanical force sensing and transmission, including junctional proteins (Cadherin 5/Vascular endothelial cadherin (CDH5/VE-cadherin), occludin), receptor kinases (vascular endothelial growth factor (VEGF) receptors, VEGFR2/KDR and VEGFR3/FLT4), integrins, focal adhesions, G-proteins, G-protein-coupled receptors, caveolae and vimentin intermediate filaments (Hahn and Schwartz, 2009). Currently, the best-studied mechanotransduction complex consists of platelet EC adhesion molecule (PECAM-1), VE-cadherin, VEGFR2, and VEGFR3 which are components of cell-cell adherens junctions (Coon et al., 2015; Tzima et al., 2005). The transmembrane domain of VE-cadherin mediates an essential adapter function by binding directly to the transmembrane domain of VEGFR2 and VEGFR3 (Coon et al., 2015). Fluid shear stress also increases tension on PECAM-1 via an upstream pathway that triggers association of PECAM-1 with the vimentin cytoskeleton. In turn, tension increases on PECAM-1 trigger the activation of a SRC-related cytoplasmic tyrosine kinase, which induces PECAM1 phosphorylation, followed by VEGFR2 phosphorylation and phosphatidylinositol-4,5-bisphosphate 3-kinase (PI3K) activation (Conway et al., 2013; Tzima et al., 2005). Hence, VEGFR2/3 are activated in a VEGF-independent manner by mechanical tension. Subsequently, integrins bind to the extra-cellular matrix (ECM) and activate GTPases, including Ras, Rho, Rac1, and CDC42. This induces the activation of transcription factors, such as NF-κB, KLF2 and NRF2/Nrf2 (Xiao et al., 2013). Rho causes the disassembly of stress fibers, while Rac1 helps newly formed stress fibers to align in the direction of flow (Tzima, 2006). eNOS is activated by caveolin (Cav)-1 via RhoA-ß1 integrin signaling, and this induces an increase in VEGFA (Yang et al., 2011). In addition, there is evidence that fluid shear-stress can activate matrix metalloproteinases which results in the release of VEGFA from the ECM and this promotes the activation of VEGFR2 (dela Paz et al., 2013). So far, it has not been investigated whether the PECAM1/VEGFR/VE-cadherin complex has a role within the endocardium.

Recently, plexin D1 was identified as a direct mechanosensor in ECs, that functions in a complex together with neuropilin-1 and VEGFR2 (Mehta et al., 2020). In adult arteries, the flow-responsive Notch receptor NOTCH1 was recently recognized as a mechanosensor that is highly sensitive to fluid shear stress levels (Mack et al., 2017). This results in differential levels of Notch signaling in distinct regions of the vessel wall and suppresses the expression

of inflammatory genes within the endothelium (Briot et al., 2015; Mack et al., 2017; Theodoris et al., 2015). Another recent study showed that, after shear stress-dependent release of NOTCH1 intracellular domain (NICD), the NOTCH1 transmembrane domain forms a complex with VE-cadherin at the adherens junctions which is essential for vascular barrier and permeability regulation (Polacheck et al., 2017). Although it is currently not known whether NOTCH1 acts as a mechanosensor within the endocardium, fluid shear stress is essential to activate Notch signaling in zebrafish EdCs (Samsa et al., 2015) and many processes such as cardiac trabeculation and valve formation are dependent on both mechanical forces and Notch signaling (MacGrogan et al., 2018).

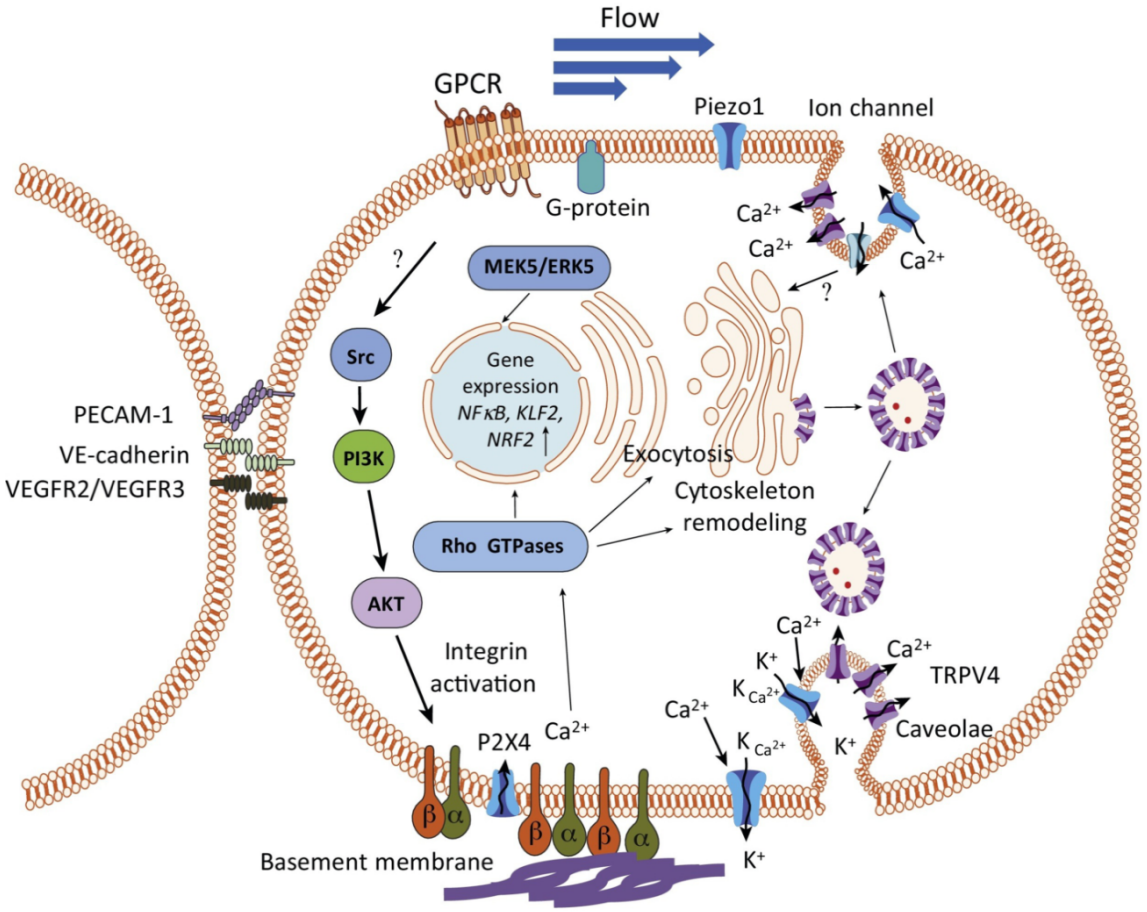

Figure 1.2. Mechanosensory pathways in endothelial cells. Blood flow-induced shear stress is applied on the plasma membrane and induces the phosphorylation of platelet endothelial cell adhesion molecule (PECAM)-1. PECAM-1 is present on adherent junctions in a mechanosensory complex with VE-cadherin and vascular endothelial growth factor receptor (VEGFR)-2/VEGFR3. This first event leads to the Src-dependent PI3K activation. Integrins are then activated to bind to extracellular matrix (ECM), and in turn transiently activate GTPases, such as Ras, Rho, Rac1, and CDC42. This causes activation of transcription factors, such as nuclear factor kappa B (NF-kB), Krüppel-like factor 2

(KLF2) and Nuclear factor-E2-related factor-2 (NRF2/Nrf2), which increase the expression of anti-inflammatory genes and antioxidant enzymes, and control endothelial barrier function. While Rho causes the disassembly of stress fibers, Rac1 helps the alignment of newly formed stress fibers in the direction of flow. RhoA activation via ß1 integrin activates caveolin (Cav)-1, which in turn activates endothelial nitric oxide synthase (eNOS). Nonselective cation channels, such as transient receptor potential (TRP)V4, are activated and in turn activate the Ca2 +-sensitive K channels (KCa2+), which in turn hyperpolarize the membrane. Adapted from Baratchi et al., 2017.

1.2.1. Mechanosensitive signaling in cardiac valvulogenesis

One of the most striking examples of interdependency between mechanical forces and molecular pathways during organogenesis is the formation of cardiac valves. Surgical alterations of mechanical forces in the chick heart, obtained by conotruncal banding or left atrial ligation or clipping, were used to create a model of increased preload in the right ventricle and decreased preload in the left ventricle, which resulted in an abnormal morphology of the AV valve (Sedmera et al., 1999). In zebrafish, EdCs of the AVC region differentiate and acquire their AV EdC identity independently from blood flow, as proven by their presence in mutants lacking blood flow due to cardiac contractility defects such as *troponin T2a* and *actin alpha 1* mutants (Bartman et al., 2004; Beis et al., 2005). However, in these mutants the further development of AV EdCs does not occur and valve leaflets do not form. Similarly, the physical occlusion of blood flow by placing beads into the inflow or outflow tract regions of the heart impairs AVC valvulogenesis (Hove et al., 2003).

Abnormal cardiac cushion development was observed in mice lacking primary cilia, which are particularly prominent on EdCs in regions of low or disturbed flow and absent in areas of high fluid shear stress (Slough et al., 2008). Indeed, differences in the type and levels of fluid shear stress result in different responses from EdCs. In chick embryos, high unidirectional fluid shear stress promotes cushion extension in the direction of flow, while low recirculating flows are involved in a pre-valvular sculpting process (Yalcin et al., 2011). In zebrafish, the AVC region at 2 days post fertilization (dpf) is characterized by an oscillatory (retrograde) flow. This is essential for the endocardial activation of the Ca^{2+} channels Pkd2/Trpp2 and Trpv4, which mediate the restriction of *klf2a* expression in this region (Heckel et al., 2015). In fact, while *klf2a* is ubiquitously expressed throughout the endocardium until 36 hpf, its expression becomes restricted to the AVC and the OFT by 48 hpf (Vermot et al., 2009). Interestingly, *pkd2* and *trpv4* mutants develop valves with aberrant morphologies, suggesting

a role for the two channels in valve morphogenesis rather than endocardial cushions specification (Haack and Abdelilah-Seyfried, 2016). Defective AV valves results also by the loss of Klf2a, in both zebrafish (Steed et al., 2016b; Vermot et al., 2009) and mice (Chiplunkar et al., 2013). In zebrafish, the knockdown of the hematopoietic gene *gata2* causes changes in the hematocrit and in a reduction of the retrograde flow fraction. Under this genetic perturbation, the expression levels of *klf2a* mRNA are reduced and the formation of AV valves is impaired (Vermot et al., 2009). These findings have raised considerable interest in the target genes of Klf2 activity within the AVC endocardium. Among those, genetic and molecular studies in zebrafish identified the gene encoding the ECM protein Fibronectin1b, which serves as the primary ligand for integrin receptor signaling. This was of particular interest since integrin receptor signaling serves an important function for the organization of the intracellular cytoskeleton and the ECM (Steed et al., 2016b) (Figure 1.3). Another target gene of Klf2 signaling within the endocardium is *Wnt9b*. Loss of murine *Wnt9b* reduced canonical WNT signaling within the neighboring mesenchymal cells and caused defective valve formation (Goddard et al., 2017). Similarly, in zebrafish, inhibition of Wnt signaling blocks the formation of cardiac cushions (Hurlstone et al., 2003) and *wnt9b* expression is dependent on both hemodynamic shear stress and *klf2a* expression (Goddard et al., 2017). Another reported Klf2a target gene is *notch1b*, a key player in valvulogenesis of zebrafish and mice. Notch signaling is highly active within the AV endocardium and its activation is flow-dependent (Samsa et al., 2015; Timmerman et al., 2004). The Notch target genes *Hey1* and *Hey2* are mainly expressed at the AVC, where they restrict the expression of Bmp2 and Tbx2 to the AV myocardium and thus contribute to patterning the AVC (Rutenberg et al., 2006). In the E9.5 mouse heart, Delta-like 4 (DLL4) and NOTCH1 are also present in the AV endocardium, as well as in the endocardium at the base of newly forming trabeculae in the ventricle, and in the atrium (MacGrogan et al., 2018). Both in zebrafish and mice, when Notch1b is blocked pharmacologically or Notch signaling is ectopically activated by the transgenic overexpression of NICD, cardiac valve leaflet morphogenesis is impaired (Beis et al., 2005; MacGrogan et al., 2016; Timmerman et al., 2004). In *Notch1* mutant mice, the endocardial cushions are acellular as a result of an impaired process of endothelial to mesenchymal transition (EndoMT), in which cells loose contacts to each other and delaminate into the cardiac jelly adopting a mesenchymal-like phenotype, to form the primordia of cardiac valves (Eisenberg and Markwald, 1995). Although the extent to which EndoMT is mechanically regulated during valvulogenesis is not yet fully understood, signaling pathways involved in EndoMT, including BMP, Transforming growth factor β

(TGFβ), Notch, and Wnt pathways, are known to be flow-sensitive, suggesting the potential for biomechanical regulation (Zhong and Simmons, 2016). Some direct evidences for the role of shear stress on EndoMT come from an *in vitro* model, in which porcine aortic valve ECs were seeded onto 3D collagen I gels and exposed to different magnitudes and type of shear stress. This revealed that low steady and oscillatory shear stress upregulated EndoMT markers (including ACTA2, Snail, Tgfβ1) and matrix invasion, when compared to static or high steady stress (Mahler et al., 2014). Experiments with chick EdCs suggested that the induction of EndoMT in the AV EdCs depends on the flow-dependent activation of Tgfβ/Alk5 signaling. This signaling becomes activated in EdCs once they have lost primary cilia (Ten Dijke et al., 2012; Egorova et al., 2011), whose distribution is also shear stress-regulated and appears to be one of the factors that biases EdC responses to blood flow (Koefoed et al., 2014). One study in zebrafish showed that flow-sensitive primary cilia activate ventricular endocardial *notch1b* expression, a process essential for cardiac trabeculation (Samsa et al., 2015).

Given the importance of *klf2a* for biomechanical signaling at the AVC, its expression levels must be strictly controlled. In tune with this notion, the cerebral cavernous malformation (CCM) proteins Ccm1 and Ccm2 tightly restrict *klf2a* expression levels within the heart (Donat et al., 2018; Renz et al., 2015). Interestingly, the expression of Heg1, the transmembrane protein of the CCM complex, is dependent on both blood flow and Klf2a, suggesting that Klf2a acts in a negative feedback loop to control its own expression (Donat et al., 2018). *klf2a* and *notch1b* levels are also regulated by the protein kinase D2 (Pdk2), which phosphorylates and inhibits the suppressive activity of nuclear Histone deacetylase 5 (Hdac5) activity (Just et al., 2011). In fact, zebrafish *pkd2* mutants have impaired AV valves, as a result of *klf2a* and Notch target genes severe downregulation.

The development of cardiac valves is also affected by epigenetic regulators including the microRNAs (miRs) miR-*21* and *miR-23.* The expression of these miRs is regulated in response to the strength of blood flow (Banjo et al., 2013). In zebrafish, *miR-23* expression at the AVC regulates the production of the ECM component hyaluronic acid by the enzyme hyaluronan synthase 2 (Has2), which is necessary for endocardial cushion and valve formation (Lagendijk et al., 2011). Similarly, mouse embryos deficient for Has2 fail to undergo EndoMT at cardiac cushions (Camenisch et al., 2000). Zebrafish mutants that lack an enzyme essential for heparan sulphate, chondroitin sulphate, and hyaluronic acid production [uridine 5′-diphosphate (UDP)-glucose dehydrogenase] also fail to form

endocardial cushions (Walsh and Stainier, 2001). One major component of the cardiac ECM is fibronectin and zebrafish *fibronectin1b* mutant develop abnormal cardiac valves. Hence, the correct composition of the ECM, which also impacts its stiffness, is essential for valve development.

In zebrafish, another characteristic marker of AV EdCs at 48 hpf is the strong expression of the cell adhesion protein Alcam and the adherens junction protein Cdh5 (Beis et al., 2005; Steed et al., 2016b). After the remodeling of the monolayered AVC EdCs into multilayered valve leaflets, high-resolution live imaging of transgenic zebrafish embryos revealed that the blood flow-exposed (luminal) EdCs exhibit high levels of Klf2a and Notch signaling and maintain Cdh5 and Alcam expression, while abluminal EdCs show high Wnt/β-catenin signaling (Pestel et al., 2016; Steed et al., 2016b). The precise mechanism that regulates the molecular differences between the distinct layers of valve leaflets is still not well understood.

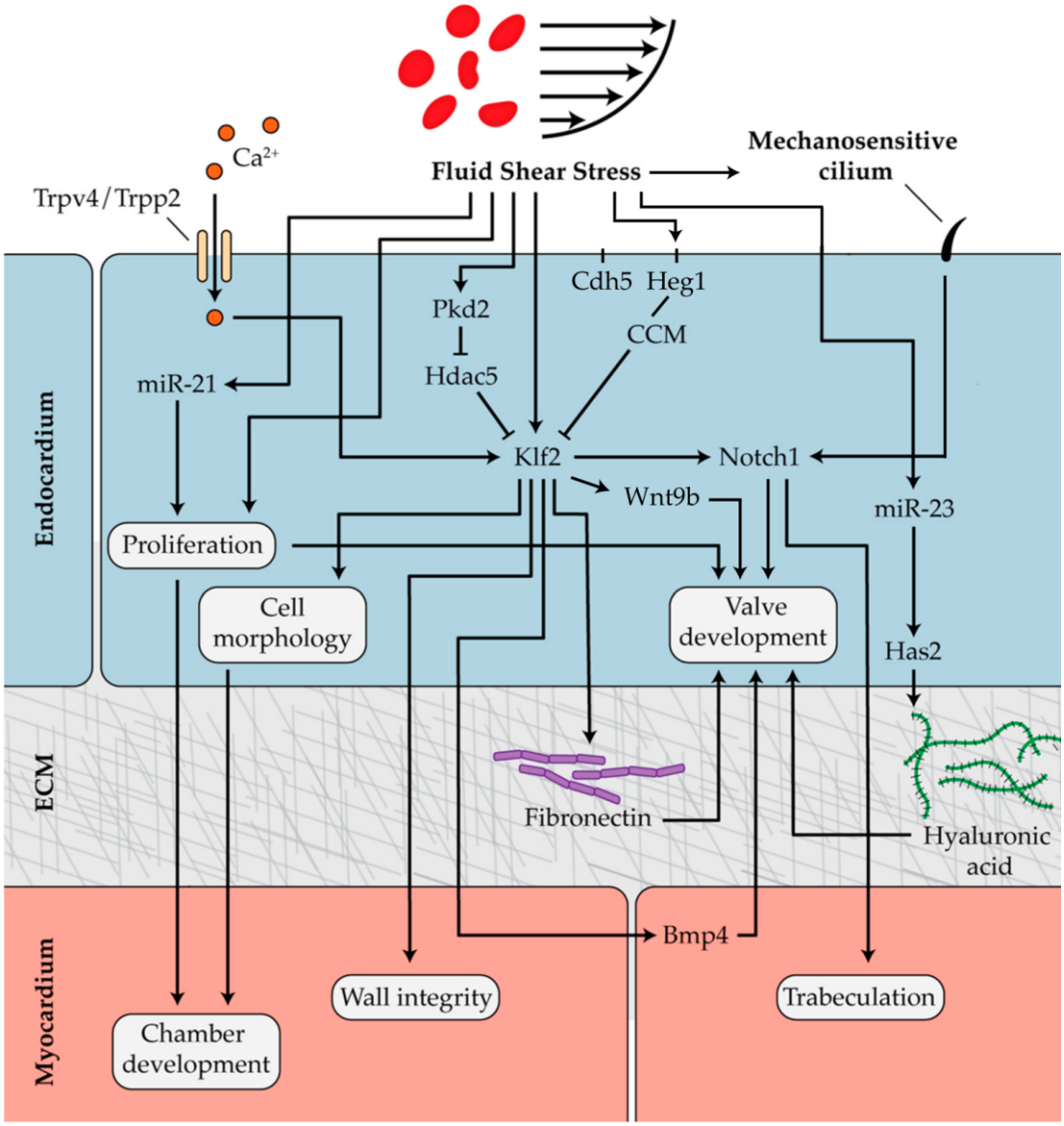

Figure 1.3. Mechanosensitive pathways involved in heart and valve development. During heart morphogenesis, hemodynamic forces control endocardial cell (EdCs) proliferation and morphology, mainly through Klf2. Through the endocardium, the myocardium is also impacted by blood flow because endocardial Klf2 signaling has a role in myocardial wall integrity, and endocardial cilia activate Notch1 signaling which regulates trabeculation. During valvulogenesis, flow-responsive *miR-21* regulates proliferation and Klf2a activates myocardial Bmp4 and Fibronectin synthesis which is deposited into the extracellular matrix (ECM). Another important component of the ECM is hyaluronic acid, produced by hyaluronan synthase 2 (Has2), which, in turn, is regulated by *miR-23*. Klf2a is positively regulated by the mechanosensitive ion channels Trpv4 and Trpp2 and suppressed by cerebral cavernous malformation (CCM) proteins and the chromatin modifier Hdac5. Adapted from Jarrell et al., 2019.

1.3. Morphological aspects of cardiac development in mammals

The heart of mammals and birds is comprised of two atrial and two ventricular chambers that are each composed of cells derived from different embryonic origins. The first cells committed to a cardiogenic fate are progenitors that are located in bilateral regions of the anterior lateral plate mesoderm. In humans this occurs at approximately embryonic day (E) 15 while this stage corresponds to E7 in mice (de Boer et al., 2012; Sizarov et al., 2011) (Figure 1.4A). During embryonic folding, these bilateral regions are brought into close proximity at the cardiac crescent (the primary heart tube). At this stage, this tissue consists of an inner endocardial and an outer myocardial layer, both of which are separated by a layer of ECM, which is referred to as cardiac jelly (DeRuiter et al., 1992). This biomaterial is mainly composed of proteoglycan glycosaminoglycans, of which hyaluronan and chondroitin sulfates are the major components (Lockhart et al., 2011).

The tissue involved in the early phases of cardiac development has been termed the first heart field (FHF) (Moorman and Christoffels, 2003). Upon heart tube formation, primitive cardiomyocytes stop proliferating and the myocardium further expands by addition of cells that are derived from the second heart field (SHF) (Cai et al., 2003). While cells from the FHF will contribute to the definitive left ventricle and the AVC, cells from the SHF will form the right ventricle, outflow tract (OFT), and atria (Kelly et al., 2001; Zaffran et al., 2004). In humans between E22-26, corresponding to E8-8.5 in mouse, the linear heart tube loops to the right (Figure 1.4B-C). The cardiomyocytes at the outer curve initiate proliferation which results in ballooning of the ventricles and, slightly later, of the atria (Soufan et al., 2006). At the same time, cells of the AVC, the OFT, and the sinus venosus maintain features of the

original primary heart tube (Van Den Berg et al., 2009). E26 in humans and E9.5 in mice mark the beginning of chamber septation, ventricular trabeculation, and growth of the epicardium (de Boer et al., 2012; Sizarov et al., 2011) (Figure 1.4D-E). After septation events and myocardial trabeculation, a four-chambered heart has formed by murine E15.5 (Figure 1.4F-G).

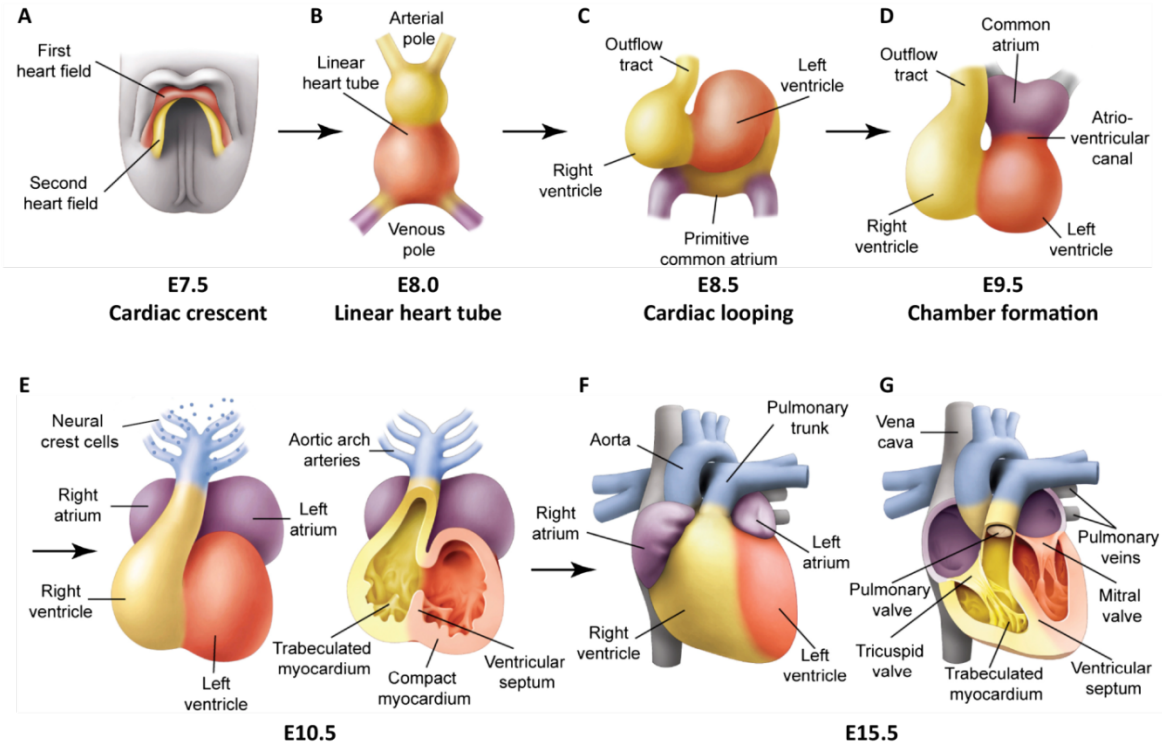

Figure 1.4: Schematic representation of cardiac development in murine embryos. (A) During gastrulation, cardiac progenitors originate from mesodermal cells and migrate to the splanchnic mesoderm to form the cardiac crescent. At E7.5, the cardiac crescent can be divided into two heart field lineages: a first heart field (red) and a second heart field (yellow), located posteriorly and medially to the first heart field. (B) At E8.0, a linear heart tube is formed. (C) At E8.5, cardiac chambers grow and undergo looping. The outflow tract forms at the arterial pole, while the inflow tract and primitive atria are present at the venous pole. (D) By E9.5, the atrioventricular canal is formed between the superior common atrium and the inferior ventricles. (E) By E10.5, cardiac neural crest cells from the dorsal neural tube migrate via the pharyngeal arches to the outflow tract. (F, G) Further cardiac developmental processes involve septation events and myocardial trabeculation, which result in a four-chambered heart at E15.5 Adapted from Epstein et al., 2015.

1.3.1. Cardiac valve development in mammals

A mature mammalian heart has four valves and four chambers, septated such that systemic circulation is separated from pulmonary circulation and blood flow is unidirectional (Figure 1.4F). The cardiac valves are divided into the inlet atrioventricular (AV) valves (mitral and tricuspid) and the outlet semilunar valves (aortic and pulmonic) (Figure 1.4G). The AV valves are complex structures, composed of the annulus, the leaflets, and the supporting tension apparatus and, in the definitive heart, are separated by the septum. The proper function of cardiac valves is largely dependent on their embryonic development and valve abnormalities related to developmental defects contribute to a wide range of cardiac diseases (e.g. arrhythmia, regurgitation, valve prolapse, stenosis, myocardial hypertrophy, heart failure) (Hinton and Yutzey, 2011). Valve morphogenesis begins with the looping of the heart tube, which becomes segmented into the atrium, the AVC, the ventricle, and the OFT. During rightward looping, the myocardium at the AVC and at the OFT upregulates the secretion of ECM, causing the cardiac jelly to swell towards the lumen of the heart tube. These tissue swellings between the endocardial and myocardial layer are termed endocardial cushions (de Vlaming et al., 2012). Stimulated by local signals, a subset of AV and OFT EdCs loose cell–cell contacts and delaminate into the cardiac jelly adopting a migratory, mesenchymal-like phenotype (Figure 1.5). This process has been referred to as EndoMT (Eisenberg and Markwald, 1995). Following their delamination, mesenchymal cells of the cushions receive cues from the endocardium that promote their proliferation, which ceases as the cells move towards the myocardium. Important molecular signals for proliferation include FGF growth factors (Sugi et al., 2003), and the transcription factors Twist, Msx-1, and Tbx20 (Chen et al., 2008; Shelton and Yutzey, 2007, 2008). In spite of the migration of cushion cells as individual cells, expression of Connexin45 and cell morphology suggest that their movements are coordinated collectively (Kumai et al., 2000). How the migration and polarization of cushion cells are regulated is still a major open question of valvulogenesis. It is well-recognized that moving cells respond to an evolving morphogenetic and biomechanical environment through sensors, and cell polarity was linked with morphogens, different concentrations of matrix components, and/or biomechanical signals (Vlaming *et al.*, 2012). Nevertheless, the molecular changes induced by each of these signals are poorly understood. Following delamination and proliferation, mesenchymal cells differentiate into valve interstitial fibroblasts that remodel into mature leaflets with their supporting apparatus. These cells are characterized by an increased synthesis of collagens and decreased expression

of the mesenchymal marker genes *twist* and *snail* (Chakraborty et al., 2010; Tan et al., 2011). The superior and inferior cushions at the AV junction fuse in the middle and form the AV septum. The AV septum eventually merges with both the developing ventricular septum and the interatrial septum into a valvuloseptal complex to which the mitral and tricuspid valves will eventually be anchored (de Vlaming et al., 2012). In addition to endocardium-derived cells, other cell lineages contribute to the building of the AV valves. These are epicardial-derived cells (Wessels et al., 2012; Zhou et al., 2010), neural crest cells (Nakamura et al., 2006), and cells of a bone marrow hematopoietic stem cell origin (Hajdu et al., 2011; Visconti et al., 2006).

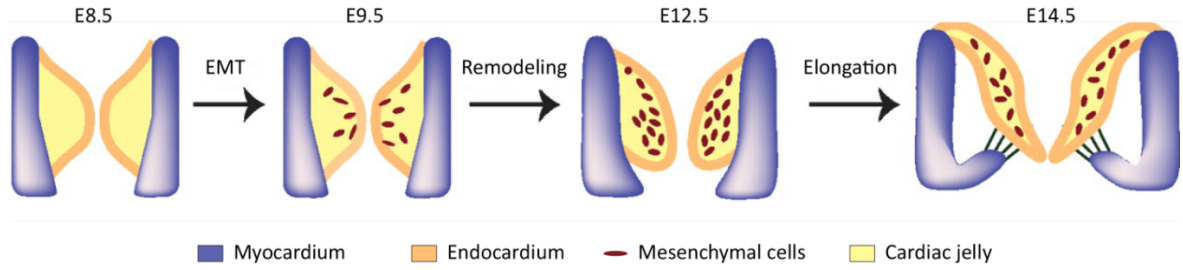

Figure 1.5. Schematic representation of atrioventricular valve formation in mice. At E8.5, endocardial cells in the AV cushions undergo endothelial-to-mesenchymal transformation and generate mesenchymal cells. The cushions then remodel and elongate to form primitive valves, which mature into valve leaflets. Adapted from Lin et al., 2012.

1.4. Morphological aspects of cardiac development in zebrafish

In zebrafish embryos, heart development initiates at 5 hours post fertilization (hpf), with the specification of myocardial and endocardial progenitor cells (Figure 1.6). While myocardial cells already have chamber-specific regional distribution (the atrial cells are located more ventrally in the lateral marginal zone than ventricular cells) (Keegan et al., 2005; Stainier et al., 1993), endocardial progenitors are not chamber-specified and are located close to a marginal region of the embryo (Lin et al., 2012b; Schoenebeck et al., 2007). During gastrulation and early somitogenesis, endocardial and myocardial progenitor cells migrate dorsally towards the embryonic midline where they reach the left and right anterior lateral plate mesoderm. Here, endocardial progenitor cells are located more anteriorly. Subsequently, endocardial progenitors move medially and posteriorly (Baker et al., 2008; Veerkamp et al., 2013), while the two lateral myocardial progenitor cell populations migrate

towards the midline, where they fuse by 19 hpf. This process results in the formation of a flat disc, which is termed cardiac cone (Stainier et al., 1993). At 24 hpf, the primitive heart tube has then formed in a series of events termed cardiac cone tilting and cardiac extension and jogging towards the left. During this later process, both endocardial and myocardial progenitor cells migrate in a left and anterior direction, causing the cardiac cone to undergo an asymmetric leftward movement and a three-dimensional conformational change (Rohr et al., 2008; Stainier et al., 1993; Yelon et al., 1999). At the same time, cardiomyocytes initiate contractions at the venous pole of the heart tube and blood passes through the heart from the inflow tract (IFT), through atrium, ventricle, and OFT (Beis et al., 2005). While at 24 hpf the heart is still incompletely lumenized and the blood flow rate is low, at about 28 hpf the lumen has opened and the heart has a regular heartbeat. During each cardiac contraction cycle, the contraction wave starts at the IFT and propagates with uniform speed to the OFT, which generates a pulsatile flow pattern. At this stage, the heart tube works as a valveless pulsatile pump and the flow rate is mostly influenced by the lumen diameter rather than the heart rate (Boselli et al., 2015; Goetz et al., 2014). After 36 hpf, the heart tube undergoes the looping process with a rightward bending that results in a rightward-placed future ventricle and a leftward positioned-future atrium (Bakkers, 2011). The two cardiac chambers become separated by a constriction which is being referred to as the AV canal (AVC). This is the site of the future AV valves. During cardiac looping morphogenesis, the ventricle and the atrium expand their volume, during cardiac ballooning. Cardiac ballooning requires functional heart contractions and blood flow, and results in a bean-shaped smaller ventricle and larger atrium (Auman et al., 2007; Hove et al., 2003). While the primitive heart tube is formed by cells derived from the FHF, the further growth and elongation of the myocardium is mostly supported by cells from the SHF (Zhou et al., 2011). In contrast, the endocardium grows by proliferation, without a contribution of external cells (Dietrich et al., 2014). The endocardial proliferation is triggered by blood flow and Bmp signaling, and is interconnected to the expansion of the myocardium (Bornhorst et al., 2019; Dietrich et al., 2014). In fact, an increase of the myocardial chamber generates higher junctional forces within endocardial cell junctions. The increase in mechanical forces is transduced by VE-cadherin and leads to the activation of Yap1 and consequent endocardial proliferation (Bornhorst et al., 2019).

At 72 hpf, cardiomyocytes initiate delamination from the ventricular wall to form cardiac trabeculae. These are muscular ridges lined by EdCs within the ventricular lumen and increase myocardial surface area which can be used for improved blood oxygenation (Liu et

al., 2010). The maturation of the heart involves formation of the coronary vasculature and the cardiac conduction system development (Burkhard and Bakkers, 2018; Samsa et al., 2013). Until early adult stages, the ventricle undergoes remodeling from a grossly pyramidal shape to a more-rectangular morphology and becomes positioned ventrally to the atrium (Singleman and Holtzman, 2012).

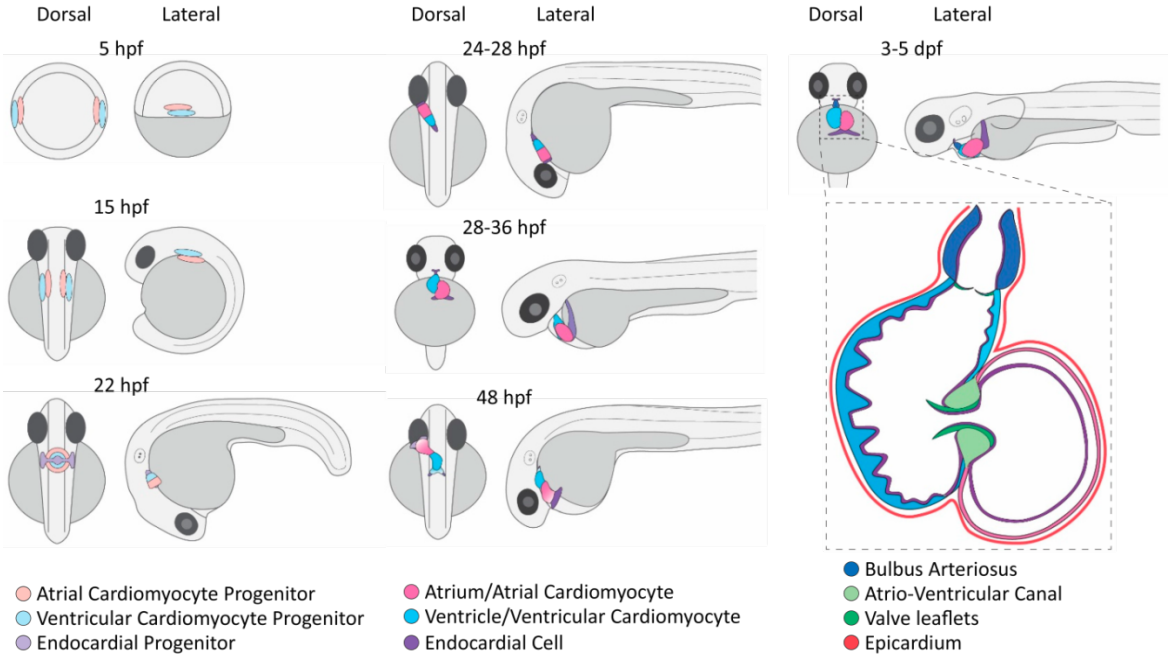

Figure 1.6. Schematic representation of zebrafish heart development. At 5 hpf, cardiac progenitors are located at the lateral margin. By 15 hpf, these cells initiate a midline directed migration and by 22 hpf, cardiac progenitors and developing endocardial cells have fused to form the cardiac cone. Cardiomyocytes begin to contract between 22 and 24 hpf. From 24 to 28 hpf, the cone elongates into the linear heart tube, begins leftward migration and then initiates a looping process. From 28 to 36 hpf, accretion of myocardial cells from the secondary heart field causes a tissue growth at the arterial and venous poles. By 48 hpf, the heart is composed of two chambers which are separated by the atrioventricular region (AVC). Between 3 to 5 dpf, the heart generates trabeculae (located primarily in the outer ventricle wall), cardiac valves at the AVC, the outflow tract, and an outer epicardial layer. Adapted from Brown et al., 2016.

1.4.1. Formation of cardiac valves in zebrafish

The mature zebrafish heart consists of a series of several chambers (sinus venosus, atrium, ventricle, and bulbus arteriosus). The cardiac valves that are positioned at the AVC are essential to maintain a unidirectional blood flow and to prevent a retrograde flow from the ventricle to the atrium during the contraction of the ventricular chamber. The formation of cardiac valves initiates at 36 hpf, concomitant with the cardiac looping process, which results in a manifest AVC region as a morphological constriction between ventricle and atrium. During this morphological process, AVC cardiomyocytes expand their basolateral while constricting their apical membrane compartments, which results in a bottlenecking of these cells. Within the endocardium, atrial cells move with the direction of flow and ventricular cells against this direction. This forms an endocardial convergence zone at the AVC (Figure 1.7A). The convergence is dependent on mechanical stimulation, since this process fails in embryos lacking heart beat and blood flow (Boselli et al., 2017). Once EdCs have converged at the AVC, signals from the AVC myocardium cause these cells to change their shape from squamous to cuboidal, and to express the activated leukocyte cell adhesion molecule a (Alcama) (Figure 1.7B-C). Hence, cells at the AVC region become morphologically and molecularly distinct from the rest of the cardiac cells. One of the best characterized signaling within the AVC myocardium is Wnt/b-catenin activity, which is essential for the communication to the AVC endocardium and to induce in this tissue proliferation and cell differentiation (Hurlstone et al., 2003). From the myocardium, Wnt/b-catenin signaling induces the expression of BMP2/4 (Verhoeven et al., 2011). Both in zebrafish and in mice, Tbx2 represses Nppa expression at the AVC (Christoffels et al., 2004; Ma et al., 2005). This contributes to the formation of AVC versus chamber cardiac tissues.

As in mammals, myocardial and endocardial layers at the AVC are separated by a thickened deposition of cardiac jelly. After 50 hpf, some ventricular chamber EdCs generate protrusions and migrate into the cardiac jelly, in a process that is blood flow-dependent (Beis et al., 2005; Heckel et al., 2015; Pestel et al., 2016; Steed et al., 2016a; Vermot et al., 2009) (Figure 1.7D). This initiates the formation of a double-layered immature valvular leaflet to which both ventricular and atrial EdCs contribute. While ventricular EdCs follow the first group of EdCs that ingressed into the ECM and contribute the abluminal part of the valve leaflet, atrial EdCs move towards the AVC where they maintain the lumen-facing side of the valve leaflet (Pestel et al., 2016; Steed et al., 2016b) (Figure 1.7E). Differently from valvulogenesis in

mammals, zebrafish EdCs that extend protrusions into the cardiac jelly apparently undergo a collective migration and move as a coherent sheets of cells rather than individual cells (Gunawan et al., 2019; Scherz et al., 2008). Resulting luminal and abluminal AV EdCs differ with respect to molecular marker expression. High shear stress induces Klf2 and Notch among luminal cells and sustains the expression of Alcam and of the adherens junction-component VE-cadherin. Abluminal EdCs have a strong Wnt/β-catenin activity and progressively lose the expression of Alcam and VE-Cadherin. The AV superior valve leaflet has formed by 76 hpf, while the development of the inferior is delayed by some 36 hours. However, by 96 hpf, valve leaflets are fully functional and prevent retrograde blood flow (Scherz et al., 2008). By 6 dpf, the superior AV valve leaflet is lined by valve EdCs, while the cells within the valve leaflet, derived from the abluminal EdCs that started to form by ECM-ingression from 50 hpf, have completely lost endothelial characteristic (Gunawan et al., 2020). These fibroblast-like cells are then referred to as valve interstitial cells (VICs). Between 4 and 6 dpf, VICs contribute to the elongation of the valve leaflets by proliferation events and ECM deposition. VIC development is promoted by the transcription factor Nfatc1, which regulates recruitment of EdCs and neural crest–derived cells and promotes proliferation. After the elongation stage, no significant morphological changes appear in the AV valve until the maturation stage, starting from 20 dpf. In this phase, VICs become multilayered and flatten, while providing the secretion and the maintenance of ECM, and valve leaflet further elongate, flattening of VICs are essential for. The establishment of a mature valve is completed by 30 dpf (Gunawan et al., 2020; Martin and Bartman, 2009).

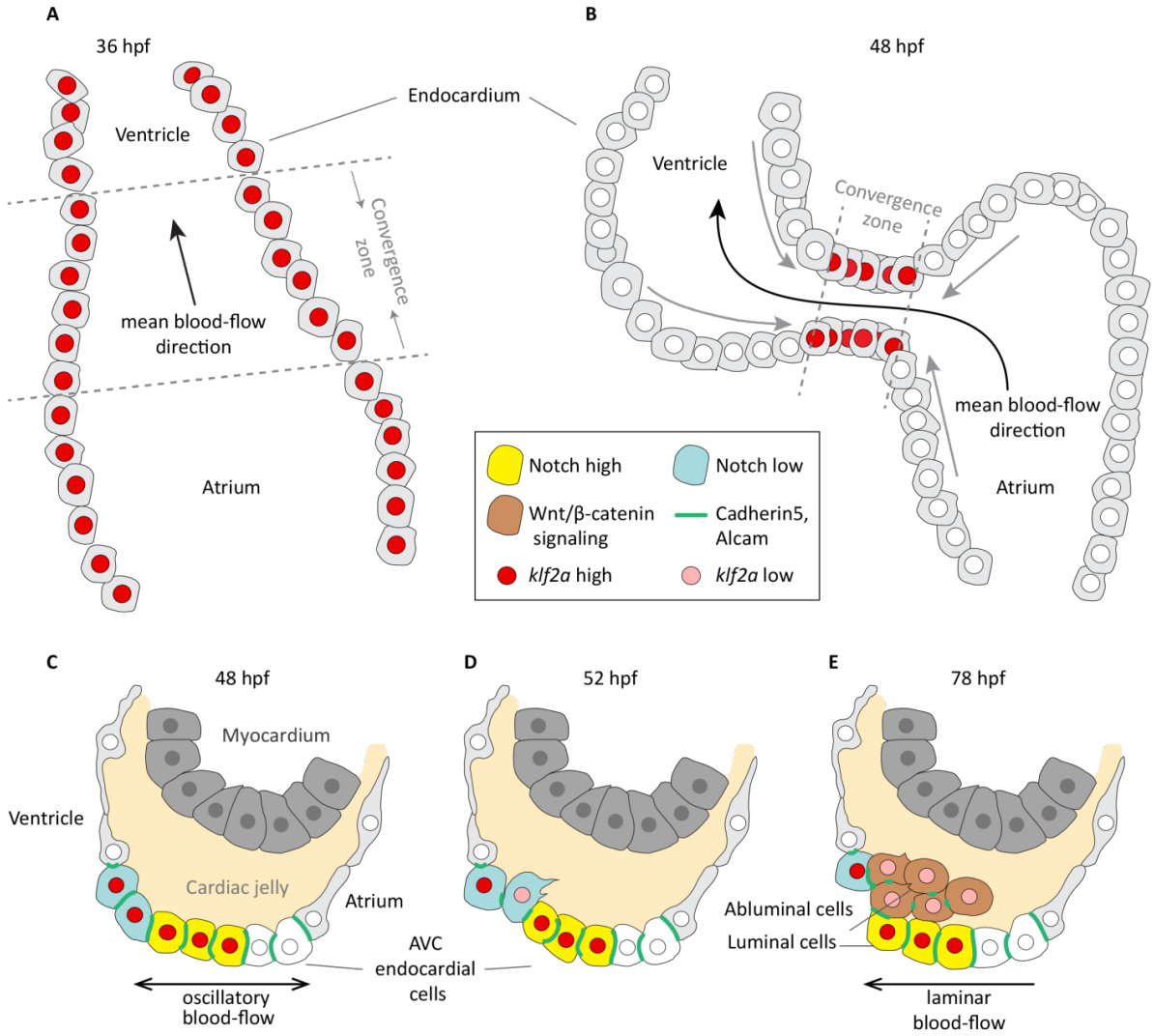

Figure 1.7. Schematic representation of zebrafish atrioventricular valve development. (A) The clustering of ventricular and atrial endocardial cells (EdCs) towards a convergence zone at the atrioventricular canal (AVC) is blood flow-dependent. **(B)** By 48 hpf, this early morphogenetic event is completed and the expression of the blood flow-responsive genes *klf2a* and *notch1b*, which at 36 hpf is throughout the entire endocardium, becomes restricted to high shear stress regions such as the AVC. Grey arrows indicate the direction of EdCs convergence movements. **(C-E)** Model of superior AV valve leaflet development. **(C)** At 48 hpf, AV EdCs adopt a cuboidal shape. **(D)** At 54 hpf, a few EdCs start protruding and migrate into the cardiac jelly, **(E)** where they will form the abluminal side of the immature valve leaflet. These cells have low expression levels of *klf2a*, *notch1b*, and cell adhesion proteins, while they have high levels of Wnt/β-catenin signaling. Adapted from Paolini and Abdelilah-Seyfried, 2018.

1.5. Biology of Vascular endothelial growth factor signaling

Over the past few decades, VEGFs and their receptors VEGFRs have emerged as main drivers of blood and lymphatic vessels development and maintenance. The field of VEGF/VEGFR signaling was established by the discoveries of the functional role of VEGFA as an endothelial growth factor (Leung et al., 1989) and the following identification of the receptor tyrosine kinases VEGFR1 [Fms-like tyrosine kinase (FLT1)], VEGFR2 (KDR/FLK1) and VEGFR3 (FLT4) (Alitalo et al., 1992; Matthews et al., 1991; Shibuya et al., 1990; Terman et al., 1991), which are dedicated to binding of VEGFs. In vertebrates, the VEGF family includes also VEGFB, VEGFC, VEGFD, and placenta growth factor (PLGF) (Joukov et al., 1997; Maglione et al., 1991; Olofsson et al., 1996; Park et al., 1994) (Figure 1.8). VEGFRs consist of seven immunoglobulin homology domains containing the ligand-binding part and a split tyrosine kinase domain, which transduces the association of growth factors to the receptors. Ligand binding induces VEGFR homodimerization or heterodimerization of the receptors, which activates the tyrosine kinase and causes the auto-phosphorylation of several dedicated regulatory tyrosine residues. Upon their phosphorylation, adapter molecules can bind and initiate various intracellular signaling pathways that result in immediate changes of vascular permeability, and longer-term responses that require gene regulation, including endothelial cell survival, migration and proliferation (Simons et al., 2016). As previously described, the dimerization and activation of VEGFRs can also occur in a VEGF ligand-independent manner, when triggered by mechanical forces or binding of non-VEGF ligands (Jin et al., 2003; Tzima et al., 2005).

The tight regulation of VEGFR signaling takes place by spatial and temporal changes in the expression levels of receptors, ligands, and VEGF-binding co-receptors (neuropilins and heparan sulfate proteoglycans). Non-VEGF-binding auxiliary proteins (such as integrins and ephrin B2) and inactivating tyrosine phosphatases, as well as the rate of receptor cellular uptake and extent of degradation and speed of recycling (Simons et al., 2016) also contribute to VEGFR signaling regulation. Therefore, it is important to study the localization of the VEGF signaling components within the different endothelial tissues. While the three receptors are all expressed within ECs during development, VEGFR2 has the broadest expression domain and, upon binding of its ligand VEGFA, is the main signaling receptor for angiogenesis, i.e. the process of forming new blood vessels from pre-existing ones (Simons et al., 2016). VEGFR1 is expressed also in monocytes and macrophages, vascular smooth

muscle cells and neuronal cells (Selvaraj et al., 2015). The other receptor VEGFR1 has a high-affinity to VEGFB, PLGF and VEGFA, but serves as a negative regulator of VEGFA/VEGFR2 signaling by limiting the availability of VEGFA for binding to VEGFR2 homodimers (Karaman et al., 2018). In fact, *Vegfr1−/−* mouse embryos die at E8.5–9 from excessive endothelial cell proliferation and disorganized vasculature, due to increased VEGFR2 signaling and enhanced angiogenesis (Fong et al., 1995). Expression of a splice variant encoding a soluble VEGFR1 (sVEGFR1) also reduces VEGFR2 signaling, by acting as a VEGF trap (Shibuya, 2013; Wild et al., 2017). Thus, both full-length membrane VEGFR1 and sVEGFR1 are viewed as anti-angiogenic decoy receptors. The third VEGF receptor, VEGFR3, plays an essential role in lymphangiogenesis upon binding of its ligand VEGFC (Karkkainen et al., 2004) and, to a minor extent, VEGFD. In *Vegfc*-deficient murine embryos, lymphatic endothelial cell (LEC) fail to detach from the cardinal vein to form the dorsal peripheral longitudinal lymphatic vessel and the ventral primordial thoracic duct which causes embryonic lethality between E15.5 and E17.5 (Hägerling et al., 2013; Karkkainen et al., 2004). However, a complete knockout of VEGFR3 in mice causes embryonic lethality at around E9.5, prior to lymphangiogenesis, due to vascular remodeling defects and pericardial fluid accumulation (Dumont et al., 1998). This suggests a further involvement of VEGFR3 in early cardiovascular development. Conversely, *Vegfc/Vegfd* double knockout mice, which display abnormal lymphangiogenesis, have normal blood vasculature development, suggesting a VEGFR3 ligand-independent mechanism in early cardiovascular development (Haiko et al., 2008). Together with the emergence of the lymphatic vessels, VEGFR-3 expression increases in these vessels and decreases in the blood endothelial cells (Kaipainen et al., 1995). Similar to mammalian embryos, zebrafish lymphatic cells are derived as sprouts from the posterior cardinal vein (PCV), migrate dorsally and congregate as parachordal lymphangioblasts along the trunk horizontal myoseptum between 48–60 hpf. Parachordal lymphangioblasts then continue migrating along arterial intersegmental vessels both ventrally and dorsally, to coalesce and form the thoracic duct (Küchler et al., 2006; Yaniv et al., 2006). The formation of parachordal lymphangioblasts and the thoracic duct formation is impacted in both *vegfc* and *vegfr3* zebrafish mutants (Hogan et al., 2009a). Despite its similarity to VEGFC and its high affinity for VEGFR3, VEGFD is dispensable for developmental lymphangiogenesis in mammals (Baldwin et al., 2005), although its absence leads to decreased lymphatic vessel caliber in the skin (Paquet-Fifield et al., 2013) and inhibition of facial lymphangiogenesis in zebrafish (Bower et al., 2017). After proteolytic processing by furin or the proprotein convertases PC5 and PC7 (McColl et al., 2003, 2007; Siegfried et al.,

2003), human VEGFC and VEGFD can also bind to VEGFR2 in human (Achen et al., 1998; Joukov et al., 1996, 1997; Stacker et al., 1999), but not in mouse (Baldwin et al., 2001).

Within the ECs, VEGFR3 has an important role in the regulation of Notch signaling. Endothelial-specific deletion of *VEGFR3* causes a decrease in Notch levels, which leads to excessive angiogenic sprouting and branching (Tammela et al., 2011). Notch, in turn, controls VEGF signaling, mainly acting via Dll4 as a negative feedback regulator to control the expression of VEGFRs and the co-receptor Nrp1 and regulate angiogenesis (see also 1.6 and 3.6). VEGFR3 has also a role in the modulation of VEGFA/VEGFR2 signaling, which impacts vascular permeability (Heinolainen et al., 2017). Despite its predominant expression in venous and lymphatic cells, VEGFR3 is expressed at lower levels in arterial ECs of zebrafish and mouse (Baeyens et al., 2015; Tammela et al., 2008). Interestingly, the expression of VEGFR3 within the murine thoracic aorta is not uniform. Regions of the aorta that experience higher fluid shear stress have lower levels of VEGFR3 expression (such as the outer curvature or some portions of the carotid artery), while inner curvature regions that are associated with lower fluid shear stress have stronger expression levels (Baeyens et al., 2015). Thus, expression of VEGFR3 in lymphatic and blood endothelial vessels suggests a negative correlation with shear stress. This finding led to the hypothesis that tissue-specific differences in VEGFR3 expression levels could explain why ECs have different levels of sensitivity in their responses to blood flow (Baeyens et al., 2015). Within the endocardium, VEGFR3 is expressed in at least a subset of murine cells at E13.5 (VanDusen et al., 2014). Recently, human mutations in *VEGFR3* have been correlated with Tetralogy of Fallot, a congenital cardiac disease with abnormal cardiac valvulogenesis (Jin et al., 2017; Reuter et al., 2018). Nevertheless, the functional role of VEGFR3 in the endocardium has not been studied further.

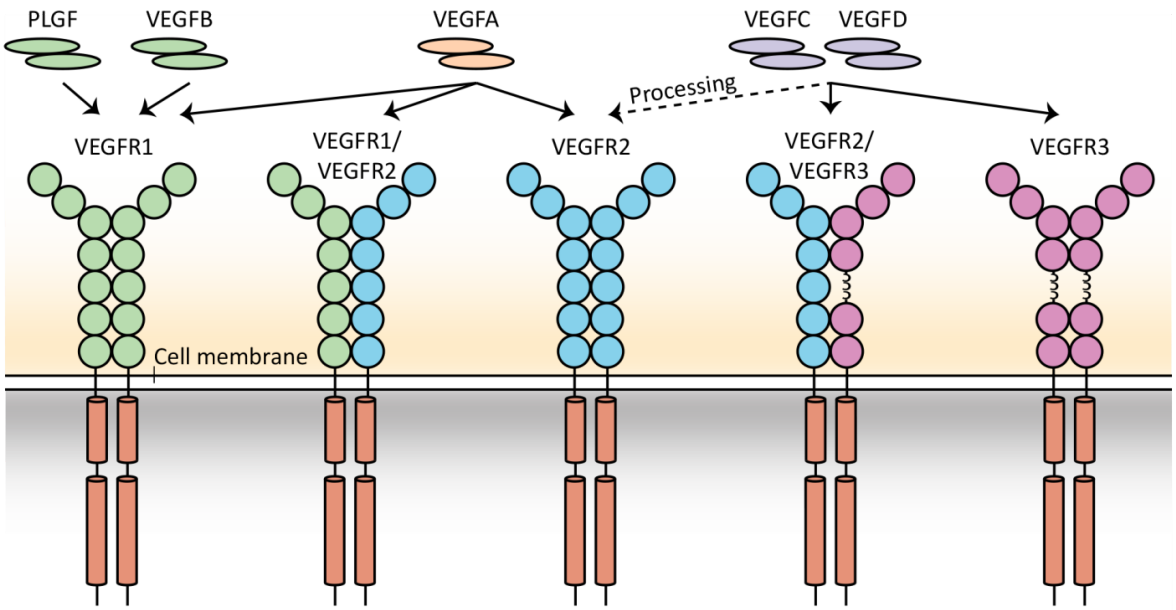

Figure 1.8. Vegf receptors and ligands in endothelial cells. Vascular endothelial growth factors (VEGFs) bind to the three VEGF receptor (VEGFR) tyrosine kinases, leading to the formation of VEGFR homodimers and heterodimers. Proteolytic processing of VEGFC and D allows for binding to VEGFR2. Adapted from Olsson et al., 2006.

1.6. Biology of Notch signaling

Notch signaling is a highly conserved intercellular signaling pathway with key roles in cardiovascular development and homeostasis (MacGrogan et al., 2018; Mack and Iruela-Arispe, 2018). In mammals, the Notch receptor family includes four transmembrane receptors (Notch1–4). Each receptor harbors a large amino-terminal Notch extracellular domain (NECD), a single-pass transmembrane domain and a short intracellular domain (NICD) which is required for the transcriptional activation of Notch target genes. The NICD contains a RAM (recombination signal-binding protein for immunoglobulin kappa J (RBPJ) Association Module) domain, seven ankyrin repeats (ANK), a transcription activation domain (TAD) and a PEST domain, involved in NICD degradation by proteolysis. During canonical Notch signaling, its activation is ligand-mediated and involves Notch ligands of the Delta-like (Dll) family (Dll1, Dll3, Dll4) as well as Jagged 1 and Jagged 2. Similar to their Notch receptors, the ligands are all type I transmembrane proteins with an extracellular domain (Pompa et al., 2016). Receptor–ligand interactions lead to proteolytic events that require ADAM metalloproteases and γ-secretase. The processing of the Notch receptor releases the

NICD from the membrane, which translocates into the nucleus where it functions as a transcriptional coactivator through cooperation with RBPJ (Mack and Iruela-Arispe, 2018). Among the key target genes and effectors of Notch are HES (hairy enhancer of split) and Hey (hairy/enhancer of split-related with YRPW motif) (Davis and Turner, 2001).

During development, Notch signaling is implicated in the differentiation of cells and tissues by promoting distinct fates within an initially homogenous group of cells. This is achieved through transactivation when a ligand-expressing cell (signaling cell) sends an inhibitory signal to a neighboring receptor- expressing cell (receiving cell), which prevents other cells within the group of cells from adopting the same fate. In turn, Notch pathway activation works through a positive feedback loop, reinforcing expression of the ligand in the signaling cell and the receptor in the receiving cell (Niessen and Karsan, 2008). Hence, transactivation leads to the process of lateral inhibition, where ligand- and receptor-expressing cells adopt unique cell fates and become segregated, resulting in a "salt and pepper" distribution (Lewis, 1998). An example of this mechanism was identified in the establishment of tip/stalk cell identity during sprouting angiogenesis. In this context, VEGF induces Dll4 expression within the cell at the end of the sprout (tip cell), which activates Notch1 in neighboring cells that adopt a stalk cell fate. In turn, Notch activation suppresses DLL4 expression (Hellström et al., 2007; Lobov et al., 2007; Suchting et al., 2007).

Notch signaling is essential for proper development of the vasculature (Hofmann and Iruela-Arispe, 2007). Cardiovascular defects were observed in murine embryos lacking Notch1, Notch3, Notch4, Notch ligands Jagged1, DLL1 or DLL4 (Niessen and Karsan, 2007). Notch signaling plays a critical role in arterial specification, by repressing venous fate, both in zebrafish and mouse (Lawson et al., 2001; Roca and Adams, 2007).

Within the heart, Notch signaling is involved in many processes. Besides its already mentioned role in the AV valve development, Notch acts in the outflow tract formation, where it regulates WNT and BMP in SHF progenitors to arrest proliferation and promote differentiation (Kwon et al., 2009) and, later on, EndoMT (High et al., 2009). NOTCH1 mutations cause bicuspid aortic valve and predispose to calcific aortic valve disease (Garg et al., 2005). Notch pathway plays an essential role also during cardiac trabeculation, promoting an endocardial signaling to the myocardium (Grego-Bessa et al., 2007). During zebrafish heart regeneration, endocardial Notch signaling mediates fibrotic tissue deposition and cardiomyocyte proliferation (Münch et al., 2017; Raya et al., 2003; Zhao et al., 2014).

1.7. The flow-regulatd transcription factor Klf2

Klf2 is the best characterized flow-regulated transcription factor. A study on ECs exposed to flow reported that 46% of the most highly flow-regulated genes depended on KLF2 upregulation (Parmar et al., 2006). KLF2 is a member of the zinc finger family of DNA-binding transcription factors. In murine ECs, *Klf2* expression is detectable from E8.5 and, with the onset of pulsatile blood flow, rises within ECs and EdCs exposed to high shear stress. At E14.5, its expression is detectable within the developing heart valves but only among those cells that are positioned on the flow-exposed sides of the valve leaflets. By E18.5, *Klf2* becomes activated within the endocardium lining the intraventricular papillary muscles (Lee et al., 2006). Loss of Klf2 in mouse causes embryonic lethality by E14.5 because of intraembryonic and intraamniotic hemorrhages (Lee et al., 2006; Wani et al., 1998).

In zebrafish, two Klf2 orthologues are present, encoded by *klf2a* and *klf2b* (Oates et al., 2001). This reflects the fact that teleosts underwent a partial genome duplication of their genome during evolution (Taylor et al., 2003). Both genes are expressed in a flow-dependent manner within the developing vasculature and the endocardium (Novodvorsky et al., 2015; Renz et al., 2015; Vermot et al., 2009). In *klf2a/b* double mutant zebrafish, the diameter of axial blood vessels is reduced and flow-induced endothelial cell polarization is affected. This indicates a conserved role of KLF2 in the regulation of vascular tone (Kwon et al., 2016). Klf2a is important for flow-stimulated angiogenesis during aortic arch development, by inducing the expression of an endothelial-specific microRNA, *miR-126*, to activate VEGFA/VEGFR2 signaling (Nicoli et al., 2010). Other studies showed that Klf2a negatively regulates endothelial proliferation by inhibiting Vegf receptor expression (Atkins and Jane et al., 2007; Dekker et al., 2006). Klf2a plays a role also in another flow-regulated process, which is the maintenance of hematopoietic stem cells (Wang et al., 2011). Klf2a and blood flow also contributes to the regulation of EdCs sizes. In *klf2a* morphant hearts, which have normal contractility, ventricular EdCs are enlarged, whereas overexpression of *klf2a* leads to smaller EdCs (Dietrich et al., 2014). Interestingly, Klf2 is activated also in a manner that is independent of blood flow. For instance, a group of zebrafish mutants that lack proteins of the CCM complex and that fail to form a functional heart (thus, lack blood flow) have an increased expression of *klf2a* mRNA levels. This activation of *klf2a* expression is triggered in a process mediated by β1-integrin signaling and cellular tension (Donat et al., 2018; Renz et al., 2015). In mice, the loss of CCM proteins activates the mitogen-activated protein kinase

kinase kinase 3 (Map3k3/Mekk3) signaling pathway. This results in an increase of ADAM metallopeptidase expression, which degrade cardiac jelly, and increased levels of Klf2 (Zhou et al., 2015).

1.8. Aims of this study

The development of the heart and the vasculature is intrinsically interconnected with biomechanical stimuli caused by blood flow. While many studies focused on mechanosensitive transduction pathways within endothelial cells, less is known about molecular mechanisms of flow-sensitivity within the endocardium. In particular, the formation of cardiac valves is strictly dependent on fine-tuned mechanosensitive signaling and involves the remodeling of the endocardium into subpopulations that are differently exposed to flow-induced forces.

In this study, I will analyze new players involved in flow-mediated valvulogenesis, with a focus on the following questions:

1. Which are flow-regulated genes within endocardial cells?
2. What are the molecular mechanisms involved in the formation of endocardial subpopulations during cardiac valve development?
3. What is the role of the flow-regulated receptor Flt4 during cardiac valve formation?
4. How does Flt4 interact with known mechanosensitive signaling pathways?

2. Results

2.1. Flt4 is negatively regulated by blood flow within the endocardium

Biomechanical stimulation induced by blood flow is essential for cardiac valve leaflet formation (Beis et al., 2005; Pestel et al., 2016; Steed et al., 2016b; Vermot et al., 2009). In order to identify molecular players involved in zebrafish cardiac mechanosensitive signaling during valvulogenesis, my colleague Dr. Timm Haack (Hannover Medical School) performed a comparative RNA-sequencing (RNA-seq) analysis (in collaboration with the Research Core Unit "Transcriptomics" of Hannover Medical School) of isolated cardiac tissue (Lombardo et al., 2015) from wild-type (WT) versus embryos injected with an antisense oligonucleotide morpholino (MO) against *troponin T type 2a* (*tnnt2a*). *tnnt2a* encodes a sarcomeric protein essential for cardiac contraction, thus *tnnt2a* morphant embryos lack blood flow (Sehnert et al., 2002). Cardiac tissue was collected at 54 hpf, the developmental stage at which EdCs at the AVC initiate the morphogenetic processes leading to valve leaflets. Previous studies had shown that shear stress-responsive genes are downregulated in *tnnt2a* morphants, including *notch1b* (Samsa et al., 2015) and *heart development protein with EGF-like domains* (*heg1*) (Donat et al., 2018). In tune with this finding, *notch1b* and *heg1* were downregulated in our *tnnt2a* RNA-seq sample as well (Figure 2.1A). Interestingly, one of the most strongly upregulated genes was *fms-related tyrosine kinase 4* (*flt4*). *flt4* encodes Vegfr3/Flt4, a receptor which is part of the family of VEGFRs. Within the endothelium, Flt4 has been described as co-receptor of the junctional mechanosensitive Pecam/VE-cadherin/Vegfr2 complex (Coon et al., 2015) and as a mediator of cell responses to shear stress (Baeyens et al., 2015). Among the other genes encoding VEGF receptors, *kinase insert domain receptor like* (*kdrl*, also known as *vegfr2*) and *kinase insert domain receptor* (*kdr*) mRNA levels did not change in response to a lack of blood flow and *fms-related tyrosine kinase 1* (*flt1,* also known as *vegfr1*) expression was downregulated (Figure 2.1A). I confirmed these data by replicating the experimental set up and by analyzing mRNA levels on 54 hpf WT versus *tnnt2a* morphant hearts by quantitative real-time PCR (RT-qPCR) analysis (Figure 2.1B).

The physiological expression of *flt4* in the zebrafish heart has not been investigated so far. In mice, *Vegfr3* is expressed in at least a subset of EdCs (VanDusen et al., 2014), but its biological function within this tissue has not been clarified. To analyze *flt4* expression within the zebrafish heart, I took advantage of the transgenic reporter line *Tg(flt4BAC:mCitrine)*^{hu7135}, which reveals endogenous gene expression from the *flt4* locus

(van Impel et al., 2014). Enhancement of mCitrine expression with an antibody against green fluorescent protein, which also detects mCitrine, revealed *flt4:mCitrine* expression in the 54 hpf endocardium, albeit at low levels (Figure 2.1C). In 54 hpf *tnnt2a* morphants, *flt4:mCitrine* expression was visibly upregulated within the endocardium, especially within the ventricular chamber. Compared to WT, the fluorescence intensity increased by 83% in *tnnt2a* morphant ventricular and AVC EdCs and by 61% in atrial EdCs (Figure 2.1D). In WT zebrafish embryos at the same stage, *heg1* (Donat et al., 2018), *notch1b* and Notch signaling (Samsa et al., 2015; Vermot et al., 2009) (Figure 2.1F) are expressed mainly in the ventricular endocardium and particularly high in the AV endocardium. Taking advantage of the transgenic reporter line *TgBAC(flt1:YFP)*^{hu4624} (Hogan et al., 2009b), I analyzed the expression of *flt1* in the endocardium. *flt1:YFP* was mainly expressed in the ventricular and AVC EdCs in a pattern that is similar of flow responsive genes (Figure 2.1G). Expression from the Notch activity reporter transgene *Tg(TP1:VenusPEST)*^{s940} (Ninov et al., 2012) and *TgBAC(flt1:YFP)*^{hu4624} was abolished or strongly decreased in *tnnt2a* morphant hearts (Figure 2.1G, I). Together, these data confirmed RNA-seq and qPCR data.

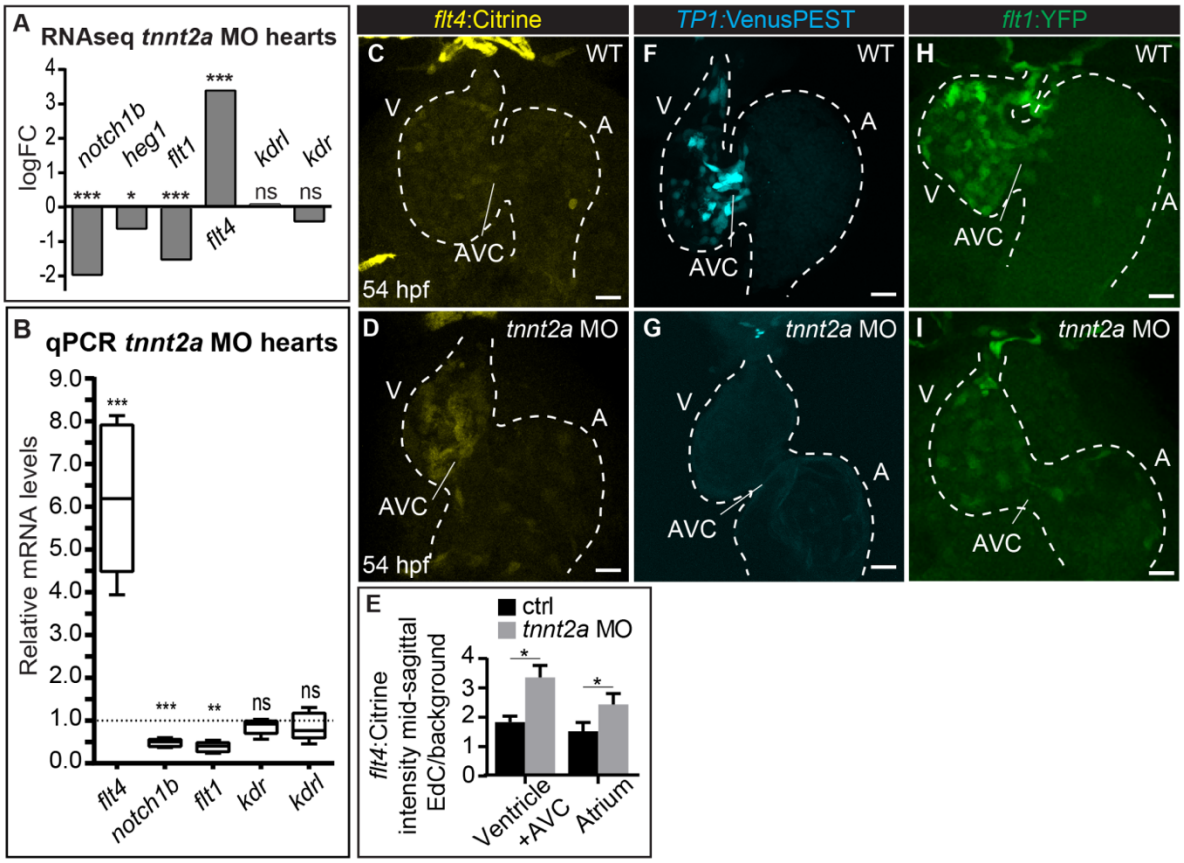

Figure 2.1: Lack of blood flow increases *flt4* mRNA and decreases *notch1b* and *flt1* mRNA expression levels. (A) Comparative mRNA expression levels from *tnnt2a* morphant compared with wild-type (WT) cardiac transcriptomes at 54 hpf. Unlike expression levels of other blood flow-sensitive genes, *flt4* mRNA is elevated upon loss of blood flow. Mean values are shown (n=3 replicates). Differential expression analysis was performed by use of Cuffdiff (*q<0.05; ***q<0.005; ns, not significant; see Materials and methods section). **(B)** Validation of RNA-sequencing results by RT-qPCR quantifications of *flt4* mRNAs, *notch1b* mRNAs, *flt1* mRNAs, *kdr* mRNAs and *kdrl* mRNAs from *tnnt2a* morphant hearts at 54 hpf, normalized to WT siblings (n=5 independent replicates). Min to max box and whisker plots are shown. Data were analyzed by ratio paired student's *t*-test (**p<0.01; ***p<0.005; ns, not significant). **(C, D, F-I)** Maximum intensity projections based on confocal z-stack images of 54 hpf hearts. **(C)** Expression from the Flt4 reporter *Tg(flt4BAC:mCitrine)*^{hu7135} is weaker in WT when compared with **(D)** *tnnt2a* morphants, **(E)** as quantified by analysing fluorescence intensity levels of mid-sagittal section planes of confocal z-scan images throughout the endocardium (control embryos, n=6; *tnnt2a* morphants, n=6). Mean values ± SD are shown and data were analyzed by unpaired student's *t*-test (*p<0.05). **(F)** Expressions of the Notch activity reporter *Tg(TP1:VenusPEST)*^{s940} and **(H)** the Flt1 reporter *TgBAC(flt1:YFP)*^{hu4624} are higher in the ventricle and AVC region in WT, while there is **(G)** no or **(I)** weak expression in *tnnt2a* morphants. V, ventricle; A, atrium; AVC, atrioventricular canal. Scale bars: (C, D, F-I) 20 µm.
Adapted from (Fontana et al., 2020).

2.2. Flt4 is expressed in atrioventricular abluminal endocardial cells

During zebrafish AV valvulogenesis, AV EdCs rearrange whereby ventricular EdCs move into the abluminal region of the developing valve leaflet, where they are not in direct contact with blood flow. At the same time, atrial EdCs remain on the luminal side where they are exposed to blood flow (Pestel et al., 2016; Steed et al., 2016b). To visualize the spatio-temporal distribution of *flt4* mRNA expression within developing AV valve leaflets, I analyzed the *Tg(flt4BAC:mCitrine)*^{hu7135} transgenic reporter line, and counterstained the tissue with the junctional marker Alcam. Within the developing zebrafish heart, Alcam is expressed in the myocardium (especially in ventricular cardiomyocytes), and within the AV endocardium (Beis et al., 2005). At 56 hpf, prior to the formation of a multilayered valve leaflet, *flt4:mCitrine* expression was generally low and Alcam was expressed in luminal EdCs, decorating the basolateral cell membrane compartments between neighboring cells (Figure 2.2A). In comparison, Alcam expression levels were lower and less continuous at the cell membranes of ingressed EdCs. By 78 hpf, AV EdCs had acquired a multilayered S-shaped structure. At this stage, the expression of Alcam within abluminal EdCs was strongly diminished while *flt4:mCitrine* expression was higher in abluminal EdCs of the developing superior AV valve leaflet (Figure 2.2B-B''). At the same stage, expression from the Notch activity reporter transgene *Tg(TP1:VenusPEST)*^{s940} was restricted entirely to the opposing luminal side (Figure 2.2C) (Pestel et al., 2016). Similarly, the *TgBAC(flt1:YFP)*^{hu4624} reporter line was expressed mainly within luminal EdCs (Figure 2.2D). Thus, luminal and abluminal regions of the developing atrioventricular valve leaflets have complementary expression patterns with luminal EdCs exhibiting Notch activity and *flt1* expression and abluminal EdCs expressing *flt4* mRNA.

In order to check whether more mature valve tissue remained responsive to blood flow, I next carried out a short-term pharmacological inhibition of blood flow. For this experiment I used the calcium channel blocker felodipine (8μM), that prevents cardiomyocyte contraction (Kokkas 1993; Otten *et al.*, 2018), in a narrow time window between 72-78 hpf. This resulted in an upregulation of cardiac *flt4* mRNA expression levels and in a downregulation of *notch1b* (Figure 2.2E). This is in tune with higher expression levels of *flt4* mRNA in cells not exposed to blood flow. Together, these results showed that a lack of blood flow results in increased expression levels of *flt4* mRNA while diminishing Notch activity within the endocardium.

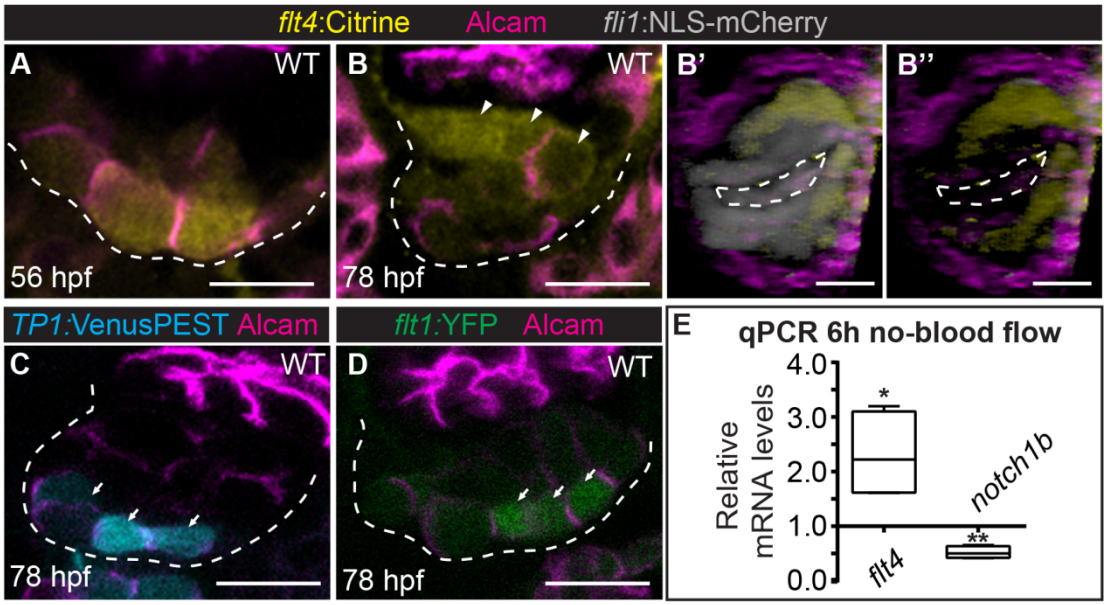

Figure 2.2: Luminal EdCs exhibit Notch and Flt1 activity, while abluminal EdCs express *flt4*. **(A-D)** Single confocal z-section images of the AVC region, immunolabeled with Alcam. **(A)** Immunohistochemical labeling of green fluorescent protein in *Tg(flt4BAC:mCitrine)*^{hu7135} embryos reveals expression in cardiac cushion EdCs at 56 hpf, **(B)** and higher expression levels in abluminal EdCs cells (arrowheads) at 78 hpf. **(B', B'')** Atrial view of transverse section from 3D reconstructed wild-type (WT) heart shown in (B), using Imaris software. Dotted line indicates AVC lumen. In **(B')**, endocardial cells are marked by *Tg(fli1:NLS-mCherry)*^{ubs10}. **(C)** In contrast, *Tg(TP1:VenusPEST)*^{s940} and **(D)** *TgBAC(flt1:YFP)*^{hu4624} have high expression in luminal EdCs of the endocardial AVC region (arrows). **(E)** RT-qPCR quantifications of cardiac *flt4* and *notch1b* mRNAs of embryos with a pharmacological inhibition of blood flow between 72-78 hpf (8 µM felodipine) normalized to dimethylsulfoxide (DMSO)-treated control embryos. Min to max box and whisker plots are shown (n=4 independent experiments). Data were analyzed by ratio paired student's *t*-test (*p<0.05; **p<0.01). Scale bars: (A-D) 20 µm, (B', B'') 10 µm. Adapted from (Fontana et al., 2020).

2.3. Flt4 is required for atrioventricular valvulogenesis

After discovering that *flt4* mRNA expression levels change dynamically within EdCs in reponse to alterations in their exposure to blood flow during cardiac AV valvulogenesis, I investigated the possible role of this receptor protein in sculpting the AV valve. In order to do that, I analyzed *flt4*^{hu4602} mutants (Hogan et al., 2009b). Although considered a hypomorphic allele, in *flt4*^{hu4602} mutants VEGFR3 signaling is impaired and mutant embryos exhibit a fully penetrant phenotype with the expected defects in the formation of facial lymphatic vessels, parachordal lymphatics, and the thoracic duct (Astin et al., 2014; Hogan et al., 2009b). After confirming that *flt4*^{hu4602} mutants showed parachordal lymphatics defects at 56 hpf (Figure 2.3A,B), I analyzed their heart beat rate, since an increase or a reduction in the heart rate have been shown to induce valvulogenesis defects (Vermot et al., 2009). The number of heart

beats/minute were similar between WT and *flt4*^{hu4602} embryos at 78 hpf (WT, n=10 embryos: 156 ± 5 heart beats/min; *flt4*^{hu4602}, n=10 embryos: 154 ± 5 heart beats/min). At this stage, developing AV valve leaflets were disorganized and abnormally multilayered, compared to WT (Figure 2.3C-D). Strikingly, the expression of the cell adhesion marker Alcam, which in the WT endocardium is mostly restricted to luminal EdCs (Beis et al., 2005; Donat et al., 2018), was present also within abluminal EdCs in 70% of *flt4*^{hu4602} mutant embryos (Figure 2.3C-E). This observation was further quantified based on Alcam intensity levels in luminal versus abluminal EdCs (Figure 2.3F). Since these findings suggested that gene expression and cellular properties at the developing valve leaflet were affected in *flt4*^{hu4602} mutants, I further investigated whether molecular signaling involved in valvulogenesis was influenced by the loss of Flt4. To this end, I analyzed the expression from Notch and Wnt transgenic reporter lines at 78 hpf. During atrioventricular valvulogenesis, EdCs on the luminal side show Notch activity, while those on the abluminal side exhibit strong Wnt/β-catenin signaling as visualized with the stable transgenic reporter strain *Tg(7xTCF-Xla.Siam:nls-mCherry)*^{ia5} (Figure 2.3G) (Moro et al., 2012; Pestel et al., 2016). Among luminal EdCs, I found that Notch activity was strongest within those cells of the two juxtaposed valve leaflets that are the first to come into contact with each other during every cardiac contractile cycle (I refer to these cells as “heel cells“) (arrows in Figure 2.3G). Strikingly, the loss of Flt4 caused an ectopic presence of Notch reporter-expressing cells within abluminal positions of the atrioventricular valve leaflets, which in some cells was overlapping with Wnt/β-catenin signaling (arrowheads in Figure 2.3H). Conversely, Wnt/β-catenin signaling was expressed also ectopically at the luminal side of the AV valve leaflet (Figure 2.3H). Altogether, these observations point at an abnormal morphology of the developing AV valve leaflet upon loss of Flt4.

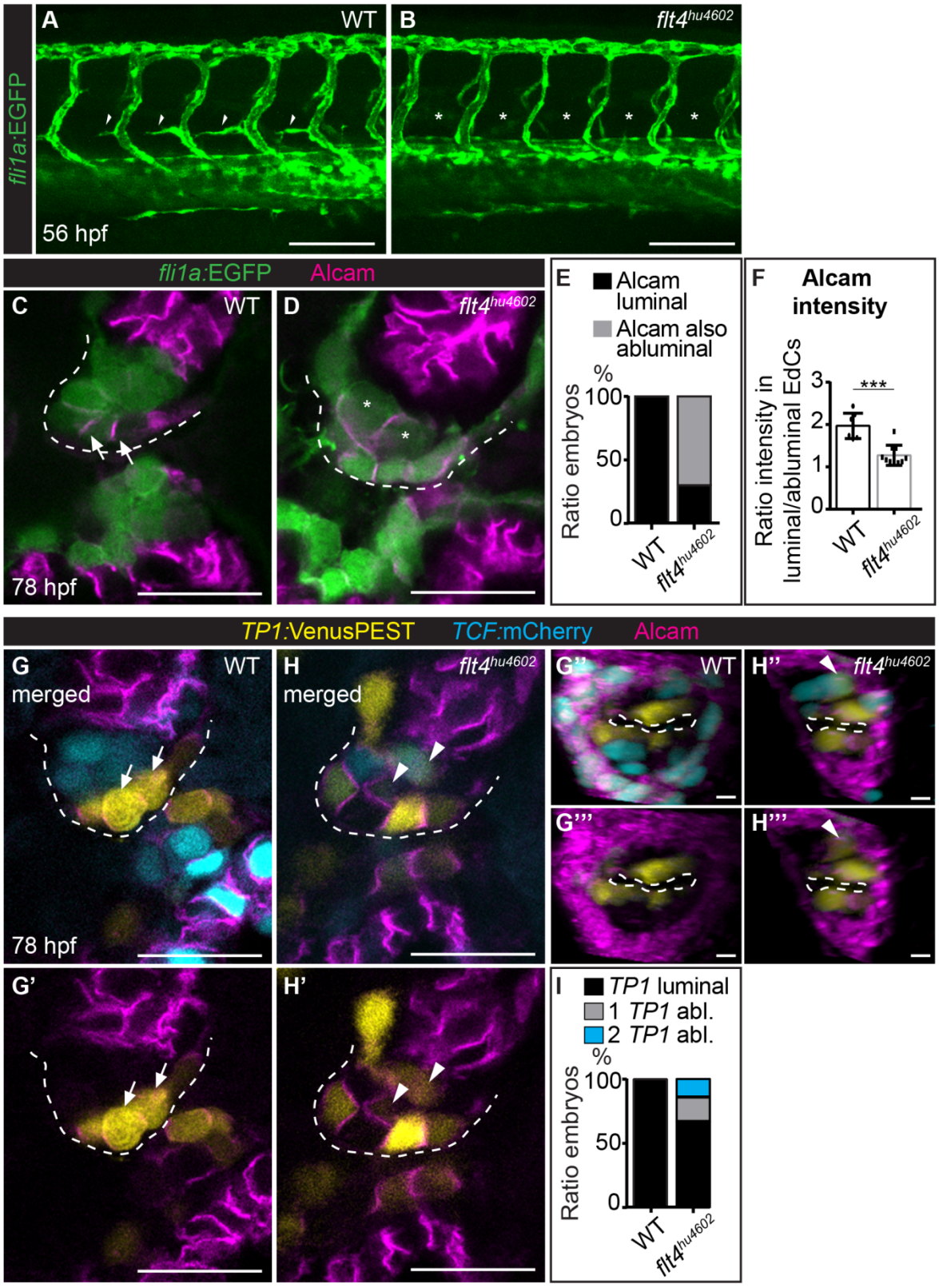

Figure 2.3: Flt4 is required for proper atrioventricular valvulogenesis. (A-B) Maximum intensity projections of confocal z-section images of trunk regions. **(A)** At 56 hpf, *Tg(fli1a:EGFP)*^{y1} expression marks the presence of parachordal lymphangioblast segments at the horizontal myoseptum in wild-type (WT) (arrowheads), while they are absent **(B)** in *flt4*^{hu4602} mutants (asterisks). **(C, D)** Single confocal z-section images of the AVC region at 78 hpf. **(C)** EdCs cells are marked by *Tg(fli1a:EGFP)*^{y1} expression and Alcam staining labels cell junctions mostly of luminal EdCs (arrows)

in WT. **(D)** In *flt4*^{hu4602} mutants, expression of Alcam is present also in abluminal positions (asterisks) and the morphogenesis of the superior valve leaflet is impaired. **(E)** Quantification of the ratio of embryos with an expression of Alcam in luminal EdCs versus embryos with Alcam expression also in abluminal EdCs (WT, n=9 embryos; *flt4*^{hu4602}, n=20 embryos). **(F)** Quantifications of Alcam fluorescence intensity in luminal/abluminal EdCs at mid-sagittal section planes of confocal z-scan images (WT, n=7 embryos; *flt4*^{hu4602}, n=10 embryos). Mean values ± SD are shown and data were analyzed by unpaired student's *t*-test (***p<0.005). **(G, H)** Single confocal z-section images of the AVC region at 78 hpf. **(G, G')** In WT, luminal EdCs express the Notch reporter *Tg(TP1:VenusPEST)*^{s940} (particularly strong in "heel EdCs"; arrows), while expression of the Wnt signaling reporter *Tg(7xTCF-Xla.Siam:nls-mCherry)*^{ia5} is in abluminal positions. **(H, H')** In *flt4*^{hu4602} mutants, EdCs expressing *Tg(TP1:VenusPEST)*^{s940} are present also in abluminal positions (arrowheads). **(G''-H'')** Atrial view of transverse section from 3D reconstructed WT hearts shown in (G) and (H), using Imaris software. Dotted line indicates AVC lumen. **(I)** Quantification of the ratio of embryos with an expression of *TP1*:Venus in only luminal AV EdCs versus embryos expressing one or two *TP1*:Venus-positive AV EdCs within abluminal positions (WT, n=9; *flt4*^{hu4602}, n=21). Abl, Abluminal. Scale bars: (A, B) 100 µm; (C, D, G-H') 20 µm; (G''-H''') 5 µm. Adapted from (Fontana et al., 2020).

The AV valve phenotype in *flt4*^{hu4602} mutant was only lowly penetrant (Figure 2.3E,I). This may be due to the hypormorphic nature of this allele, which still results in the full-length Flt4 protein, but affected in its kinase domain function (Hogan et al., 2009b). To verify the *flt4*^{hu4602} cardiac phenotype with an independent knockdown tool, I injected a well-characterized Flt4-specific morpholino (MO) (Covassin et al., 2006; Kok et al., 2014). This MO has been reported to cause similar lymphatic defects as the *flt4*^{hu4602} mutation and in my study resulted in a reduction of lymphatic precursors at 56 hpf (Figure 2.4A,B). Consistent with the endocardial defects observed in *flt4*^{hu4602} mutants, mophants had a dysmorphic AV valve leaflet phenotype at 78 hpf, with a more persistent Alcam and Notch expression at the abluminal side (Figure 2.4C-G). This phenotype was similar to *flt4*^{hu4602}, but with a higher penetrance (Figure 2.4E,H). The expression of the adherens junction protein VE-Cadherin, which in WT is restricted to luminal EdCs (Steed *et al.*, 2016), was persistent in *flt4* morphant abluminal EdCs (Figure 2.4I,J). Dr. Timm Haack measured the surface area of Notch-expressing cells at the AVC at 78 hpf, and found that *flt4* morphant cells were larger compared to WT (WT, n=12 cells, 19.12 ± 1.11 µm^2; *flt4* morphant, n=20 cells, 29.23 ± 1.47 µm^2, p<0.001). Shear stress reduces surface area sizes and contributes to the elongation of zebrafish EdCs (Dietrich et al., 2014). Their enlargement in *flt4* morphants suggested an impaired mechanosensitivity of AV EdCs under these conditions.

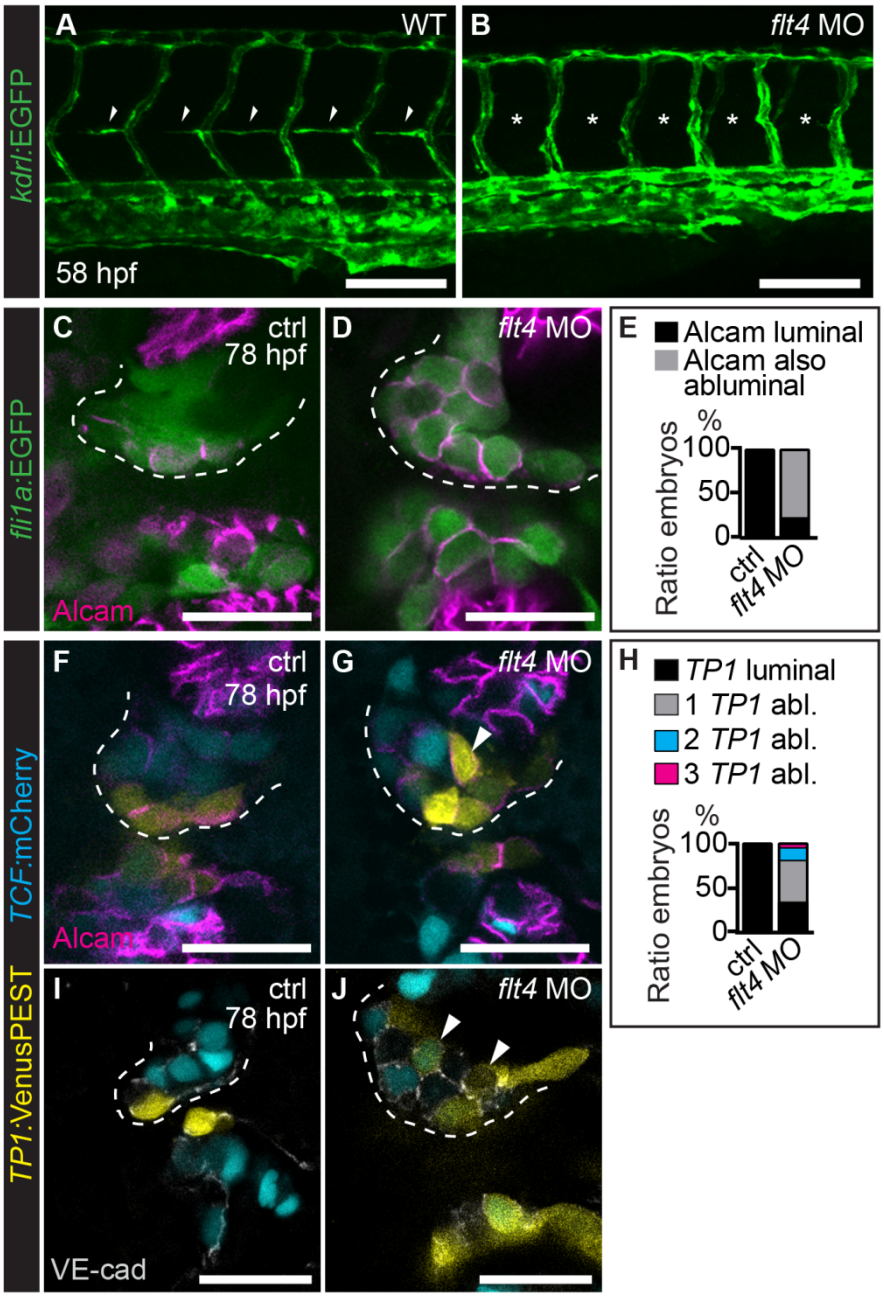

Figure 2.4: Morpholino-induced loss of Flt4 causes AV valve defects. (A-B) Maximum intensity projections of confocal z-section images of trunk regions. At 58 hpf, parachordal lymphangioblast segments are present **(A)** in wild-type (WT), while being absent **(B)** in *flt4* morphants. **(C, D)** Single confocal z-section images of the AVC at 78 hpf. **(C)** In control embryos, *Tg(fli1a:EGFP)*^{y1} marks EdCs cells and Alcam staining is present mainly at cell junctions of luminal EdCs. **(D)** In *flt4* morphants, Alcam is expressed also in abluminal positions. **(E)** Quantification of the ratio of embryos with an expression of Alcam in luminal EdCs versus embryos with Alcam expression also in abluminal EdCs (ctrl n=18, *flt4* MO n=23). **(F-G)** Single confocal z-section images of the AVC region at 78 hpf. **(F)** In control embryos, luminal EdCs express the Notch reporter *Tg(TP1:VenusPEST)*^{s940}, while expression of the Wnt signaling reporter *Tg(7xTCF-Xla.Siam:nls-mCherry)*^{ia5} is in abluminal positions. **(G)** In *flt4* morphants, *Tg(TP1:VenusPEST)*^{s940}-positive EdCs are present also in abluminal positions (arrowheads). **(H)** Quantification of the ratio of embryos with an expression of *TP1*:Venus in only luminal AV EdCs versus embryos expressing one, two or three *TP1*:Venus also within abluminal AV EdCs (ctrl n=17, *flt4* MO n=21). Abl, Abluminal. **(I, J)** Single confocal z-section images of the

AVC region at 78 hpf. **(I)** The adherens junction protein VE-Cadherin is present in luminal EdCs in control embryos, **(J)** while its present also in abluminal positions in *flt4* morphants. Scale bars: (A, B) 100 µm; (C, D, F, G, I, J) 20 µm. Adapted from (Fontana et al., 2020).

As a second independent tool to impact Flt4 signaling activity, I treated embryos between 24-78 hpf with 25 µM of the Vegfr inhibitor MAZ51, which has a high affinity for Flt4 (Benedito et al., 2012). MAZ51 is an indolinone that was reported to inhibit the phosphorylation of VEGFR3 and therefore block its signaling, both in a ligand-dependent and independent manner (Benedito et al., 2012). This treatment also resulted in a dysmorphic AV valve leaflet, with a persistent expression of Alcam and the occurrence of Notch activity within abluminal AV cells (Figure 2.5A-F). Taken together, these three independent lines of evidence strongly suggest that signaling via Flt4 plays a role in AV valvulogenesis.

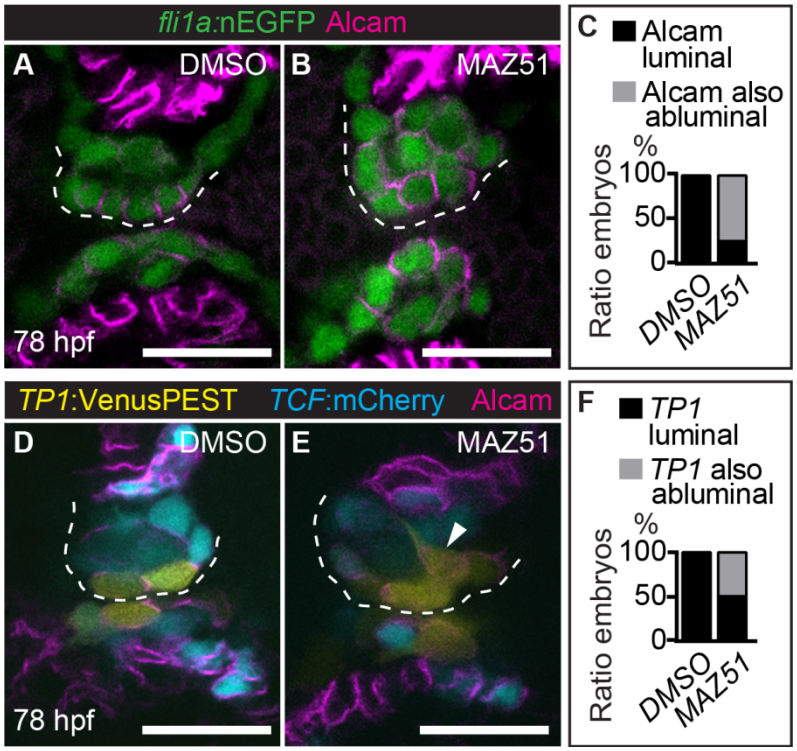

Figure 2.5: Flt4 signaling- inhibitor MAZ51 causes AV valve defects. (A-B) Single confocal z-section images of the AVC at 78 hpf. **(A)** In DMSO-treated embryos, *Tg(fli1a:nEGFP)*^{y7} marks EdCs cells and Alcam staining is present mainly at cell junctions of luminal EdCs. **(B)** In embryos treated with MAZ51 between 24-78 hpf to inhibit Flt4 signaling, Alcam is expressed also in abluminal positions. **(C)** Quantification of the ratio of embryos with an expression of Alcam in luminal EdCs versus embryos with Alcam expression also in abluminal EdCs (DMSO n=7, MAZ51 n=16). **(D-E)** Single confocal z-section images of the AVC region at 78 hpf. **(D)** In DMSO-treated embryos, luminal EdCs express the Notch reporter *Tg(TP1:VenusPEST)*^{s940}, while expression of the Wnt signaling reporter *Tg(7xTCF-Xla.Siam:nls-mCherry)*^{ia5} is in abluminal positions. **(E)** In embryos treated with the Flt4 signaling- inhibitor MAZ51, *Tg(TP1:VenusPEST)*^{s940}-positive EdCs are present also in abluminal positions (arrowheads). **(F)** Quantification of the ratio of embryos with an expression of *TP1*:Venus in

only luminal AV EdCs versus embryos expressing one *TP1*:Venus also within abluminal AV EdCs (DMSO n=5, MAZ51 n=10). Abl, Abluminal. Scale bars: (A, B, D, E) 20 µm. Adapted from (Fontana et al., 2020).

2.4. Flt4 acts within the AVC EdCs in a Vegfc-independent manner

During the formation of the lymphatic vessels, Flt4 plays an essential role mainly acting through its ligand Vascular endothelial growth factor C (Vegfc) (Jeltsch et al., 1997; Karkkainen et al., 2004; Küchler et al., 2006; Yaniv et al., 2006). Conversely, endothelial cell mechanotransduction has been associated with Vegfc-independent Flt4 activity (Baeyens et al., 2015). In order to verify whether Flt4 signaling at the AVC involves Vegfc-dependent signaling, I used a well-characterized *vegfc* MO (Ober et al., 2004) which produced the characteristic lymphatic defects at 54 hpf (Figure 2.6A,B). However, in contrast to the loss of Flt4, *vegfc* morphants did not exhibit any significant perturbations of Alcam expression or of Notch or Wnt/β-catenin signaling at the developing AV valve leaflets at 78 hpf. (Figure 2.6C-H). Thus, Vegfc is these dispensable for AV EdC mechanosensation. This finding suggests that Flt4 controls important signaling events during AV valve leaflet morphogenesis in a Vegfc-independent manner.

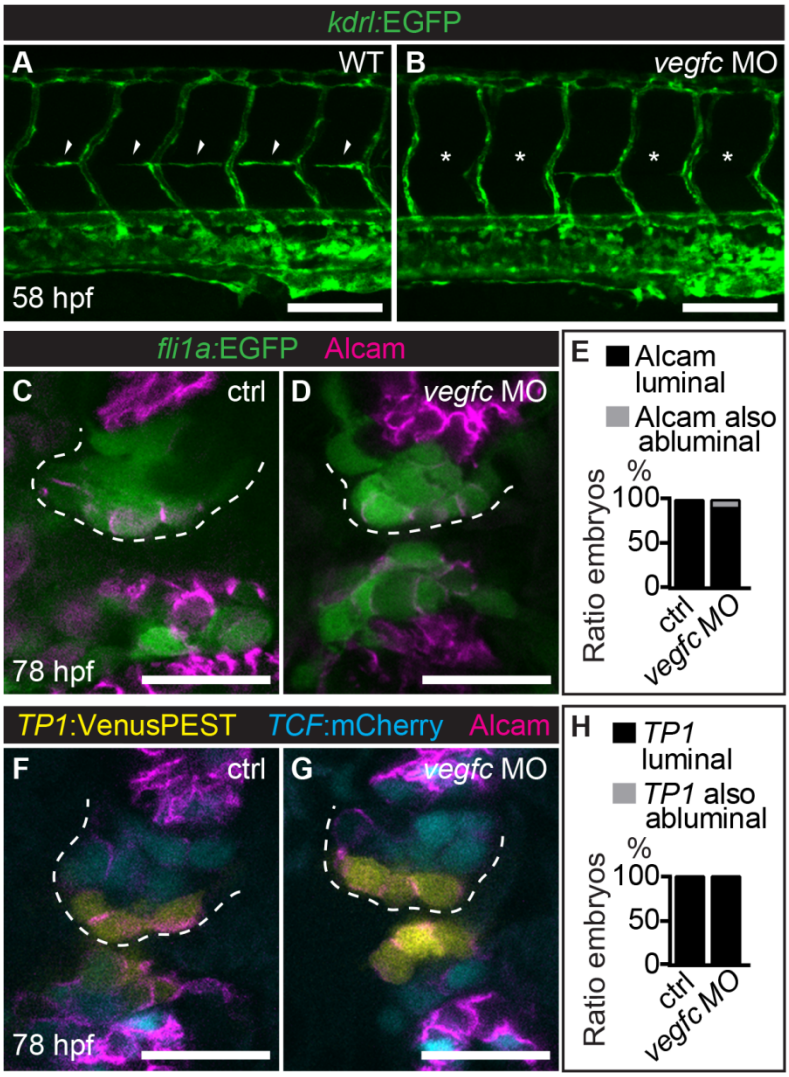

Figure 2.6: The Flt4 ligand Vegfc is dispensable for AV valve development. (A-B) Maximum intensity projections of confocal z-section images of trunk regions. At 58 hpf, parachordal lymphangioblast segments are present (A) in WT, while being absent (B) in *vegfc* morphant embryos. **(C-D)** Single confocal z-section images of the AVC at 78 hpf. **(C)** In control embryos, *Tg(fli1a:EGFP)*^{y1} marks EdCs cells and Alcam staining is present mainly at cell junctions of luminal EdCs. **(D)** In *vegfc* morphants, developing valve leaflets have a normal morphology and Alcam expression is present mostly within luminal EdCs. **(E)** Quantification of the ratio of embryos with an expression of Alcam in luminal EdCs versus embryos with Alcam expression also in abluminal EdCs (ctrl n=18, *vegfc* MO n=22). **(F-G)** Single confocal z-section images of the AVC region at 78 hpf. **(F)** In control embryos, luminal EdCs express the Notch reporter *Tg(TP1:VenusPEST)*^{s940}, while expression of the Wnt signaling reporter *Tg(7xTCF-Xla.Siam:nls-mCherry)*^{ia5} is in abluminal positions. **(G)** In *vegfc* morphants, expression of *Tg(TP1:VenusPEST)*^{s940} and *Tg(7xTCF-Xla.Siam:nls-mCherry)*^{ia5} is similar to WT. **(H)** Quantification of the ratio of embryos with an expression of *TP1*:Venus in only luminal AV EdCs versus embryos expressing *TP1*:Venus also within abluminal AV EdCs (ctrl n=17, *vegfc* MO n=14). Abl, Abluminal. Scale bars: (A-B) 100 µm; (C, D, F, G) 20 µm. Adapted from (Fontana et al., 2020).

2.5. Flt4 impacts mechanosensitive signaling within the endocardium

In order to better understand the molecular players implicated in Flt4 signaling at the AV endocardium, I extracted total RNA from purified 54 hpf cardiac tissue using a well-established protocol (Lombardo et al., 2015) of WT or *flt4* morphants. This was used for a comparative RNA-sequencing analysis that was performed at the Research Core Unit "Transcriptomics" of Hannover Medical School. After comparing the number of reads obtained for each gene and setting the adjusted P-value threshold to <0.05, 1187 genes were found downregulated and 1414 upregulated in *flt4* morphant hearts compared to WT. For biological pathway annotation of those differentially expressed genes, I used the Database for Annotation, Visualization and Integrated Discovery (DAVID) bioinformatics tool (Huang et al., 2009). The Kyoto Encyclopaedia of Genes and Genomes (KEGG), a biological pathways resource, identified 16 significantly downregulated pathways (including the p53 signaling pathway, glycolysis, cell cycle) and 16 significantly upregulated pathways (including p53 signaling pathway, tight junctions, focal adhesions, ECM-receptor interactions) (Table 2.1).
These findings indicate that proliferation and apoptosis events could be misregulated in *flt4* morphant hearts. Increase in endocardial cell number is dependent on blood flow-induced shear stress (Renz et al., 2015). Hence, misregulation of cell cycle-related genes suggests impairment in mechanosensitivity upon loss of Flt4. Within the endothelium, it has been reported that blood flow mediates cytoskeletal remodeling (le Noble et al., 2008). Mechanosensory integrins connect the endothelial cell to the ECM and induce cell proliferation by activation of the Focal Adhesion Kinase in response to shear stress (Renshaw et al., 1999; Zhao et al., 1998). An upregulation of adhesion-, junction- and ECM-related genes (including *actininα1*, *occludin a* and *b*, *claudin*-, *laminin*-, *collagen*-, *integrin*- family member genes) in *flt4* morphant hearts may be another indication for affected mechanotransduction processes.

Downregulated KEGG pathways	logFC	PValue
p53 signaling pathway	3.585	<0.001
Carbon metabolism	2.581	<0.001
Ribosome	2.408	<0.001
Oocyte meiosis	2.002	0.010
Biosynthesis of amino acids	2.333	0.012
Glycolysis / Gluconeogenesis	2.431	0.014
Phagosome	1.886	0.014
Glyoxylate and dicarboxylate metabolism	3.422	0.014
Butanoate metabolism	3.872	0.017
Cell cycle	1.871	0.022
Biosynthesis of antibiotics	1.593	0.029
Cardiac muscle contraction	2.017	0.034
Spliceosome	1.820	0.034
Alanine, aspartate and glutamate metabolism	2.824	0.034
Pentose phosphate	3.123	0.039
Pyruvate metabolism	2.627	0.047

Upregulated KEGG pathways	logFC	PValue
Ribosome biogenesis	2.895	<0.001
Aminoacyl-tRNA biosynthesis	2.997	<0.001
Cytosolic DNA-sensing	3.516	<0.001
p53 signaling	2.381	0.003
Tight junction	1.992	0.006
Protein processing in endoplasmic reticulum	1.705	0.007
Salmonella infection	2.024	0.008
RNA polymerase	3.152	0.011
Focal adhesion	1.521	0.015
NOD-like receptor signaling	2.381	0.021
ECM-receptor interaction	1.975	0.022
Glycosphingolipid biosynthesis	2.963	0.026
Apoptosis	1.981	0.028
RNA transport	1.601	0.031
Insulin resistance	1.632	0.040
Glycosaminoglycan biosynthesis	3.571	0.045

Table 2.1: KEGG pathway analyses of RNA-sequencing results. Ranking of (left side) downregulated and (right side) upregulated pathways by P values, from cardiac *flt4* MO mRNAs compared to WT.

Interestingly, blood-flow responsive genes including *notch1b* or *klf2a* were misregulated. The expression of *klf2a* is induced by blood flow within EdCs and is important for cardiac valve formation (Steed et al., 2016b; Vermot et al., 2009) and the control of EdC size (Dietrich et al., 2014). Within the heart, Klf2a was reported to regulate *notch1b* expression (Vermot et al., 2009). Strikingly, from *flt4* MO cardiac transcriptome analysis *klf2a* was significantly downregulated (log2= -1.695), while *notch1b* was upregulated (log2= 0.584). Hence, these data implied for the first time that the endocardial regulation of *notch1b* can be independent from Klf2a. To validate the RNA-seq analysis, I performed RT-qPCR analyses on cardiac tissue extracted from *flt4*^{hu4602} mutants versus WT at 54 hpf. Also in the *flt4*^{hu4602} mutants, *klf2a* mRNA levels were downregulated and *notch1b* mRNA levels were upregulated (Figure 2.7A). This suggests that the regulation of *klf2a* and *notch1b* mRNA expression levels is

independent within the endocardium. It also implies that the misregulation of *notch1b* expression upon loss of Flt4 is not simply induced by a possible alteration in the shear stress levels, since that would be expected to have a similar impact on *klf2a* levels as well. Also, heart rate analyses of *flt4*^{hu4602} mutants at 54 hpf indicated normal values (WT, n=10: 147 ± 4 heart beats/min; *flt4*^{hu4602} mutants, n=10: 146 ± 4 heart beats/min), suggesting that the misregulation of *klf2a* and *notch1b* is directly caused by the loss of Flt4. To assess the AVC-specific temporal expression pattern of *klf2a* upon loss of Flt4, I took advantage of the transgenic reporter line *TgBAC(klf2a:YFP)*^{mu107}, which permits visualizing expression from the *klf2a* genomic locus (Sugden et al., 2017), and analyzed its expression in *flt4* morphants. In tune with the *klf2a* downregulation detected by RT-qPCR, *klf2a*:YFP expression at the superior AVC was generally lower upon loss of Flt4 (Figure 2.7B,C). At 78 hpf, *klf2a:YFP* expression was particularly high within "heel cells" at the luminal side of the developing WT valve leaflets (Figure 2.7D), while this expression was lower in *flt4* morphants (Figure 2.7E).

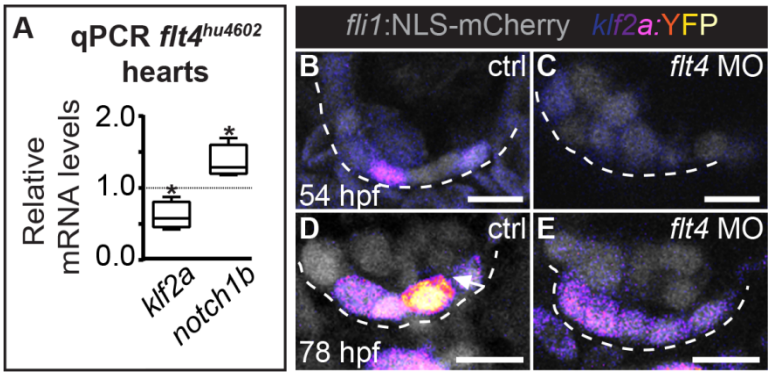

Figure 2.7: Loss of Flt4 impacts mechanosensitive *notch1b* and *klf2a* within the heart. (A) RT-qPCR quantifications of cardiac *notch1b* and *klf2a* mRNAs in *flt4*^{hu4602} mutants normalized to WT embryos. Min to max box and whisker plots are shown (n=4 independent experiments). Data were analyzed by ratio paired student's *t*-test (*p<0.05). **(B-E)** Single confocal z-section images of the superior AVC region. The *klf2a*:YFP signal is shown as FireLUT (ImageJ application) to highlight differences in fluorescence intensities (white=highest; black=no signal) **(B)** At 54 hpf, *Tg(klf2a:YFP)*^{mu107} is expressed within control EdCs at the AVC, **(C)** while expression is weaker in *flt4* morphants. **(D)** At 78 hpf, *Tg(klf2a:YFP)*^{mu107} expression is particularly high within "heel cells" at the luminal side of the developing valve leaflets in WT. **(E)** This expression is lower in the *flt4* morphant AVC region. Scale bars: (B-E) 10 µm. Adapted from (Fontana et al., 2020).

2.6. Klf2 suppresses *flt4* mRNA expression in a Notch-independent manner

My discovery that *flt4* mRNA levels are regulated by blood flow led me to investigate whether the shear stress-activated Klf2 has a role in this regulation. The loss of Klf2a induced by a genetic mutation has been associated with cardiac valve defects, although only with incomplete penetrance (Steed et al., 2016b). In zebrafish, the human *KLF2* gene has a second *kl2b* paralog. To overcome potential issues with genetic redundancy, I generated mutant alleles of *klf2b* using CRISPR/Cas9-mediated genome editing. In order to do that, a guide RNA was designed to target a sequence within the *klf2b* gene that transcribes for the transrepression domain. The injection of the *klf2b* gRNA together with *cas9* mRNA in one-cell stage embryos led to the identification, in the following generation, of three stable alleles. Two of these *klf2b* alleles resulted in nucleotide deletions (Δ1, *pbb42* and Δ7, *pbb43*) and one in a one nucleotide insertion (*pbb44*). All of these alleles are frame shift mutations encoding predicted premature protein deletions and truncated proteins containing only a small part of the transrepression domain and missing the zinc finger domains (Figure 2.8A). Nevertheless, homozygous *klf2b* mutants for each allele did not reveal any obvious morphological defects and reached adulthood. Next, I combined each of the three *klf2b* mutant alleles with the *klf2a*^{sh317} allele, which has been reported to have a normal vasculature and normal heart rate with expected blood flow velocities (Novodvorsky et al., 2015). Phenotypic analyses revealed similar phenotypes of all three *klf2a*^{sh317}*;klf2b* double mutant combinations and their overall embryonic morphologies appeared normal until 54 hpf when compared to WT (Figure 2.8B-G). Pericardial edema developed in *klf2* mutants by 78 hpf (Figure 2.8H-K). Given these findings, all further analyses were performed with the *klf2a*^{sh317}*; klf2b*^{pbb42} allele combination (hereafter referred to as *klf2* mutants).

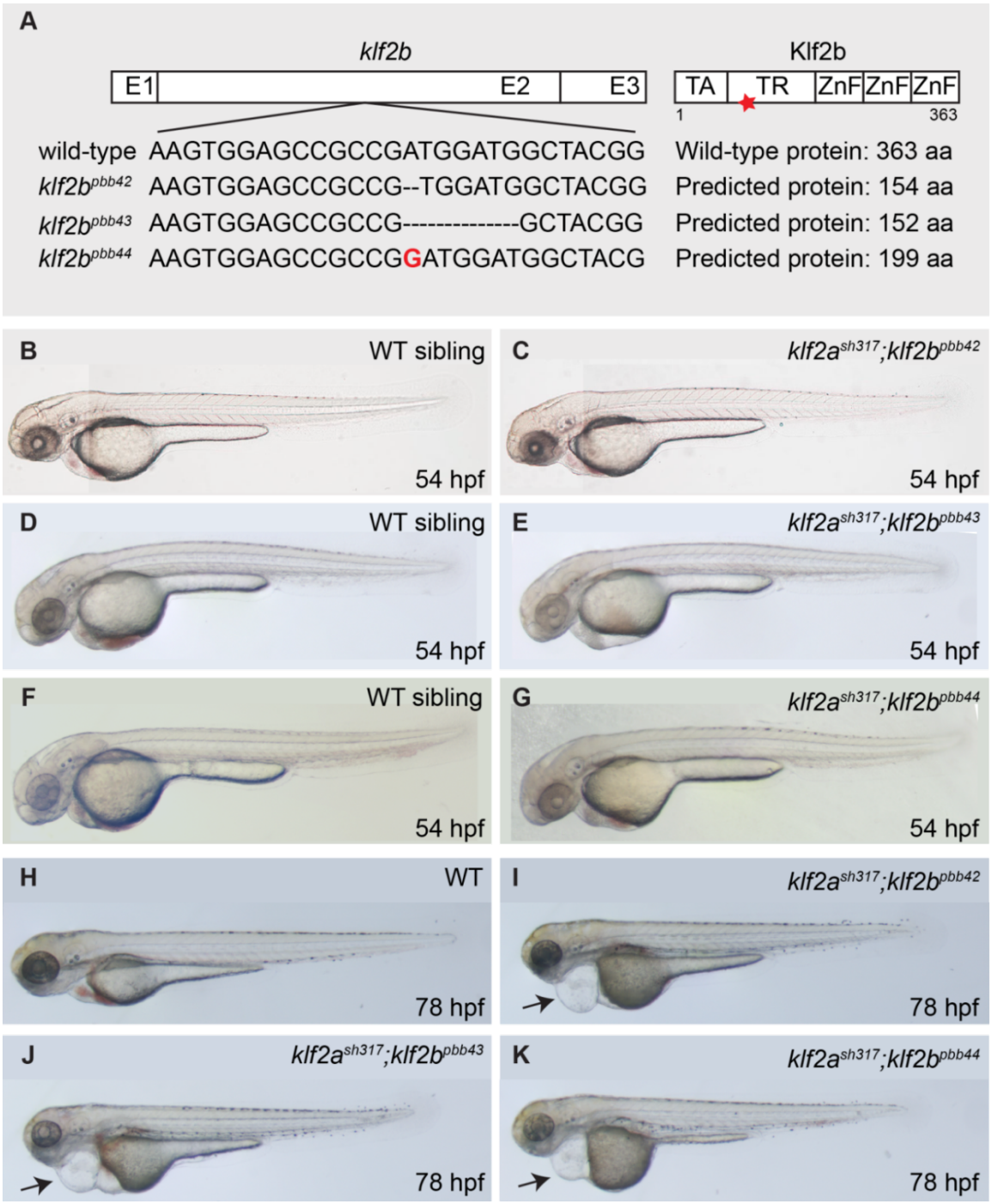

Figure 2.8: CRISPR/Cas9 mutagenesis-derived alleles of *klf2b* and *klf2* double mutants. (A) Shown is the nucleotide sequence (left side) and predicted protein structure (right side) encoded by the *klf2b* alleles generated by CRISPR/Cas9 mutagenesis. Two *klf2b* alleles carry nucleotide deletions (*klf2b*^{pbb42} with a one base pair deletion and *klf2b*^{pbb43} with seven-base pair deletion), while one *klf2b* allele carries a one nucleotide insertion (in red, *klf2b*^{pbb44}). All three alleles result in a frameshift and premature stop codons within the region encoding the transrepression domain (TR, the star indicating mutation sites). Therefore, all predicted truncated proteins contain only a small part of the transrepression domain and lack the zinc finger domains (ZnF). **(B-K)** Lateral views of zebrafish embryos. **(B, D, F)** Wild-type (WT), **(C)** *klf2a*^{sh317}*; klf2b*^{pbb42}, **(E)** *klf2a*^{sh317}*; klf2b*^{pbb43} or **(G)** *klf2a*^{sh317}*; klf2b*^{pbb44} embryos at 54 hpf present a similar morphology. **(H)** WT embryos at 78 hpf appear normal, while **(I-K)** all *klf2* mutant combinations present pericardial edema (arrow). **(A-C)** Adapted from (Fontana et al., 2020).

At 54 hpf, *klf2* mutants showed normal blood flow and EdCs at the AVC expressed Alcam in a WT pattern. However, the tissue was mono-layered and EdCs apparently failed to ingress into the cardiac jelly (Figure 2.9A, B). By 78 hpf, *klf2* mutants had impaired atrioventricular valve leaflets due to a mono-layered organization of EdCs (n=14/25 embryos) or due to a partial infolding of AVC endocardium (n=11/25) (Figure 2.9C, D). This finding was in tune with previous observations (Rasouli et al., 2018).

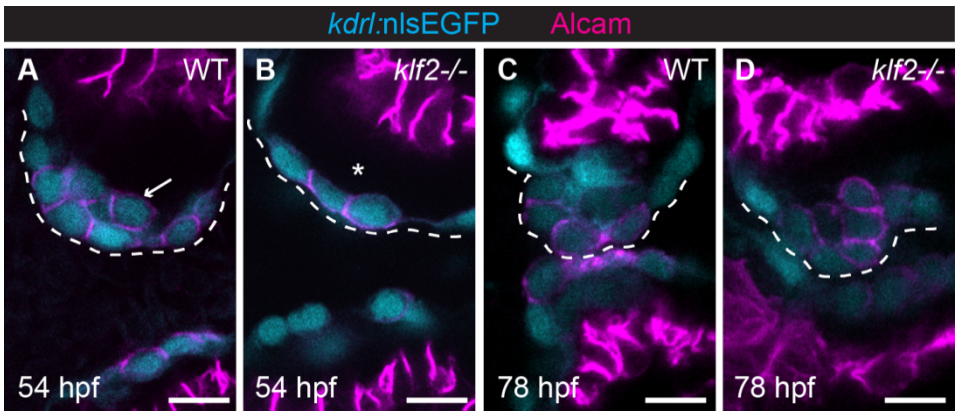

Figure 2.9: Loss of Klf2 impacts AV valve development. (A-D) Single confocal z-section images of the AVC region. **(A)** In 54 hpf wild-type (WT) embryos, *Tg(kdrl:nlsEGFP)*^{ubs1} expression marks EdCs, a few AV EdCs have migrated into the cardiac jelly (arrow) and Alcam staining labels AVC EdC junctions. **(B)** *klf2* mutants properly express Alcam in AVC EdCs, but cells fail to invade the cardiac jelly (asterisk). **(C)** At 78 hpf, the WT AVC region has developed into an S-shaped multi-layered structure and junctional Alcam is present only within EdCs in luminal positions. **(D)** In *klf2* mutants, the AV valvular region is abnormally altered and Alcam is expressed also in abluminal positions. Scale bars: 20 µm. Adapted from (Fontana et al., 2020).

To investigate whether a loss of Klf2 affects the cardiac expression of *flt4* mRNA, I extracted *klf2* mutant or WT hearts at 54 hpf and compared *flt4* mRNA levels by RT-qPCRs. Although *klf2* mutants are exposed to normal blood flow at 54 hpf, the expression of *flt4* mRNA was upregulated in *klf2* mutant hearts (Figure 2.10A). To check how *flt4* expression was altered at the AVC, I crossed the *Tg(flt4BAC:mCitrine)*^{hu7135} reporter line into the *klf2* mutant background. At 56 hpf, *flt4BAC:mCitrine* fluorescence intensity, enhanced by anti-GFP immunohistochemistry, was increased at the superior AVC in *klf2* mutants compared to WT (Figure 2.10B-D). This suggests a possible role of Klf2a/b in mediating the blood flow-dependent downregulation of *flt4* mRNA expression.

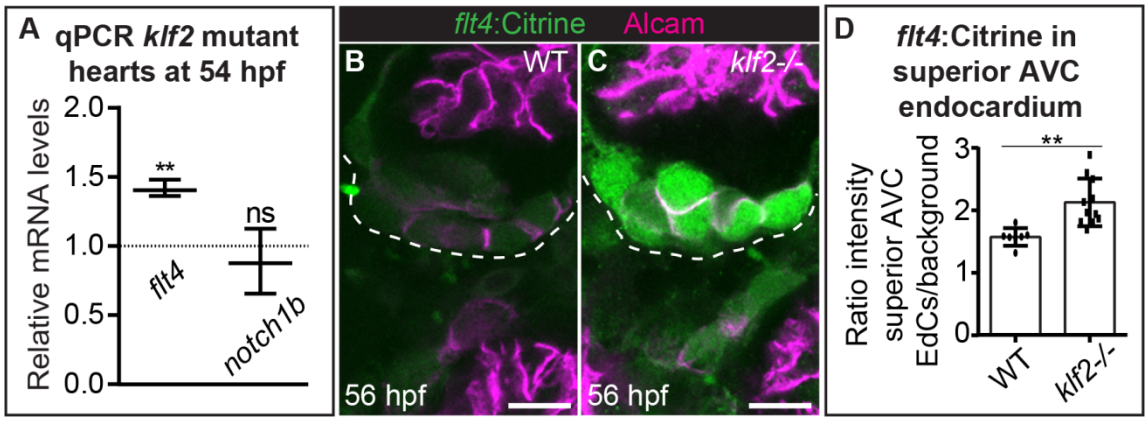

Figure 2.10: Loss of Klf2 increases *flt4* mRNA cardiac expression. (A) RT-qPCR quantifications of *flt4* and *notch1b* mRNA levels in 54 hpf *klf2* mutant cardiac tissue normalized to WT. Min to max box and whisker plots are shown (n=3 independent experiments). Data were analyzed by ratio paired student's *t*-test (**p<0.01). (F-G) Single confocal z-section images of the AVC region. **(B, C)** Single confocal z-section images of the AVC region. **(B)** Immunohistochemical labeling of green fluorescent protein in *Tg(flt4BAC:mCitrine)*^{hu7135} embryos reveals lower expression in the superior AVC region of WT embryos at 56 hpf, **(C)** compared to *klf2* mutants. **(D)** Quantification of the ratio intensities of *flt4*:Citrine expressing EdCs within the superior AVC relative to background levels (WT, n=7 embryos, *klf2*, n=11 embryos). Mean values ± SD are shown and data were analyzed by unpaired student's *t*-test (**p<0.01). Scale bars: 20 µm. Adapted from (Fontana et al., 2020).

To further investigate the link between Klf2 and Notch1 in the endocardium, I tested the expression of *notch1b* in *klf2* mutant hearts at 54 hpf. RT-qPCRs revealed that *notch1b* mRNA levels were not statistically changed in *klf2* mutant compared to WT hearts (Figure 2.10A). This finding was also in support with my observation that *klf2* mutants had normal blood flow, which induces the expression of *notch1b.* To investigate whether the spatial distribution of Notch activity was affected in *klf2* mutant hearts, I introduced the Notch reporter transgene *Tg(TP1:VenusPEST)*^{s940} into the *klf2* mutant background. In tune with my previous observations, between 58-74 hpf, EdCs exhibited an abnormal mono-layered arrangement (Figure 2.11A-D). Nevertheless, Notch activity persisted at the AVC of *klf2* mutants (Figure 2.11B, D). These findings suggest that Notch activity at the AVC is independent of Klf2 but that the ingression of AVC EdCs is dependent on Klf2.

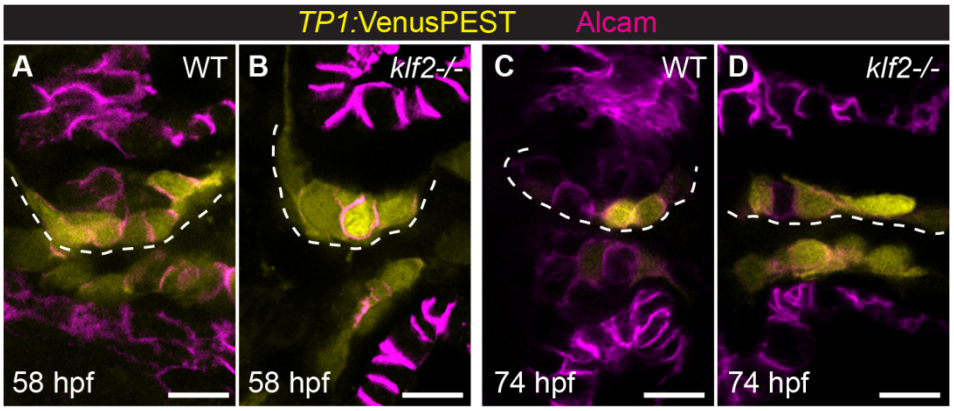

Figure 2.11: Notch activity at the AVC is independent of Klf2. (A-D) Single confocal z-section images of the AVC region. **(A)** At 58 hpf, some WT AVC EdCs have formed the abluminal side of the developing superior valve leaflet. The Notch reporter *Tg(TP1:VenusPEST)*^{s940} is strongly expressed within luminal EdCs. **(B)** In *klf2* mutants, AVC EdCs express *Tg(TP1:VenusPEST)*^{s940} and EdCs do not protrude towards the cardiac jelly. **(C)** At 74 hpf, *Tg(TP1:VenusPEST)*^{s940} expression in WT is particularly strong within "heel cells" at the luminal side. **(D)** In *klf2* mutants, *Tg(TP1:VenusPEST)*^{s940} is expressed but EdCs in the AVC region are in a mono-layered arrangement. Scale bars: 20 μm. Adapted from (Fontana et al., 2020).

2.7. Notch signaling suppresses *flt4* mRNA expression in a Klf2 -independent manner

The above findings suggested that Klf2 regulates the endocardial expression of *flt4*, in a Notch-independent manner. Since both *klf2a* and *notch1b* are flow-sensitive genes and have a similar endocardial expression, next I addressed whether also Notch played a role in regulating the expression of cardiac *flt4* mRNA. To test this, I inhibited the processing and activity of Notch, by incubation with the γ-secretase inhibitor RO4929097 (RO) between 52-78 hpf (Huynh et al., 2011; Munch et al., 2013). RO-treated fish had blood flow at 78 hpf, although the hearts were not properly ballooned (Figure 2.12A, B). As previously reported (Timmerman et al., 2004), Notch inhibition prevented a normal AV valve development and AV EdCs appeared in a monolayer or the AVC endocardium was only partially folded, when compared to the multilayered valve structure in WT embryos (Figure 2.12A', B'). At 78 hpf, I extracted cardiac mRNA from RO treated- versus DMSO-treated embryos and performed RT-qPCRs analyses. This analysis revealed that levels of *flt4* mRNA were upregulated in Notch-inhibited hearts. Conversely, RO treatment did not significantly affect *klf2a* mRNA levels (Figure 2.12C). The efficiency of RO-mediated Notch inhibition was validated by the

abolishment of the TP1 signal in *Tg(TP1:VenusPEST)*^{s940} embryos treated between 52-78 hpf (Figure 2.12D, E).

In a complementary approach, I tested the impact of an endothelial and endocardial-specific overactivation of Notch signaling on *flt4* mRNA levels. To do that, I crossed the transgenic lines *Tg(fli1a:Gal4FF)*^{ubs3}*;Tg(5xUAS-E1b:6xMYC-notch1a-intra)*^{kca3} obtaining embryos expressing NICD under the endothelial *fli1a* promoter. The efficiency of the Notch overexpression was assessed based on the upregulation of the *Tg(TP1:VenusPEST)*^{s940} reporter line expression (Figure 2.12D, F). These embryos were used for cardiac RNA extractions at 78 hpf. Next, I performed RT-qPCR analyses to assess the levels of *flt4* mRNA expression in these hearts, and found that its levels were significantly downregulated in NICD-overexpressing hearts compared to WT siblings (Figure 2.12C). Interestingly, the same analysis on *klf2a* mRNA levels indicated a downregulation in NICD-overexpressing hearts. While blood flow circulation was visible in these fish by visual inspection, I cannot rule out that a change in the heart shape had influenced the blood flow rate and, consequently, *klf2a* levels. Further experiments would be required to verify whether *klf2a* downregulation in NICD-overexpressing hearts is directly mediated by Notch signaling. Regarding the regulation of *flt4*, I can rule out that the downregulation of *flt4* mRNA in NICD-overexpressing hearts is mediated by the downregulation of *klf2a*, since I had found that *flt4* levels are increased in *klf2* mutants. Hence, the suppressive effects of Notch signaling on Flt4 are Klf2a-independent.

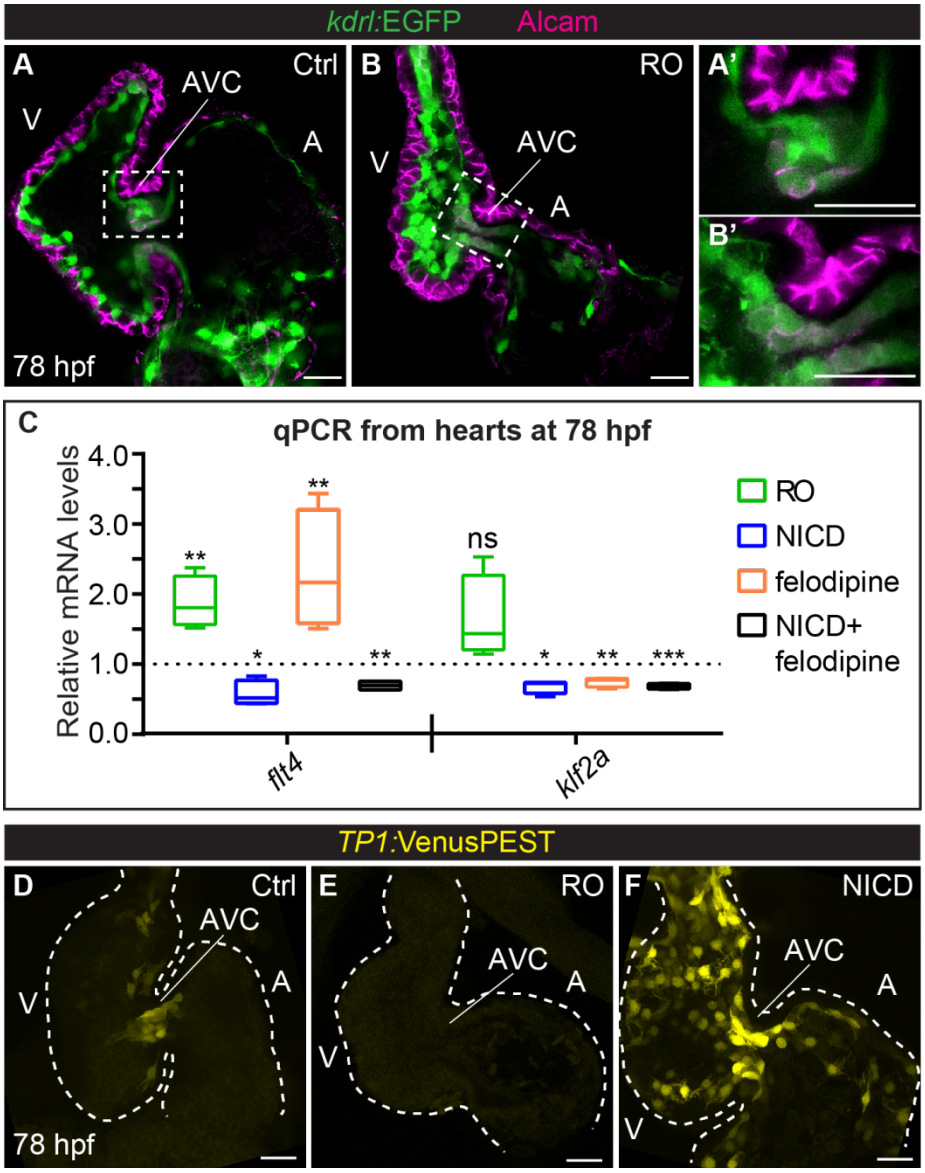

Figure 2.12: Notch levels impact *flt4* expression within the heart. (A-B) Single confocal z-section images of 78 hpf hearts. **(A)** While wild-type (WT) heart is ballooned and **(A')** AV superior valve is multi-layered structured, **(B)** RO-treated heart is less ballooned and **(B')** AV superior valve is only partially folded. **(C)** RT-qPCR quantifications of cardiac *flt4* and *klf2a* mRNA levels from embryos treated with the Notch signaling inhibitor RO (between 52-78 hpf,), embryos with an endothelial-specific overactivation of Notch signaling (NICD) [*Tg(fli1a:Gal4FF)*^{ubs3}*;Tg(5xUAS-E1b:6xMYC-notch1a intra)*^{kca3}], embryos treated with felodipine to stop the heart beat (between 72-78 hpf), or *Tg(fli1a:Gal4FF)*^{ubs3}*;Tg(5xUAS-E1b:6xMYC-notch1a intra)*^{kca3} embryos treated with felodipine between 72-78 hpf (NICD+felodipine), each normalized to DMSO-treated sibling fish (n=4 independent replicates). Min to max box and whisker plots are shown. Data were analyzed by ratio paired student's *t*-test (*p<0.05; **p<0.01; **p<0.005; ns, not significant). Adapted from (Fontana et al., 2020). **(D-F)** Maximum intensity projections based on confocal z-stack images of 78 hpf hearts. **(D)** In WT heart, the Notch reporter *Tg(TP1:VenusPEST)*^{s940} is expressed mainly at the AVC region and weakly in the ventricle. **(E)** In RO-treated heart, *TP1:VenusPEST* expression is abolished. **(F)** In endocardially NICD-overexpressing heart, *TP1:VenusPEST* signal is increased and present in both endocardial chambers. V, ventricle; A, atrium; AVC, atrioventricular canal. Scale bars: 20 µm.

2.8. Notch signaling mediates the blood flow impact on *flt4* mRNA expression

My observations indicated that *flt4* mRNA levels are negatively regulated by blood flow and by Notch activity. Also, levels of Notch activity are contingent to the strength of blood flow. Therefore, I next tested whether Notch activity mediates the effect of blood flow on *flt4* expression. To assess this possibility, I analyzed how *flt4* mRNA levels change in conditions of overexpressing Notch signaling in the absence of blood flow. When treating *Tg(fli1a:Gal4FF)^{ubs3};Tg(5xUAS-E1b:6xMYC-notch1a intra)^{kca3}* embryos with felodipine between 72-78 hpf, to also block cardiac contraction, cardiac *flt4* mRNA levels decreased in NICD-overexpressing embryos, when compared to DMSO-treated control embryos and to embryos lacking blood flow (Figure 2.12C). These data suggest that the upregulation of *flt4* mRNA levels under no-blood flow conditions can be suppressed by Notch activity.

In comparison, *klf2a* mRNA expression levels were reduced upon both loss of blood flow and Notch signaling overexpression (Figure 2.12C). Since my previous findings indicated an upregulation of *flt4* levels upon loss of Klf2, the concurrent downregulating effects of Notch activity on *flt4* and *klf2a* mRNA expression indicate that suppressive role of Notch signaling on Flt4 does not involve Klf2a in the same pathway.

2.9. Notch activity is dependent on mechanical forces, in a Flt4-independent manner

My data suggest that Flt4 has a repressive effect on Notch activity and *notch1b* mRNA levels. Thus, I next wondered whether the downregulation of Notch activity which occurs in the absence of blood flow was mediated by an upregulation of Flt4 levels. This led me to test whether Notch activity would be restored in no- blood flow conditions when Flt4 signaling was also knocked out. To this end, I injected *tnnt2a* MO into *flt4^{hu4602}* mutant embryos, obtaining embryos that lack Flt4 signaling and have no cardiac contractility, and found that those embryos exhibited no expression from the *Tg(TP1:VenusPEST)^{s940}* Notch activity reporter (Figure 2.13C, D). This suggests that blood flow is necessary for Notch activation in a manner that is independent of Flt4.

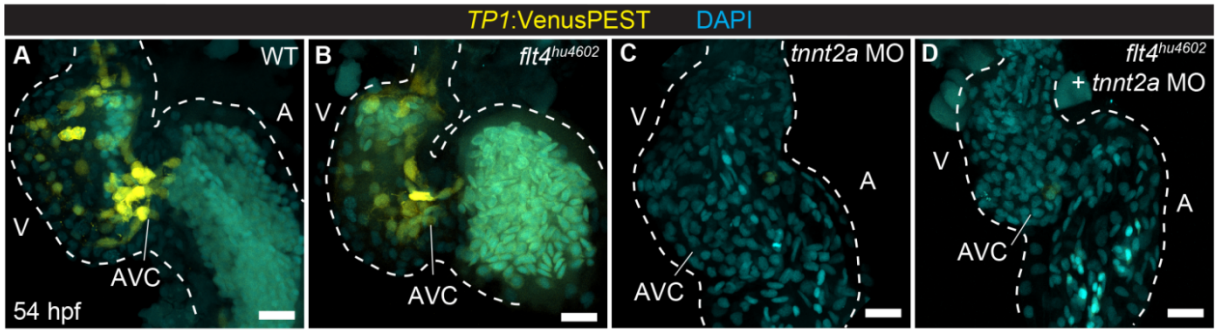

Figure 2.13: Notch activation requires blood flow in a Flt4 independent-manner. (A-D) Maximum intensity projections of confocal z-stack images of 54 hpf hearts. **(A)** The Notch reporter *Tg(TP1:VenusPEST)*^{s940} is expressed in wild-type (WT) and **(B)** in *flt4*^{hu4602} ventricular and AVC endocardium. **(C)** Notch activity is abolished in *tnnt2a* morphant hearts lacking blood flow. **(D)** The loss of Flt4 in *flt4*^{hu4602} does not restore *Tg(TP1:VenusPEST)*^{s940} expression in embryos lacking blood flow due to injection of *tnnt2a* MO. N=3 embryos/condition. V, ventricle; A, atrium; AVC, atrioventricular canal. Scale bars: 20 µm. Adapted from (Fontana et al., 2020).

This finding raised the question of how Flt4 expressing cells and Notch activated cells interact within AV valve leaflets. I had observed that in *flt4*^{hu4602} mutants, Notch activity occurred in abluminal positions where EdCs are not exposed to blood flow (Figure 2.14B, 2.3H). To directly test with a high temporal resolution the effects of blood flow on the Notch reporter in *flt4*^{hu4602} mutant abluminal AV EdCs, I treated *flt4*^{hu4602} mutants between 72-78 hpf with felodipine and stopped cardiac contraction. This short temporal inhibition of blood flow caused a decreased Notch activity, both in *flt4*^{hu4602} mutant and WT background (Figure 2.14C, D). Strikingly, Notch activity was not observed in felodipine-treated *flt4*^{hu4602} mutant abluminal AV EdCs (Figure 2.14D). This suggests that Notch activity within abluminal *flt4*^{hu4602} mutant AV EdCs is dependent on blood flow between 72-78 hpf (period of felodipine treatment). In tune with this finding, the cardiac *notch1b* mRNA upregulation mediated by the lack of Flt4 signaling was suppressed in *flt4*^{hu4602} mutants lacking blood flow. Expression of *klf2a* mRNA, which was found downregulated in *flt4*^{hu4602} mutants, was similarly downregulated in fish lacking both Flt4 and blood flow (Figure 2.14E). In summary, these data showed that while blood flow activates both Klf2 and Notch1b expression, they respond to the stimulus independently of each other and negatively affect *flt4* mRNA expression within the heart.

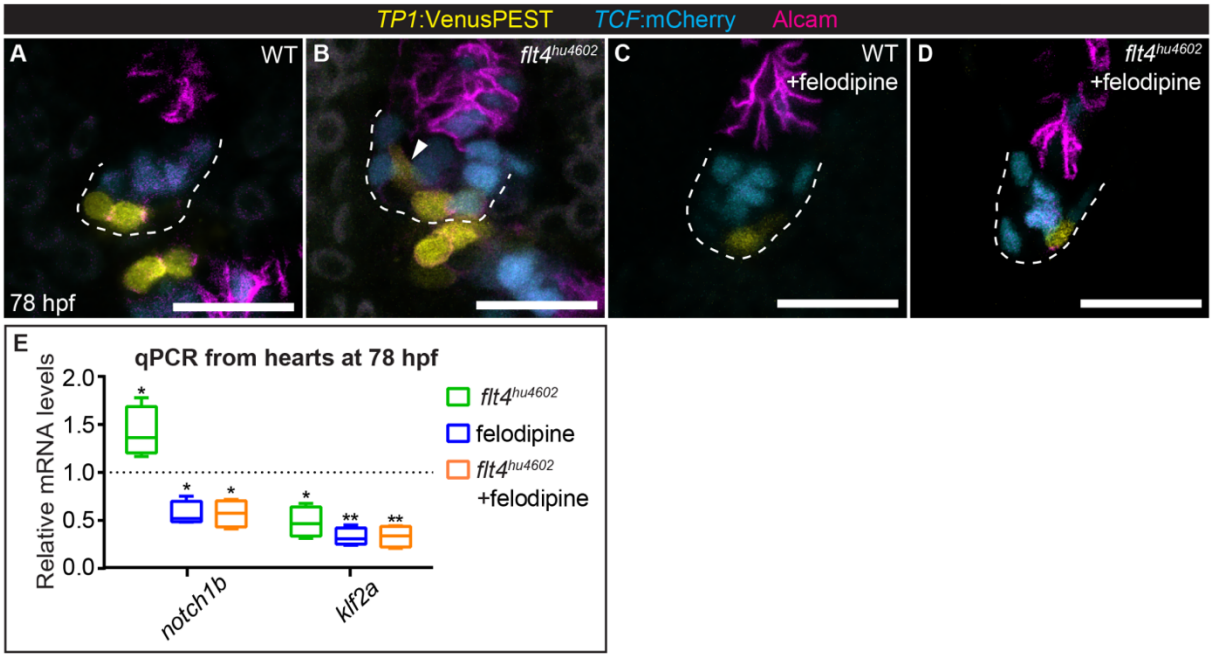

Figure 2.14: Abluminal Notch activity upon loss of Flt4 is blood flow dependent. (A-D) Single confocal z-section images of the superior AV valve leaflet at 78 hpf, expressing the Notch reporter *Tg(TP1:VenusPEST)*^{s940} and the Wnt reporter *Tg(7xTCF-Xla.Siam:nls-mCherry)*^{ia5}, counter-stained against Alcam. **(A)** In WT, Notch signaling is active in luminal EdC "heel cells", while Wnt signaling marks abluminal EdCs (n=4/4 embryos). **(B)** In *flt4*^{hu4602} mutants, Notch-expressing EdCs are also present in abluminal positions (arrowhead, n=3/10 embryos). **(C)** Treatment with felodipine to stop the heart beat between 72-78 hpf in the WT decreases the expression of Notch reporter in luminal EdCs (n=7/7 embryos). **(D)** *flt4*^{hu4602} mutants treated with felodipine have a decreased expression of Notch signaling in luminal EdCs and Notch activity is absent from abluminal EdCs (n=10/10 embryos). **(E)** RT-qPCR quantifications of cardiac *notch1b* and *klf2a* mRNA levels at 78 hpf from *flt4*^{hu4602} mutants, from embryos treated with felodipine to stop the heart beat (between 72-78 hpf) or from *flt4*^{hu4602} mutants treated with felodipine between 72-78 hpf, each normalized against DMSO-treated embryos (n=4 independent replicates). Min to max box and whisker plots are shown. Data were analyzed by ratio paired student's *t*-test (*p<0.05; **p<0.01). Scale bars: 20 µm. Adapted from (Fontana et al., 2020).

3. Discussion

The morphogenesis of cardiac valve leaflets in the zebrafish embryo involves the remodeling of EdCs at the AVC from a single layer of cells into a multi-layered structure. This process leads to the formation of two subpopulations of EdCs that are on luminal and abluminal sides of the valve leaflet. EdCs on the abluminal side of the valve leaflet are not exposed to fluid shear stress. This remodeling is sensitive and dependent on biomechanical stimuli by blood flow. Several molecular pathways become activated by fluid shear stress. However, much less is known about molecular signaling within EdCs that lack the exposure to shear stress. It has been suggested that during mammalian valvulogenesis, these cells undergo a process of EndoMT and start to express genes related to a mesenchymal cell fate. In tune with this notion, during zebrafish valvulogenesis, EdCs downregulate the expression of junctional proteins, including Alcam and VE-Cadherin. However, in contrasts to mammalian valvulogenesis, these cells remain connected and form a coherent sheet-like structure (Gunawan et al., 2019; Scherz et al., 2008). These observations have raised great interest in the molecular events that occur within abluminal EdCs. In my work, I discovered that valve leaflet morphogenesis requires not only the activation of high-shear stress programs in EdCs on the luminal side, but also the downregulation of programs characteristic of no-shear stress regions, and that both effects are dependent on blood flow. The expression of the angiogenesis receptor Flt4 is suppressed by blood flow in a manner that is dependent on Notch and Klf2a. Consequently, Flt4 is mainly expressed among AV abluminal EdCs, which are not exposed to shear stress. The lack of shear stress within these EdCs is apparent also by the lack of known flow-induced proteins, including Notch1b and Klf2a. In functional studies, I found that Flt4 plays an important role in shaping of the abluminal region of the developing zebrafish AV valve leaflet. Flt4 also antagonizes the presence of Notch activity within abluminal AV EdCs and of Wnt activity within luminal AV EdCs (Figure 3.1).

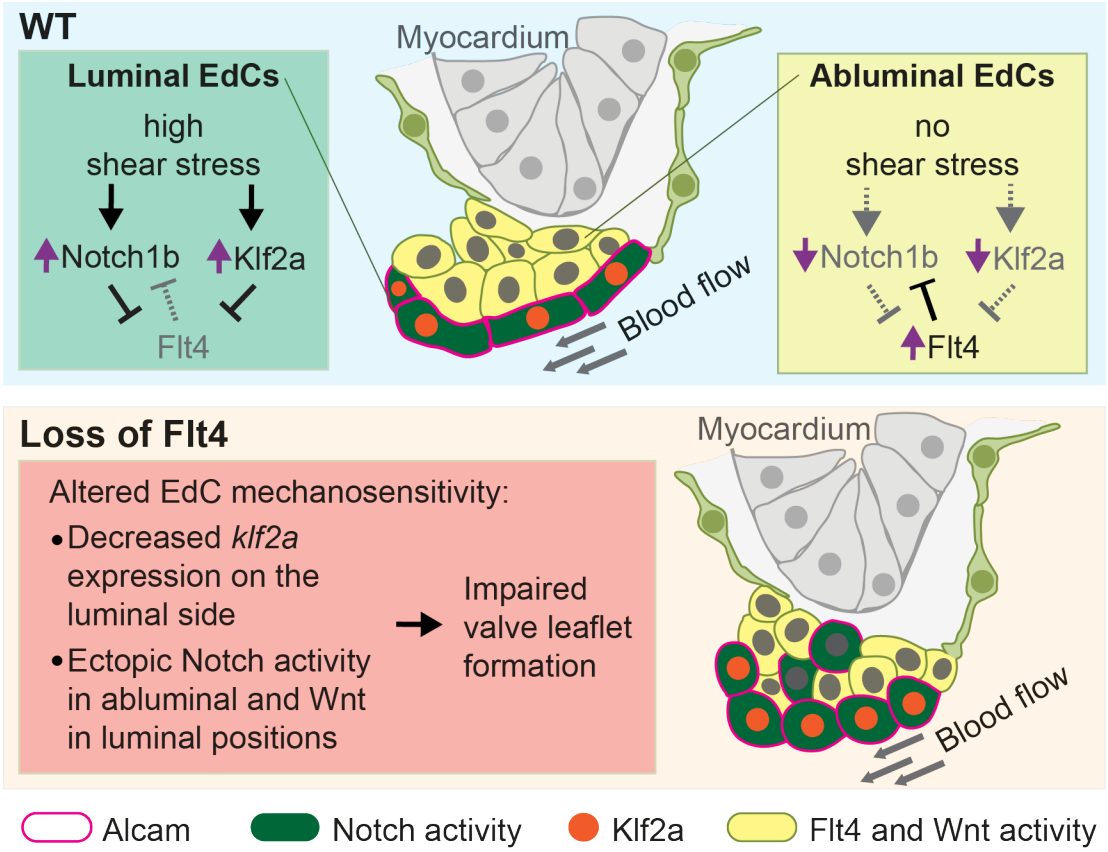

Figure 3.1: Model of molecular pathways involved in zebrafish atrioventricular valve development. At 78 hpf, wild-type (WT) AV EdCs are organized in an S-shaped multi-layered structure. Biomechanical stimuli induced by blood flow activate two independent pathways, which activate Notch signaling and Klf2a activity within luminal cells. Both pathways negatively regulate Flt4, which is expressed only within abluminal EdCs. Upon loss of Flt4, valve morphogenesis is disrupted and the AV luminal EdC junctional marker Alcam and Notch signaling are present also within EdCs in abluminal positions, while Wnt/β-catenin is ectopically active within luminal EdCs. Their ectopic expression patterns contribute to disrupted valve morphogenesis.

3.1. Fluid shear stress positively regulates the endocardial expression of *notch1b* and *flt1*, while downregulating *flt4*

The development of cardiac valve leaflets initiates when a single layer of EdCs at the AVC remodels into a multilayered structure composed by a luminal and an abluminal cell population. Previous studies demonstrated that this process is influenced by biomechanical stimuli triggered by blood flow (Beis et al., 2005; Hove et al., 2003; Vermot et al., 2009). In spite of the great importance of fluid shear stress for the maturation of endocardium, we are far from a comprehensive understanding of the molecular signaling events involved in mechanotransduction in this tissue. During my work, I analyzed transcriptome data that my colleague Dr. Timm Haack had generated, to compare which genes are highly expressed in

beating versus non-beating zebrafish hearts. As a model system, zebrafish embryos are particularly well-suited for blood flow-manipulation studies, since they can survive without a functional heart up to 7 days post fertilization (Sehnert et al., 2002). For this analysis, heart contractility was impaired by knocking down the sarcomeric protein Tnnt2a which is essential for cardiac contractility and blood flow. Hence, the endocardium in *tnnt2a* morphants lacked exposure to fluid shear stress and was used to screen for flow-regulated genes. We found that Notch signaling, and in particular the receptor Notch1b, are downregulated under no-flow conditions, which was in tune with previous studies (Samsa et al., 2015). This analysis also revealed that some members of the angiogenesis VEGF receptor family are regulated by blood flow. Similar with *notch1b*, *flt1*/*vegfr1* was downregulated in the absence of blood flow whereas *flt4/vegfr3* was upregulated. The levels of the other genes encoding VEGFRs (*kdrl*/*vegfr2* and *kdr*) did not change in response to a lack of blood flow. The roles of VEGFRs have been well-characterized for their roles in angiogenesis and vasculogenesis within ECs (reviewed in (Simons et al., 2016)). In human umbilical vein endothelial cells (HUVECs), VEGFR2 expression increased when exposed to arterial shear stress (Paz et al., 2012), indicating a role in mediating fluid shear stress response. More importantly, the junctional mechanosensitive Pecam-1/VE-cadherin/Vegfr2/Vegfr3 complex is essential for sensing and transducing fluid shear stress *in vitro* and *in vivo* within ECs (Coon et al., 2015; Tzima et al., 2005). In particular, it has been reported that the different levels of Flt4 in different endothelial tissues are crucial to set the level of fluid shear stress to which the cells will respond (Baeyens et al., 2015). This concept, known as fluid shear stress set point, is based on the observation that, while relative changes in fluid shear stress levels induce a similar response in arterial, venous or lymphatic cells, the absolute value of shear stress to which cells respond is different for each type of EC. The higher the levels of Flt4, the lower the levels of shear stress needed to induce cell remodeling. In tune with it, lymphatic cells upregulate Flt4 expression and respond to low levels of fluid shear stress. Instead, arterial cells are exposed to high levels of shear stress and express low levels of Flt4. Hence, Flt4 appear to control the sensitivity to shear stress within the different vascular beds (Baeyens et al., 2015).

Currently, there is no evidence for a mechanosensitive role of Flt1 or Kdr within ECs or the endocardium, nor it is clear whether they are integrated in pathways downstream the flow-responsive Klf2 or Notch signaling. While ECs and EdCs share fundamental characteristics, they differ in developmental origin, molecular expression profile, cell shape, cytoskeletal organization, and permeability (Brutsaert and Andries, 1992). Thus, specific studies on

mechanosensitive signal transduction pathways within EdCs are of great importance. The no-flow transcriptome analysis was based on 54 hpf cardiac tissue in which the lack of blood flow prevented the initiation of AV EdC remodeling. At 54 hpf, flow-responsive genes including *notch1b* or *klf2a* are expressed strongly at the AVC. Hence, the misregulated genes from this RNA-seq analysis were good candidates with a potential role during valvulogenesis. When I performed a control experiment, by pharmacologically inhibiting blood flow between 72 and 78 hpf, I found that *notch1b* was downregulated and that *flt4* was upregulated which suggested that the mechanisms involved in the endocardial response to blood flow are fine-tuned with high temporal resolution. One limitation of these RNA-seq analyses is that mRNAs were extracted from whole hearts, therefore comprising both myocardium and endocardium. Also, this approach did not separate different regions of the endocardium, leading to a lack of spatial resolution and to a lower detectability of changes in the levels of genes expressed in small regions. Nevertheless, I focused on genes known to have an endocardial expression and with a strong expression at the AVC under WT conditions. Also, I analyzed promoter-specific transgenic reporter lines, to be able to visualize gene expression changes within the heart. Another limitation of our approach is that, in order to block fluid shear stress, cardiac contractility was inhibited. The contraction of cardiomyocytes induces a mechanical stress within EdCs and, therefore, changes in endocardial genes expression levels may derive also from a lack of stretching forces. Uncoupling cardiac contractility and blood flow has been difficult to achieve in functional studies. Different strategies have been adopted to address this question. Hove and colleagues surgically positioned beads in the zebrafish heart to obstruct blood flow but not contractility, and found that valve development was impaired (Hove et al., 2003). However, this invasive approach resulted in other disturbed aspects of cardiogenesis, including a reduced bulbus formation, a lack of heart looping, a collapse of the lateral walls of the sinus and outflow tract and the formation of pericardial edema. All these defects made it difficult to distinguish primary from secondary effects. Bartman and colleagues performed a series of dose-increasing pharmacological inhibition experiments to reduce cardiac contractility, showing that embryos with an impaired heart beat but a blood flow circulation develop affected valves (Bartman et al., 2004). However, lowering myocardial contractility intrinsically also alters blood flow dynamics, which can lead to valve defects. Vermot and colleagues used the sodium channel blocker lidocaine to decrease the heart rate of zebrafish embryos by 30%. This resulted in a range of valve defects (Vermot et al., 2009). Similar defects were observed in fish exposed to higher temperature (by 2-4°C), which increases the heart rate. The authors also studied the impact of blood viscosity

on valvulogenesis. They found that a reduction of blood viscosity by *gata1/2* knockdown (while maintaining a normal heart rate) affected valve morphogenesis. Altogether, these data argued in favor of a critical role of fluid shear stress for valve development independently of myocardial contractility. Similarly, Kalogirou and colleagues showed that mutants with long-term disturbances in intracardiac flow dynamics, but not heart rate, have defective AV valves (Kalogirou et al., 2014). Hence, most of the studies indicate a direct effect of blood flow on valvulogenesis. To further prove a direct role of fluid shear stress, *in vitro* experiments with controlled alterations of shear stress can be useful to assess whether gene expression is regulated by it. During my work, I collaborated with Dr. Maria Reichenbach (Freie Universität Berlin) to assess levels of *FLT4* mRNA expression in HUVECs under cell culture conditions with variable shear stress conditions. Exposure to high (30 dyn/cm^2), but not to low shear stress conditions (1 dyn/cm^2), decreased *FLT4* mRNA levels when compared with static conditions. Hence, shear stress regulates *FLT4* expression and this mechanism is conserved between zebrafish EdCs and human ECs. While NOTCH1 has already been reported to be a mechanosensor in arterial cells (Mack et al., 2017) and flow-responsive in the zebrafish endocardium (Samsa et al., 2015), it is currently not known how *FLT1* is influenced by shear stress. Since our data pointed out a downregulation of *flt1* expression levels in the absence of blood flow, it would be interesting to further analyze the contribution of Flt1 to mechanosensitive signal transduction.

3.2. Flt4 expression increases in atrioventricular mesenchymal- like endocardial cells

While sharing similarities in the general process of AV valvulogenesis, cardiac valve development in zebrafish and mammals differs in some aspects. At the zebrafish AVC, a mono-layered endocardium rearranges in a way that AV EdCs at the ventricular side move into the cardiac jelly, forming an abluminal population which is not in direct contact with blood flow. At the same time, AV EdCs from the atrial side remain luminally exposed and in contact with blood flow (Pestel et al., 2016; Steed et al., 2016b). Zebrafish AV EdCs that extend protrusions into the cardiac jelly migrate as sheets of cells, and not individually after delaminating (Gunawan et al., 2019; Scherz et al., 2008). Instead, in mammals, individual EdC at the AVC delaminate into the extra cellular matrix (ECM), while undergoing EndoMT (Cai et al., 2012; Wang et al., 2013). This morphological difference between zebrafish and mammalian AV abluminal EdCs is revealed also by differences in the expression of cell

adhesion markers. Mammalian delaminating AV EdCs loose cell membrane adhesion and acquire a mesenchymal cell identity as they protrude into the ECM. In the zebrafish embryo, expressions of Alcam and of the adherens junction-component VE-cadherin at the membranes of AV EdCs are not entirely and directly downregulated once AV ventricular EdCs have migrated and lost contact with the cardiac lumen. Similarly, the expression of the endothelial marker *fli1a* and *kdrl* remain longer expressed in these cells (Beis et al., 2005; Gunawan et al., 2020; Steed et al., 2016b). One limitation in the usage of transgenic reporter lines to assess the temporal expression of proteins is the persistence of the fluorescence proteins. To overcome this issue, it is possible to generate reporter lines that transcribe, under the desired promoters, destabilized fluorescence proteins. This is the case of the Notch reporter line I used in this study, *Tg(TP1:VenusPEST)*^{s940}. PEST degradation dramatically reduces the half-life of fusion proteins (from 23 to 2 hours for GFP-PEST in mammalian cells) (Li et al., 1998; Ninov et al., 2012). Another way to validate at higher temporal resolution the expression from reporter lines is the use of specific antibody for the analyzed protein. In my study, immunohistochemistry was performed to analyze the localization of the cell adhesion proteins Alcam and VE-cadherin. Another study found a similar gradual degradation within abluminal EdCs of the tight junction–associated protein ZO-1 (Gunawan et al., 2019). Hence, the transformation from AV endocardial to mesenchymal cells is more gradual and less defined in zebrafish compared to mammals. Also, in mammals the mesenchymal identity of these cells becomes defined by the well-known mesenchymal cell markers *TWIST* and *SNAIL* (Chakraborty et al., 2010; Tao et al., 2011). In particular, Snail is induced by Notch signaling in AVC and OFT endocardium, where directly represses *VE-cadherin* and thus allows these cells to break contact with neighboring cells and to migrate into the cardiac jelly (Saad et al., 2010; Timmerman et al., 2004). Whether this process is fully conserved and whether Snail1 plays a similar role in zebrafish is still under debate. After a collective AV EdC migration, by 78 hpf AV EdCs have acquired a multilayered S-shaped structure. While previous studies have characterized some of the molecular markers of the luminal cell population, which include Notch signaling and expression of Klf2, my work revealed that *flt4:mCitrine* expression was higher in abluminal EdCs, which also exhibit Wnt/β-catenin signaling (Moro et al., 2012; Pestel et al., 2016). Also, I showed that *flt1* expression is flow-responsive and localizes to the luminal side. In order to analyze the gene expression of *flt4* and *flt1*, I made use of transgenic reporter lines carrying specific promoters that drive expression of fluorescent proteins. This allowed me to continuously observe the gene expression *in vivo*. However, the visualization of fluorescent proteins, such as Citrine or YFP, rather than the

native Flt4 or Flt1 proteins sets limitations. In fact, while it reveals the endogenous activation of the promoter gene, it does not allow tracking the *in vivo* behavior of Flt4 or Flt1. For instance, as already mentioned, the physiological turnover and degradation speed may be different between the native and the fluorescent proteins. Also, *flt4:Citrine* expression in the heart is weak, and an immunolabeling against GFP was necessary to enhance the signal. Hence, for further studies it may be of advantage to obtain specific antibodies against Flt4 and Flt1. This would allow a validation of the transgenic reporter lines and to study the spatial and temporal localization of the native proteins more precisely. The spatial subcellular localization of Flt4 and Flt1 is especially relevant due to the complexity of receptor protein signaling, which needs to better characterized in order to understand the signaling events. For instance, receptor proteins may not be active or signal differently if expressed but localized in the cytoplasm. Also, as previously mentioned, differences in the levels of Flt4 account for the difference in the response to fluid shear stress within different EC types (Baeyens et al., 2015). Arterial cells are physiologically exposed to a higher shear stress level than venous cells, which in turn are subject to more shear stress than lymphatic cells. The ability to respond and adapt to different levels of shear stress has been correlated with the expression levels of Flt4. Therefore, in the zebrafish dorsal aorta *flt4:Citrine* signal is lowly detectable, but these low expression levels are functional to maintain the correct homeostasis of the vessel. In fact, upon lack of Flt4, the dorsal aorta narrowed, in a remodeling process that suggests an impairment of shear stress sensitivity (Baeyens et al., 2015). Similarly, the zebrafish endocardium is exposed to high shear stress. *flt4:Citrine* expression becomes higher within ECM-ingressed AV cells, but the levels are still lower than within the lymphatics that are constantly under low shear stress. However, a lack of Flt4 caused a phenotype within the cardiac valves. Hence, this suggests that Flt4 plays a similar role within ECs and EdCs in setting the shear stress point and may explain why low levels of expression are crucial for cardiac valve development.

Juvenile and adult AV valves are composed of an outer luminal layer of EdCs and an inner abluminal layer of valve interstitial cells (VICs). VICs are mesenchymal cells that derived in part from abluminal EdCs, and in part from neural crest cells (Gunawan et al., 2020). Since my work showed a gradual increase between 54-78 hpf in Flt4 expression levels in AV abluminal EdCs, it would be interesting to analyze its expression in more mature valve leaflets. A hypothesis may be that Flt4 becomes higher expressed within no flow-exposed VICs. Functional studies would then be required to study whether Flt4 is required for the identity of those cells.

In mice, AV EdCs acquire a mesenchymal cell identity as they protrude into the ECM (reviewed in (Macgrogan et al., 2014). Currently, *Flt4* was reported to be expressed within at least a subset of the endocardium and the epicardium at E13.5 (VanDusen et al., 2014). This expression is maintained at low levels by a negative regulation from the endocardial transcription factor Hand2. In turn, Hand2 is induced by Notch signaling. Endocardial ablation of Hand2 resulted in a failure to develop a patent tricuspid valve, and in other malformations that include intraventricular septum defects, hypotrabeculated ventricles and a higher density of the coronary lumen. While this correlates with increased levels of Flt4, a role of this protein was not further characterized and whether the expression was also within developing valves was not reported. To characterize *Flt4* expression within the murine AVC, I collaborated with Dr. Michel Puceat (MMG, Marseille), who performed single-cell RNA-seq analyses of purified mouse EdCs derived from E9.5 AVC tissue. At this stage, EdCs delaminate from the endocardium, undergo EndoMT, and invade the cardiac jelly of the cushions. Bioinformatics analyses revealed that *Flt4*-positive EdCs distributed primarily into three clusters. In one cluster, cells expressed the genes *Twist*, *Prrx2*, and *Loxl2*, marking a 'transition to mesenchymal' cell fate. In another, cells expressed endothelial markers including *Egfl7* and *Claudin-5*. The third cluster comprised cells expressing mesenchymal markers, such as *Snail1* and *Tgfb2*. Within those clusters, Flt4 expression levels were highest in the 'transition-to-mesenchymal' cell fate cluster and lowest among mesenchymal cells. This suggests that the murine process is similar to the one that takes place in zebrafish in the sense that the expression of Flt4 defines subpopulations of EdCs delaminating from luminal regions of the murine embryonic AVC cushions. Functional studies with a murine AV EdCs-specific *Flt4*-knockout would be instrumental to test the hypothesis of a conserved role of Flt4 between zebrafish and mammals during valvulogenesis.

3.3. Flt4 is required for atrioventricular valvulogenesis

With my work, I showed that Flt4 localization within AV abluminal EdCs is necessary for proper valve development. In fact, a lack of Flt4 caused the formation of dysmorphic valves, in which EdCs did not elongate as in WT. The abluminal side of the valve leaflet was affected by the ectopic expression of the cell adhesions markers Alcam and VE-cadherin and Notch activity. Within the luminal side, Notch-active cells had a larger surface area and exhibited ectopic Wnt/β-catenin signaling. To induce a lack of Flt4, I made use of three independent

tools. I used a stable loss-of-function mutant line, a morpholino-induced knockdown and an inhibitor-driven block of signaling. *flt4*^{hu4602} embryos were reported to have lymphatics defects (Astin et al., 2014; Bower et al., 2017; Le Guen et al., 2014; Hogan et al., 2009b). The *flt4*^{hu4602} allele has a point mutation predicted to change a conserved isoleucine residue into a serine at position 1042 in the split kinase domain and should represent a strong loss-of-function allele (Hogan et al., 2009b), but has been described as a hypomorphic allele (Astin et al., 2014; Vogrin et al., 2019). In my analysis, the *flt4*^{hu4602} heart phenotype was indeed lowly penetrant (33.3% had ectopic Notch expression, 70% had persistent abluminal Alcam expression) which may be due to the fact that this mutation does not cause a complete lack of Flt4 but only a predicted lack of its kinase activity. While Flt4 kinase activity is necessary for lymphangiogenesis, mutant mice with a missense mutation in the tyrosine kinase catalytic domain develop a blood vascular network (Zhang et al., 2010). In comparison, mice null for Flt4 display abnormal angiogenesis and die before the formation of lymphatic vessels (Dumont et al., 1998). These findings indicate that signaling mediated via the activation of Flt4 kinase is not required for blood vessel growth. Zhang and colleagues suggest that during angiogenesis, Flt4 forms heterodimers with VEGFR2 and modulate its phosphorylation and thus its signaling (Zhang et al., 2010). Similarly, it can be that within the endocardium, Flt4 may also have a kinase-independent role.

Another explanation for the incomplete penetrance of the *flt4* mutant phenotype may be that in homozygously mutant embryos a compensatory gene network is activated, which buffers an otherwise deleterious mutation (Rossi et al., 2015). One way of overcoming this phenomenon would be the generation of RNA-less *flt4* allele, which does not trigger a transcriptional compensation by other genes (El-Brolosy et al., 2019). This could be achieved by a mutation within the *flt4* promoter. Since such an allele was not available in the course of these studies, I used as a second independent tool to analyze Flt4 cardiac contribution, a specific morpholino which targets the ATG site of *flt4* and therefore blocks protein translation (Hogan et al., 2009b). Although recent studies showed that morpholinos can induce unspecific effects (Kok et al., 2014), both *flt4* morphants and mutants presented the expected lymphatic defects and the *flt4* MO has been recognized as a valid tool to specifically knockout Flt4. My analyses showed that a MO-induced Flt4 knockdown had a higher phenotypical penetrance than the *flt4* mutation (66.7% of *flt4* morphants had ectopic Notch expression, 78.3% of *flt4* morphants had persistent abluminal Alcam expression). The higher penetrance of the MO-induced phenotype is in support of a mutation-induced compensatory pathway (Rossi et al., 2015) that becomes activated in the *flt4*^{hu4602} mutant allele. The specificity of the cardiac

phenotype was further supported by a third tool, which was the use of MAZ51, an inhibitor for Vegfr with a high affinity for Flt4 that has been shown to inhibit its phosphorylation (Benedito et al., 2012). The use of this inhibitor enhanced the penetrance of the cardiac valve phenotype. However, the penetrance was still not complete, and this may be in tune with a kinase-independent Flt4 signaling. An additional advantage of using a pharmacological inhibition is the temporal control that this approach provides and which allows a precise staging of protein function. I used MAZ51 inhibition by treating embryos from 24 hpf, which excluded an earlier requirement of Flt4 in cardiac progenitors. Although at 24 hpf the development of valve leaflets has not yet started, the inhibitor treatment was needed that early which may relate to the efficacy of drug uptake into tissues. Further analyses will be necessary to assess the drug efficacy in blocking Flt4 signaling upon incubation. Alternatively, Flt4 may have an earlier role than anticipated. A genetic tool that can block Flt4 in a temporal-specific manner can be instrumental to verify these hypotheses. For instance, that could be obtained using the Cre-loxP system. Using that genetic tool, a transgenic line bearing a floxed *flt4* allele can be crossed to a line carrying Cre recombinase under a heat shock inducible promoter. In a similar approach, it would be possible to generate a tissue-specific lack of Flt4, by having an endothelial/endocardial promoter to drive Cre recombinase expression. This could be useful, since *flt4* is expressed not only within endocardium, but also in the other tissues including blood and lymphatic vessels. Although at the observed stages embryos did not present any obvious other severe morphological defects that could induce secondary effects on the heart, an endocardial-specific Flt4 mutant line would be helpful for this experiment. Complementary, cell transplantation assays could be performed to introduce *flt4* mutant cells into a WT background. If Flt4 function were cell-autonomous, I would expect *flt4* mutant clones to have a high expression of Notch signaling and become part of the luminal side of the AV valve leaflets.

Although my work is the first one to point out a role of Flt4 in the heart, *FLT4* mutations in humans have recently been correlated with Tetralogy of Fallot, a congenital cardiac disease with abnormal cardiac valvulogenesis (Jin et al., 2017; Reuter et al., 2018). The molecular mechanisms uncovered in my study will contribute to a better understanding of defects in valve formation which is a common feature of many congenital heart defects (Combs and Yutzey, 2009). Since the majority of *flt4*^{hu4602} mutants reach adulthood, it would be interesting to verify the condition of the cardiac valves in juvenile and adult fish and, pending the outcome, use them as a model to study the impact of congenital valve defects.

Besides the cardiac valves, mammals regulate the unidirectional flow of fluids throughout the vasculature with lymphatic valves (LV), venous valves (VV) and lymphovenous valves (LVV, which are at the sites where lymph is returned to blood circulation). The development of VVs and LVs is very similar. In both venous and lymphatic vessels, the establishment of valve territory starts with the clustering of ECs, which then undergo circumferential reorientation along the rim of the vessel and form a ring-like constriction. This structure then elongates into the vessel lumen and matures into V-shaped leaflets, with an extracellular matrix core assembly (Bazigou and Makinen, 2013). It was reported that the formation of LV in mice also depends both on shear stress (Sabine et al., 2012) and Flt4 (Liu et al., 2014), whose expression is initially high in collecting lymphatic trunks and becomes restricted to the valves once they have formed (Norrmén et al., 2009). LVVs develop in mice at the two sites of contact between the lymph sacs and the veins. LVV-forming endothelial cells (LVV-ECs) differentiate and delaminate from the vein walls with a luminal orientation, similar to LVs and VVs (Geng et al., 2016). Hence, while this process is reminiscent of an EndoMT that occurs during cardiac valve formation, in other valve types it differs with respect to the direction of the delaminating cells. While AV EdCs delaminate abluminally, away from the blood flow, LVV-ECs protrude into the lumen of the vein (Geng et al., 2016) and can withstand the force of blood flow, likely due to their association with the ECM (Geng et al., 2017). While the LVV-ECs represent the cover of the LVVs, the internal part is sustained by lymphatic endothelial cells (LECs). These cells are not in contact with blood flow and upregulate the expression of Flt4 (Geng et al., 2016). In spite of its expression in venous and lymphatic valves, the function of Flt4 in the formation of these valve types is not yet characterized. In light of the results from my work, it would be interesting to verify a possible conserved role of Flt4 within no-shear stress regions of lymphatic valves, similar to the one in the formation of cardiac valves.

3.4. At the atrioventricular valves, Flt4 acts in a Vegfc-independent manner

During lymphangiogenesis, Flt4 plays an essential role through the binding of its ligand, Vegfc (Karkkainen et al., 2004; Yaniv et al., 2006). In mechanosensitive signaling, several lines of evidence suggested that Flt4 functions in a Vegfc-independent manner (Baeyens et al., 2015; Park et al., 2017; Planas-Paz et al., 2012). As already mentioned, Baeyens and colleagues (2015) suggested that a loss of Flt4, but not of Vegfc, shrinks the caliber of the

zebrafish dorsal aorta. This phenotype could be explained by a reduction in endothelial cell mechanosensitivity and a consequent inward remodeling of the vessel, which would restore normal signaling levels. Park and colleagues (2017) reported that in the uterine endometrium, during pregnancy, shear stress regulates FLT4 independently of VEGFC. Planas-Paz and colleagues (2012) proposed that a stretching of LECs induced by high interstitial fluid volume causes activation of VEGFR3 through β1 integrins, independently of changes in VEGFC. The interactions between β1 integrin and VEGFR3 are regulated by integrin-linked kinase (ILK), which assembles with β1 integrin in quiescent LECs. Mechanical stimulation releases β1 integrin from ILK, enabling β1 integrin-VEGFR3 interaction (Urner et al., 2019). Similarly, my data show that Vegfc is dispensable for zebrafish valve morphogenesis. When I knocked down *vegfc* using MOs, the morphant heart appeared normal, although morphants exhibited fully penetrant lymphatic defects similar to a *flt4* knockdown, which demonstrated the efficacy of the *vegfc* MO mediated knockdown. From the RNA-seq data on non-beating versus beating hearts, *vegfc* mRNA levels were statistically not different between the two conditions. However, while my data support a Vegfc-independent cardiac role of Flt4, it is not possible to rule out a Flt4 signaling through a different ligand. In fact, Vegfd has as a high affinity for Flt4 and acts redundantly with Vegfc during lymphangiogenesis (Astin et al., 2014; Bower et al., 2017). Nevertheless, double *Vegfc*−/−/*Vegfd*−/− mutant mice survive until E16.5 and do not recapitulate the blood vasculature phenotype of *Flt4*−/− mutants, suggesting VEGF-C/VEGF-D-independent activation of FLT4 in mice (Haiko et al., 2008). It was also reported that FLT4 on human dermal blood ECs can be phosphorylated by collagen-I stimulation in the absence of VEGF-C/VEGF-D, and even in the presence of blocking antibodies against FLT4 (Kasey et al., 2013). A previous report also showed that endothelial cell migration requires cooperative interactions between β1-integrin and FLT4 (Wang et al., 2001). Endothelial cell adhesion to the extracellular matrix does not require the activation of receptor kinase activity. Instead, this interaction induces integrin-mediated FLT4 phosphorylation and activation of the CRKI/II-SHC (Src homology and collagen homology protein)-JNK cascade (Galvagni et al., 2010). Therefore, FLT4 mediates both ligand-dependent and extra-cellular matrix-dependent effects. In our transcriptome analysis from extracted hearts, *vegfd* mRNAs were not detected, indicating an absence or low expression levels of *vegfd* mRNA within cardiac tissue at 54 hpf. Altogether, my findings provide new insights into the modes of Flt4 regulation and the fine-tuning of mechanosensitity during cardiac valvulogenesis, which occurs in a Vegfc ligand-independent manner.

3.5. Flt4 impacts mechanosensitive signaling within the atrioventricular endocardium

My studies revealed that a lack of Flt4 leads to the formation of dysmorphic valve leaflets. Taking advantage of transgenic reporter lines, I showed that Notch activity and Wnt/β-catenin signaling are ectopically expressed within AV EdCs upon loss of Flt4. In WT, the remodeling of the AV endocardium into AV valves involves the formation of a luminal AV endocardial cell population which has an atrial origin and another abluminal cell population which is derived from the ventricular endocardium. Blood flow impacts the luminal EdC population in a way that it triggers and sustains the expression of the flow-responsive Notch and Klf2 pathways. Abluminal cells are characterized by Wnt/β-catenin activity and some will differentiate into valve interstitial cell precursors (Gunawan et al., 2020). My data revealed that at 78 hpf, AV abluminal cells lacking Flt4 have a persistent expression of cell adhesion proteins and of Notch activity. The short felodipine treatment effect suggests that the loss of Flt4 impacts the behavior of Notch positive luminal cells in way that they delaminate ectopically and enter the luminal or VIC region of the developing valves. It also suggests that Dll4-positive cells (responsive to Wnt ligands) remain at the luminal side. Together, these findings suggest that the mesenchymal transformation in these cells is defective. Recent studies indicated that the EndoMT is negatively influenced by shear stress in endothelial cells, and therefore regulated by mechanosensitive pathways (Kovacic et al., 2019; Mahmoud et al., 2017). Flt4 may have a role in mediating mechanosensation and promote EndoMT in AV EdCs. My observations also revealed that the loss of Flt4 causes an ectopic expression of Wnt signaling within luminal AV EdCs. In some cases, I observed a co-expression of Notch and Wnt signaling in AV EdCs at 78 hpf. At the beginning of AV valve formation, the mono-layered lumen-facing AV endocardium expresses both Wnt- and Notch-positive cells. Then, cell migration and resulting no-shear stress versus shear stress environments reinforce precise cell fates in the two AV endocardial subpopulations (Pestel et al., 2016). Hence, my findings that upon lack of Flt4 both luminal and abluminal cells ectopically express Wnt/β-catenin and Notch activities are in tune with affected cell fate transitions during valve remodeling. The blood flow dependency of both endocardial Wnt/β-catenin and Notch signaling (Pestel et al., 2016) strengthens the hypothesis of an impaired mechanosensitivity upon the loss of Flt4. Further studies will be needed to clarify the molecular relationship between Wnt/β-catenin and Flt4/Notch signaling pathways and whether the ectopic expression of luminal and abluminal markers is due to misregulated gene expression or abnormal cell rearrangements.

In order to get insights on other cardiac molecular players misregulated upon loss of Flt4, I performed an RNA-seq on *flt4* morphant versus WT hearts. Interestingly, tight junctions, focal adhesion and ECM-receptor interaction were among upregulated pathways. This supports the data on the ectopic persistent expression of cell adhesion molecules in abluminal positions. Among the most misregulated pathways were p53 signaling, cell cycle, and apoptosis signaling. Disturbed flow or misregulation of mechanotransduction genes have been shown to promote endothelial senescence via a p53-dependent pathway (Warboys et al., 2014). Hence, these data may be in support of an incorrect sensitivity and transduction of shear stress in *flt4* morphant cells. However, a recent study also pointed at an induction of interferon-stimulated genes and cellular stress pathways as common signatures that characterize morpholino-injected (Lai et al., 2019). Further analyses, including the use of a control MO or the analysis of the *flt4* mutant transcriptome profile, are necessary to rule out a morpholino-induced rather than a *flt4* knockdown-induced gene misregulation in *flt4* morphant hearts.

Interestingly, transcriptionally, the flow responsive genes *notch1b* and *klf2a* are differently misregulated. Whereas *notch1b* mRNA levels are upregulated in Flt4-depleted hearts, *klf2a* mRNA levels are downregulated. These data from the cardiac *flt4* morphant transcriptome were confirmed by qRT-PCR on *flt4* mutant hearts. While these results refer to whole-hearts, the use of the *klf2a*:YFP reporter line allowed me to verify that klf2a expression is downregulated within the AV endocardium. In addition to supporting a mechanoregulative role for Flt4, the different behavior of *klf2a* and *notch1b* mRNA expression levels in the Flt4-depleted endocardium implies that the misregulation of these flow-sensitive genes is not simply induced by a possible alteration of shear stress levels, since that would have a similar impact on *notch1b* and *klf2a* expressions.

3.6. Notch and Flt4 have antagonistic activities within the atrioventricular endocardium

In addition to showing that Flt4 limits the expression of Notch activity at the luminal AV side, my findings indicate that *flt4* is in turn negatively regulated by blood flow and that this suppression is mediated by Notch during cardiac valve leaflet formation. Notch signaling is involved in cell fate control, stem cell self-renewal and postnatal tissue differentiation. Genetic inactivation of either endothelial Notch1 or of the Notch ligand DLL4 results in loss

of arterial–venous specification and deregulated angiogenesis due to a failure of tip cell versus stalk cell specification (Simons et al., 2016). In the tip cell, at the vascular front of the growing vessel, VEGF stimulation of both VEGFR2 and VEGFR3 promotes the expression of DLL4, which induces Notch signaling and the Notch ligand Jagged1 in adjacent stalk cells. Jagged1 antagonizes DLL4–Notch signaling and allows stalk cells to revert to tip cells in response to VEGF. Notch activity creates a feedback loop with VEGF–VEGFR signaling, as inhibition of the DLL4–Notch pathway results in increased expression of VEGFR2 and VEGFR3 (Benedito et al., 2009). Thus, VEGF–VEGFR signaling both lies upstream of Notch and provides feedback signaling (Jakobsson et al., 2010). A similar repression has been observed in zebrafish during arterial tip cell formation, where *flt4* is ectopically expressed in the absence of Notch (Lawson et al., 2001; Siekmann and Lawson, 2007). In the mouse retina, the inhibition of Notch caused ectopic endothelial cell sprouting and proliferation mediated by FLT4 during angiogenic tip cell formation (Benedito et al., 2012). Genetic or pharmacological disruption of Notch signaling led to widespread endothelial FLT4 expression, which caused excessive sprouting (Tammela et al., 2008). However, FLT4 was also reported to act in a bimodal role in regulating angiogenesis, since endothelial-specific deletion of *Flt4* led to excessive angiogenic sprouting and branching, associated with a decreased level of Notch (Tammela et al., 2011).

Our findings imply that tip cell formation and cardiac valvulogenesis bear molecular similarities. Tip cells are thought to undergo a process of partial EMT (Welch-Reardon et al., 2015), which is another molecular resemblance between tip cell biology and valvulogenesis. The process of valve development in zebrafish, however, exhibit major differences to murine retinal tip cell sprouting. Among those, my work is in tune with previous studies (Timmerman et al., 2004) in showing that the pharmacological inhibition of Notch prevents the formation of a multi-layered AV valve structure. This means that high levels of Flt4, triggered by the pharmacological suppression of Notch, are apparently not sufficient to activate EdC sprouting and multi-layering. Rather, other Notch-dependent processes are essential for the formation of abluminal valve structures. In addition, my findings indicate that blood flow is required for Notch activation in a Flt4-independent manner.

3.7. Klf2 and Notch act independently in suppressing *flt4* mRNA expression

Previous studies reported that the expression of *notch1b* mRNA at the AVC is regulated by *klf2a* (Vermot et al., 2009). Surprisingly, I found that, upon loss of Flt4, *klf2a* and *notch1b* expression levels are regulated independently of each other. Although both require stimulation by shear stress (Samsa et al., 2015; Vermot et al., 2009), my findings indicate that the pharmacological inhibition of Notch activity does not abolish *klf2a* expression and, similarly, Notch activity at the AVC is not affected in *klf2a;klf2b* double mutants. Since blood flow is present in these conditions, shear stress may be necessary and sufficient to induce Klf2 or Notch expression. Currently, I cannot rule out the possibility that the Notch1b and Klf2a/b pathways converge at least upon a subset of common target genes and cooperate in activating the morphological processes necessary to generate multi-layered cardiac AV valve leaflets. In support of this model, my findings show that both Notch inhibition and loss of Klf2 activity caused a loss of abluminal EdCs in zebrafish. Consistent with this finding, in the mouse, the lack of Notch activity impairs the EndoMT process in the AV endocardium (Timmerman et al., 2004). Intriguingly, my work identified *flt4* as a negative target gene upon which the activities of Notch and Klf2 converge and that plays a role within the abluminal portion of the valve leaflet. Whether the regulation from Notch or Klf2a/b on *flt4* is direct or not is still an open question. To clarify this hypothesis, bioinformatics analyses would be helpful to predict potential Klf2a or Klf2b binding sites on the *flt4* promoter and a chromatin immunoprecipitation assay would be instrumental to verify the binding of these transcription factors to the *flt4* promoter DNA sequence. To clarify whether Klf2 and Notch act independently or within one signaling pathway, it would be essential to block both signaling factors at the same time, and test Flt4 expression. A more severe phenotype than the block of one of the two pathways would suggest that additional effects were caused by distinct pathways. Instead, a similar phenotype to the one induced by a single signaling knockdown would indicate that the pathways converge. In order to manipulate Notch signaling, I either inhibited or overexpressed the Notch intracellular domain. Hence, one open question is at which level of the Notch signaling pathway the interaction with Flt4 occurs. Additional genetic and biochemistry experiments, including the analysis of Flt4 levels in mutant lines for the single components of the Notch pathway, will be helpful to answer more precisely which Notch ligands and receptors are involved in the regulation of Flt4 during cardiac valve development.

3.8. Conclusions

The embryonic development of cardiac valves is a complex and precisely regulated process. Molecular pathways and physical forces are interconnected and essential for the tight regulation of the required morphological events. In my work, I investigated at cellular resolution the remodeling of the zebrafish atrioventricular endocardium into a developing valve leaflet, composed of two different subpopulations of EdCs, one on the luminal and the other on the abluminal side of the valve leaflet. I found that blood flow-driven shear stress is essential not only to directly activate molecular pathways within the luminal EdCs, but also to shape the abluminal ECM-ingressed EdC side. In particular, the lack of blood flow experienced by the ECM-ingressed EdCs causes a downregulation of Notch signaling and upregulation of Flt4. Independently of Notch, another crucial mechanosensitive protein, Klf2a, contributes to the suppression of Flt4 in EdCs that are exposed to blood flow. In turn, Flt4 prevents the expression of Notch and induces the degradation of the cell adhesion proteins Alcam and VE-cadherin within no-flow abluminal EdCs. Hence, my study introduces Flt4 as a previously uncharacterized player in the formation of the abluminal, mesenchymal-like side of the developing atrioventricular valve and identifies antagonistic signaling activities of Flt4 and Notch in fine-tuning the process that shapes cardiac valve leaflets. This is achieved by inducing unique differences in the fates of EdCs. These results are relevant not only to understanding the mechanisms of mechanotransduction during valve development, but also to identifying potential target genes connected to congenital valve malformations.

4. Materials and Methods

4.1. Consumables and equipment

Cell Strainer (100 µm Nylon)	Falcon
Centrifuge	Eppendorf
Confocal microscope LSM 710, 780, 880	Zeiss
Coverslips	Roth
Disposable Pasteur pipettes	Elkay
Dumont forceps n.4	neoLab
EOS 5 D Mark III camera	Canon
Flaming/Brown Micropipette Puller	Sutter Instrument
Gel electrophoresis apparatus	Life Technologies
Glass bottom dishes	MatTek
Glass injection needles	Brummond Scientific
Injection machine	Eppendorf
Micro tubes	Eppendorf
Microinjection 20 µL tips	Eppendorf
Micropipettes	Gilson
Microscope Glass Slides	Roth
MM33 Micromanipulator	Maerzhaeuser
MPPI-2 Pressur Injector/BP15 Back Pressure Unit	Applied Scientific Instrumentation
NanoDrop	Thermo Scientific
Parafilm	Bemis
PCR thermocycler	Biozym diagnostic GmbH
PCR tubes	Sigma-Aldrich
Petri dishes	Roth
Phase lock gel heavy (1.5 ml)	VWR
PikoReal 96 Real-Time PCR System	Thermo Scientific
Pre-separation Filters (30 µm)	Miltenyi Biotec
Stereo microscope Leica M165 FC	Leica
Stereo microscope Zeiss Discovery. V8	Zeiss
Thermomixer	Eppendorf,
Tubes	Sarstedt
Vortex Genie	Scientific Industries

4.2. Chemicals and Solutions

Agarose, Low Melting Point	Lonza
1-phenyl-2-thiourea (PTU)	Sigma-Aldrich
4', 6-diamidino-2-phenylindole (DAPI)	Sigma-Aldrich
Bovin Serum Albumin (BSA)	Sigma-Aldrich
Dimethyl sulfoxide (DMSO)	Sigma-Aldrich
Ethanol	Sigma-Aldrich
Felodipine	Cayman Chemical
Gel Loading Dye Purple (6x, no SDS)	NEB
Luna Universal qPCR Master Mix	New England Biolabs
MAZ51	Santa Cruz Biotechnology
Methanol	Roth
Midori Green Advance	Nippon Genetics
NaCl	Sigma
Normal goat serum (NGS)	Sigma-Aldrich
Paraformaldehyd (PFA)	Sigma-Aldrich
Quick Load purple 2 Log DNA Ladder	NEB
Restriction enzymes and buffers	NEB
RO4929097	Selleckchem
SlowFade Gold	Thermo Fisher Scientific
Sodium azide (2% solution)	Santa Cruz
Tricaine (3-amino benzoic acidethylester)	Sigma-Aldrich
Triton X-100	Serva
TRIzol	Thermo Fisher Scientific
TrypLE	Thermo Fisher Scientific
Tween 20	Sigma-Aldrich

4.3. Kits

Quick RNA micro-prep	Zymo Research
KAPA Sybr Fast qPCR kit	Peqlab
MegaScript T3 Transcription Kit	Thermo Fisher Scientific
MegaShortScript T7 Transcription Kit	Thermo Fisher Scientific
RevertAid H Minus First Strand cDNA Synthesis kit	ThermoFisher Scientific
TruSeq Stranded Total RNA Sample Preparation Kit	Ilumina

4.4. Buffers and Media

Danieau's buffer 1x, pH 7.2	58 mM NaCl 0.7 mM KCl 0.4 mM MgSO4 0.6 mM Ca(NO3) 5 mM HEPES
E3 medium	5 mM NaCl 0.17 mM KCl 0.33 mM CaCl2 0.33 mM MgSO4
Fish egg water	60 µg/ml Instant Ocean Sea Salts in ddH2O
PBS 1x, pH 7.4	137 mM NaCl 2.7 mM KCl 80.9 mM NaHPO4 1.5 mM KH2PO4 in ddH2O
PBST	0.1% Tween in 1x PBS
PBDT	1% DMSO in 1x PBST
Permeabilization solution	0.5% Triton X-100 in 1x PBST
PFA 4%	4% paraformaldehyde in 1x PBS
TE-Buffer, pH 8.0	10 mM Tris-HCl 1 mM EDTA in ddH2O

4.5. Software

Fiji ImageJ	(Schindelin et al., 2012)
A plasmid editor (ApE)	UT
Adobe Illustrator CS6	Adobe Systems Inc
Adobe Photoshop CS6	Adobe Systems Inc
Cufflinks suite	(Trapnell *et al.*, 2012)
Imaris 8	Bitplane

LSM Image browser 8.1	Zeiss
Office 2010	Microsoft
PikoReal software 2.2	Thermo Fisher Scientific
Prism 6	GraphPad

4.6. Zebrafish Strains and Maintenance

Handling of zebrafish was done in compliance with German and Brandenburg state law, carefully monitored by the local authority for animal protection (LUVG, Brandenburg, Germany; Animal protocol #2347-18-2015). Zebrafish were maintained under standard conditions as previously described (Westerfield et al., 1997). Zebrafish embryos were kept in egg water (60 µg/ml Instant Ocean Sea Salts (Aquarium Systems Inc., USA) supplied with 1 µg/ml Methylene blue) at 28.5°C. To inhibit pigmentation, embryos were kept in egg water with an additional supply of 0.003% (w/v) 1-Phenyl-2-thiourea (PTU) from 24 hpf. Zebrafish embryos were staged according to morphological criteria previously described (Kimmel et al., 1995) and their genotype was determined either by fluorescent protein expression, by phenotype inspection or by genetic analysis of isolated genomic DNA. Adult fish were maintained at 26.5°C in the fish facility and mutant carriers were identified by incrosses and phenotypical analysis of the offspring or by genetic analysis of genomic DNA isolated from tissue obtained by fin-clipping. The following strains of zebrafish were used: *flt4*^{hu4602} (Hogan, Bos, *et al.*, 2009), *klf2a*^{sh317} (Novodvorsky et al., 2015), *Tg(EPV.Tp1-Mmu.Hbb:Venus-Mmu.Odc1)*^{s940} [here referred to as *Tg(TP1:VenusPEST)*^{s940}] (Ninov et al., 2012), *Tg(kdrl:EGFP)*^{s843} (Jin et al., 2005), *Tg(fli1a:EGFP)*^{y1} (Roman et al., 2002), *Tg(fli1a:nEGFP)*^{y7} (Roman et al., 2002), *Tg(kdrl:nlsEGFP)*^{ubs1} (Blum et al., 2008), *Tg(flt4BAC:mCitrine)*^{hu7135} (van Impel et al., 2014), *Tg(flt1:YFP)*^{hu4624} (Hogan, Bos, *et al.*, 2009), *Tg(7xTCF-Xla.Siam:nls-mCherry)*^{ia5} (Moro et al., 2012), *Tg(klf2a:YFP)*^{mu107} (Sugden et al., 2017), *Tg(fli1a:Gal4FF)*^{ubs3} (Herwig et al., 2011), *Tg(5xUAS-E1b:6xMYC-notch1a intra)*^{kca3} (Scheer and Campos-Ortega, 1999), *Tg(fli1:nls-mCherry)*^{ubs10} (Heckel et al., 2015). Double transgenic lines were generated via out-crossing.

4.7. Isolation of genomic DNA from zebrafish tissue and genotyping

For genetic analysis of embryos, genomic DNA was extracted from a part of the tail or from entire embryos. For genotyping of adult fish, genomic DNA was extracted from fin tissue after fin-clipping. Samples were digested in 50 mM NaOH, at 95°C for 20 minutes. After cooling down (at 4°C, 5 minutes), Tris pH 7.5 were added 1:10 in each sample. Samples were stored at 4°C.

Primers used to perform polymerase chain reactions (PCRs) to genotype were the following:

Name	Sequence 5'-3'
flt4^{hu4602} genotyping Fw	AGCTCTTGATTTGGCTTTAG
flt4^{hu4602} genotyping Rv	GGAAAGTATCCTTGCTCTGC
klf2b^{pbb42}, *klf2b*^{pbb43}, and *klf2b*^{pbb44} genotyping Fw	AGAAGCACCTCCACCATACG
klf2b^{pbb42}, *klf2b*^{pbb43}, and *klf2b*^{pbb44} genotyping Rv	GCGGAGGAGTCATATTCCCG
klf2a^{sh317} TAL Fw	CAGGCGACTACAGAATGCAA
klf2a^{sh317} TAL Rv	GCCCTCTTGTTTGACTTTGG

Amplified DNA products for *flt4* and *klf2b* were cleaned by adding *ExoI* (ThermoFisher Scientific, Cat. No. EN0582) and FastAP (ThermoFisher Scientific, Cat. No. EF0651) and incubating for 30 min at 37°C and 15 min at 85°C. Then, 2 µl of 5 µM specific Fw primers were added to each sample, which was then sequenced (Sanger sequencing, LGC Genomics, Berlin, Germany). *klf2a* amplicons were incubated (3 hours, 37°C) with BstXI (NEB) restriction enzyme, which digests the WT PCR product but not the mutant *klf2a*^{sh317}.

4.8. Embryo injection

One-cell stage embryos were injected using a stereomicroscope and glass injection needles (Drummond Scientific, USA) pulled in a P-97 Flaming/Brown Micropipette puller (Sutten Instruments), fixed onto a micromanipulator (MM33 Micromanipulator, Maerzhaeuser, Germany) and connected to a microinjector (MPPI-2 Pressure Injector, BP15 Back Pressure Unit, Applied Scientific Instrumentation, USA). Injection needles were loaded with 3 µl of the working solution and the embryos were positioned in one row at the edge of a glass slide. The volume of the drop to inject was adjusted to 1 nl, volume measured with a graticule (Pyser-SGI Limited, UK). The injected embryos were transferred into Petri dishes (Greiner

bio-one, Cat. No. 633180, Germany) with egg water and maintained at 28.5°C for further development.

4.9. Antisense oligonucleotide Morpholino injections

Morpholinos (MOs) (Gene Tools, LLC, USA) were diluted in ddH_2O to 1 mM stock solution and stored at -20 °C. The following morpholinos were injected into the yolk at the one-cell stage in 1 nl total volume: *tnnt2a* MO (5'-CATGTTTGCTCTGATCTGACACGCA-3') (1 ng/embryo) (Sehnert et al., 2002), *flt4* ATG MO (5'-CTCTTCATTTCCAGGTTTCAAGTCC-3') (2 ng/embryo) (Hogan, Bos, *et al.*, 2009), *vegfc* MO (5'-GAAAATCCAAATAAGTGCATTTTAG-3') (3 ng/embryo) (Hogan, Bos, *et al.*, 2009). Morpholino working solutions were diluited in 0.3x Danieau's buffer. Control siblings were injected with 1 nl of 1X Danieau's solution.

4.10. Generation of *klf2b* mutant lines

klf2b mutants were generated using CRISPR/Cas9-mediated mutagenesis. The guide RNA (gRNA) target sequence was 5'-CCGATGGATGGCTACGGT-3' and the DNA sequence used for transcription contained a T7 promoter sequence (Gagnon et al., 2014). gRNA was transcribed *in vitro* using MegaShortScript T7 Transcription Kit (Thermo Fisher Scientific) and *cas9* mRNA was transcribed *in vitro* from pT3TS-nCas9n DNA using MegaScript T3 Transcription Kit (Thermo Fisher Scientific). *klf2b* gRNA (~150 pg/embryo) and *cas9* mRNA (~250 pg/embryo) were co-injected into the cell of one-cell stage. Primers used to genotype are listed in Table 1. Morphological analyses of $klf2b^{pbb42}$, $klf2b^{pbb43}$, and $klf2b^{pbb44}$ mutants revealed no obvious defects.

4.11. Chemical treatments

To prevent cardiac contractility, embryos were treated with 8 µM felodipine (Cayman Chemical) from 72 to 78 hpf. To block Vegfr3 signaling, embryos were treated with 25 µM MAZ51 (Santa Cruz Biotechnology) a Vegfr inhibitor with a high affinity for Vegfr3/Flt4 between 24-78 hpf. To inhibit Notch signaling, embryos were treated with 10 uM RO4929097

(Selleckchem) between 52-78 hpf. The stock solutions were solved in DMSO and control embryos were treated with 0.2% DMSO.

4.12. Heart isolation, RNA extraction, and qRT-PCR

For cardiac extractions, ~50 hearts/replicate were extracted from 54 hpf WT or *flt4*^{hu4602} mutant embryos, from 54 hpf WT or *tnnt2a* morphant embryos, and from 78 hpf DMSO-treated or felodipine-treated embryos or RO-treated embryos, as described (Lombardo et al., 2015). For 54 hpf WT and *klf2* mutant embryos, and for 78 hpf WT and *Tg(fli1a:Gal4FF)*^{ubs3}*;Tg(5xUAS-E1b:6xMYC-notch1a intra)*^{kca3} embryos (both, DMSO- or felodipine-treated), ~25 hearts/replicate were manually extracted. Hearts were pooled for each condition (at least three biological replicates) and transferred into 100 µL of RNA lysis buffer from Quick RNA micro-prep (Zymo kit). RNA was isolated according to manufacturer's instructions and the corresponding cDNA was synthesized from total RNA with the RevertAid H Minus First Strand cDNA Synthesis kit (ThermoFisher Scientific). RT-qPCR experiments were performed as described (Renz et al., 2015) using 2 ng cDNA/technical replicate and the KAPA Sybr Fast qPCR kit (Peqlab) on a PikoReal 96 Real-Time PCR System (ThermoFisher Scientific). Cycle threshold (Ct) values were determined by PikoReal software 2.2 (ThermoFisher Scientific). *eif1b* was used as a housekeeping gene for normalization. Control sample values were normalized to 1, using the comparative threshold cycle method (2– ΔΔCT) (Livak and Schmittgen, 2001). As each single biological replicate represents an independent experiment from an independent clutch of embryos, ratio paired t-tests were performed, using Prism 6 (GraphPad).

Plotted results are listed below [stg: developmental stage (hpf, hours post fertilization) of zebrafish embryos at RNA extraction; n: number of independent biological replicates analyzed per condition; p: p Value; Mean (Geometric Mean of ratios)>1 corresponds with target upregulation; Mean<1 represents target downregulation; SEM: standard error mean].

	flt4^{hu4602}			*flt4*^{hu4602}			6h-felodipine on *flt4*^{hu4602}			6h-felodipine on ctrl		
	stg (hpf): 54			stg (hpf): 78								
	n: 4			n: 4								
	Mean	SEM	p	Mean	SEM	p	Mean	SEM	p	Mean	SEM	p
notch1b	**1.349**	**0.034**	**0.033**	**1.400**	**0.038**	**0.032**	**0.557**	**0.056**	**0.020**	**0.560**	**0.044**	**0.011**
klf2a	**0.594**	**0.065**	**0.040**	**0.462**	**0.072**	**0.019**	**0.318**	**0.078**	**0.008**	**0.319**	**0.057**	**0.003**

	RO-treatment			6h-felodipine			NICD			6h-felodipine+NICD		
	stg (hpf): 78											
	n: 4											
	Mean	SEM	p	Mean	SEM	p	Mean	SEM	p	Mean	SEM	p
flt4	**1.841**	**0.042**	**0.008**	**2.674**	**0.063**	**0.007**	**0.556**	**0.065**	**0.029**	**0.693**	**0.020**	**0.004**
klf2a	**1.548**	**0.074**	**0.083**	**0.751**	**0.021**	**0.009**	**0.678**	**0.033**	**0.015**	**0.683**	**0.012**	**0.001**

	tnnt2a MO			6h-felodipine			*klf2a*^{sh317};*klf2b*^{pbb42}		
	stg (hpf): 54			stg (hpf): 78			stg (hpf): 54		
	n: 5			n: 4			n: 3		
	Mean	SEM	p	Mean	SEM	p	Mean	SEM	p
flt4	**5.983**	**0.059**	**0.0002**	**2.205**	**0.078**	**0.022**	**1.415**	**0.011**	**0.005**
notch1b	**0.477**	**0.036**	**0.001**	**0.510**	**0.048**	**0.009**	**0.865**	**0.068**	**0.450**
flt1	**0.368**	**0.063**	**0.002**						
kdr	**0.842**	**0.046**	**0.179**						
kdrl	**0.810**	**0.077**	**0.302**						

The following primers were used for RT-qPCR:

Name	Sequence 5'-3'
flt4 qPCR Fw	CTCTCTTCTCGTTAGTGCCG
flt4 qPCR Rv	ATGATGTGTGCTGGCTGTTT
notch1b qPCR Fw	AATGTCCACCGGGTTTTACG
notch1b qPCR Rv	AGGCATTTGGGACTCTTGTG
klf2a qPCR Fw	CTGGGAGAACAGGTGGAAGGA
klf2a qPCR Fw	CCAGTATAAACTCCAGATCCAGG
flt1 qPCR Fw	AACTCACAGACCAGTGAACAA
flt1 qPCR Rv	ATGCGTTTGCTGATAATGGC
kdr qPCR Fw	TGGAGTTCCAGCACCCTTTA
kdr qPCR Rv	CGTCCTTCTTCACCCTTTCA
kdrl qPCR Fw	CAGATCACGGTGGATACAT
kdrl qPCR Rv	AAGAGGAGGAAGAGCAAGAG
eif1b qPCR Fw	CAGAACCTCCAGTCCTTTGATC

eif1b qPCR Rv	GCAGGCAAATTTCTTTTTGAAGGC

4.13. RNA-sequencing

For RNA sequencing, ~100 hearts/replicate were extracted from 54 hpf WT siblings and *tnnt2a* morphant embryos (*sih*MO RNAseq experiment), or from 54 hpf WT siblings and *flt4* morphant embryos (*flt4*MO RNAseq experiment), as previously described (Lombardo et al., 2015). Hearts were pooled for each condition (*sih*MO RNAseq: n=3 biological replicates/condition; *flt4*MO RNAseq: n=3 biological replicates/WT condition, n=6 biological replicates/*flt4*MO condition). For *sih*MO RNAseq experiment, total RNA was extracted with Trizol (Sigma-Aldrich) using Phase Lock Gel Heavy tubes (1.5 mL, Prime 5). For *flt4*MO RNAseq experiment, hearts were put in 100 µL of RNA lysis buffer from Quick RNA micro-prep (Zymo kit) and RNA was isolated according to manufacturer's instructions. cDNA libraries for both RNAseq experiments were prepared starting from 100 ng of RNA/replicate, using "TruSeq Stranded Total RNA Sample Preparation Kit" (Low Sample Protocol) (Ilumina). The fragment length distribution of generated libraries was monitored and the quantification was performed using the D1000 ScreenTape System (Agilent Technologies). Equal molar amounts of individual libraries were pooled, denatured with NaOH and diluted to 1.5pM. 1.3 ml of denatured pool sample were run on an Illumina NextSeq 500 sequencer using a High Output Flow cell for 75bp single reads (#FC-404-2005; Illumina) and reads were aligned to the *Danio rerio* reference genome (GRCz10) using STAR (Dobin et al., 2013). Differential expression analysis was finally performed by use of Cuffdiff as part of Cufflinks suite (Trapnell et al., 2012). For this, the library type was set to "fr-firststrand" (--library-type=fr-firststrand). The master transcriptome provided by Cuffmerge was provided as input. All other settings were left as default. For biological pathway annotation of differentially expressed genes, gene ontology and KEGG pathway enrichment analysis were performed using the Database for Annotation, Visualization and Integrated Discovery (DAVID) bioinformatics tool (Huang et al., 2009).

4.14. Whole-mount immunohistochemistry

Embryos were fixed at the desired developmental stage and fixed with 4% paraformaldehyde overnight at 4°C or for 2 hours at RT. Embryos were washed 3 times for 5 min in PBT and

then blocked for 2 hours at room temperature in PBT with 5% NGS and incubated at 4°C overnight with the primary antibody in PBT with 5% NGS. For anti-GFP labeling of hearts from *Tg(flt4BAC:mCitrine)*^{hu7135} embryos at 78 hpf, hearts were first dissected from fixed embryos and then immuno-labeled. After washing 6 times for 30 min in PBT, embryos were incubated with fluorescently conjugated secondary antibodies (1:200) overnight at 4°C. The following day, the embryos were washed 6 times for 30 min in PBT. For the Cdh5 antibody staining, embryos were fixed with 2% PFA overnight and permeabilized with PBST with 0.5% Triton X-100 for 1 hr and subsequently incubated with primary antibody diluted in PBST with 0.2% Triton X-100, 1% BSA, and 5% NGS. In Figure 2.13, nuclei were visualized by DAPI (4,6-diamidino-2-phenylindole; Sigma) staining.

The following primary antibodies were used:

Rabbit anti-VE-Cadherin (1:200)	Donation from Markus Affolter (Blum *et al.*, 2008)
Mouse anti-Zn-8/Alcam (1:100)	Developmental Studies Hybridoma Bank
Chicken anti-GFP (1:200)	Aves labs
Rabbit anti-VEGFR3 (1:200)	Abcam

The following secondary antibodies were used (1:200):

Alexa Fluor 488 Goat anti-rabbit IgG (H+L)	Thermo Fisher Scientific
Alexa Fluor 633 Goat anti-rabbit IgG (H+L)	Thermo Fisher Scientific
Alexa Fluor 546 Goat anti-mouse IgG (H+L)	Thermo Fisher Scientific
Alexa Fluor 633 Goat anti-mouse IgG (H+L)	Thermo Fisher Scientific
Fluorescein-conjugated goat anti-chicken IgY	Aves labs

4.15. Imaging acquisition and processing

Hearts were manually extracted and mounted in SlowFade Gold (Life Technologies, Cat. No. S36936) on a slide (Menzel-Gläser Superfrost, ThermoFisher Scientific, 76x26 mm) with a coverslip (High Precision No. 1.5H, 170±5 µm, 18x18 mm; Roth, Germany). To image whole embryos, specimens were embedded in 1% low melting agarose on a glass-bottom dish (Lonza). Images were acquired using the following Zeiss confocal microscopes: LSM 710 with 10x/dry, 25x/water, 40x/oil or multi-immersion; LSM 780 40x/oil; 40x/oil or multi-immersion objectives. Images were processed with Imaris (Bitplane, Version 8.1) or Fiji software (Schindelin et al., 2012). Overview brightfield images of the embryos were recorded

with 10x or 20x objectives on an Axioskop (Zeiss, Jena, Germany) with an EOS 5 D Mark III (Canon) camera and processed using Photoshop (CS6, Version 13.0.1, Adobe Systems).

4.16. Quantifications of the heart rate

Heart beats of 10 mutant or morphant embryos and of WT or their respective sibling embryos were counted over a 1-minute period under a dissecting microscope.

4.17. Measurements of cells size

Measurements were performed by Dr. Timm Haack on confocal z-section images of AVC regions in *Tg(TP1:VenusPEST)*^{s940} control (n=12 cells) or *flt4* morphant embryos (n=20 cells) at 78 hpf. The tissue was counter-stained with an antibody against VE-cadherin to highlight cell borders between AVC EdCs. Measurements were performed using the free draw tool implemented in the Fiji software.

4.18. Measurements of fluorescence intensity

In figure 2.1E, measurements of *flt4*:Citrine intensity were performed at 54 hpf on control injected embryos or *tnnt2a* morphants. After anti-GFP immunochemistry to increase the signal, hearts were imaged on the same microscope using the same settings. To measure fluorescence intensity levels, the mid-sagittal heart plane of a confocal z-stack was chosen and the ventricular+AVC endocardium (V) or the atrial endocardium (A) were selected as region of interest. ImageJ was used to calculate average pixel intensities of the signal area, which was normalized to the background intensity levels (control embryos, n=6; *tnnt2a* morphants, n=6).

Mean+SD Average Pixel intensities	
tnnt2 ventricle: 1.836+0.201	Ctrl ventricle: 3.356+0.408
*tnnt2*atrium: 1.495+0.304	Ctrl atrium: 2.407+0.373

In figure 2.3F, measurements of Alcam intensity were performed on WT embryos or *flt4*^{hu4602} mutants at 78 hpf. The mid-sagittal heart plane of a confocal z-stack was chosen and ImageJ was used to calculate average pixel intensities in luminal cells and abluminal cells. The values represent the ratio between the intensity averages in luminal and abluminal cells (WT, n=7 embryos; *flt4*^{hu4602}, n=10 embryos).

Mean±SD Luminal/ Abluminal intensities	
flt4^{hu4602}: 1.274±0.225	Ctrl: 1.971±0.280

In figure 2.10D, measurements of *flt4*:Citrine intensity were performed on WT embryos or *klf2* mutants at 56 hpf. After anti-GFP immunochemistry to increase the signal, hearts were extracted and imaged on the same microscope using the same settings. ImageJ was used to calculate average pixel intensities of maximum intensity projections of the superior AVC, which was normalized to background intensity levels (WT, n=7 embryos, *klf2*, n=11 embryos).

Mean±SD Signal/ Background	
klf2 mutants: 2.128±0.364	Ctrl: 1.575±0.131

4.19. Statistical analysis

All statistical analyses were performed with GraphPad Prism (version 6). Data representations and P values calculations are indicated in the figure legends. All indicated P values are two-tailed and significance was defined as $P < 0.05$.

5. Bibliography

Achen, M.G., Jeltsch, M., Kukk, E., Mäkinen, T., Vitali, A., Wilks, A.F., Alitalo, K., and Stacker, S.A. (1998). Vascular endothelial growth factor D (VEGF-D) is a ligand for the tyrosine kinases VEGF receptor 2 (Flk1) and VEGF receptor 3 (Flt4). Proc. Natl. Acad. Sci. U. S. A. *95*, 548–553.

Alitalo, R., Aprelikova, O., Korhonen, J., Kaipainen, A., Alitalo, K., and Pertovaara, L. (1992). FLT4 Receptor Tyrosine Kinase Contains Seven Immunoglobulin-like Loops and Is Expressed in Multiple Human Tissues and Cell Lines. Cancer Res. *52*, 5738–5743.

Astin, J.W., Haggerty, M.J.L., Okuda, K.S., Le Guen, L., Misa, J.P., Tromp, A., Hogan, B.M., Crosier, K.E., Crosier, P.S., Guen, L. Le, et al. (2014). Vegfd can compensate for loss of Vegfc in zebrafish facial lymphatic sprouting. Development *141*, 2680–2690.

Auman, H.J., Coleman, H., Riley, H.E., Olale, F., Tsai, H.J., and Yelon, D. (2007). Functional modulation of cardiac form through regionally confined cell shape changes. PLoS Biol. *5*, 0604–0615.

Baeyens, N., and Schwartz, M.A. (2016). Biomechanics of vascular mechanosensation and remodeling. Mol. Biol. Cell *27*, 7–11.

Baeyens, N., Nicoli, S., Coon, B.G., Ross, T.D., Van den Dries, K., Han, J., Lauridsen, H.M.M., Mejean, C.O.O., Eichmann, A., Thomas, J.-L.L.L., et al. (2015). Vascular remodeling is governed by a VEGFR3-dependent fluid shear stress set point. Elife *2015*, 1–16.

Baker, K., Holtzman, N.G., and Burdine, R.D. (2008). Direct and indirect roles for Nodal signaling in two axis conversions during asymmetric morphogenesis of the zebrafish heart. Proc. Natl. Acad. Sci. U. S. A. *105*, 13924–13929.

Bakkers, J. (2011). Zebrafish as a model to study cardiac development and human cardiac disease. Cardiovasc. Res. *91*, 279–288.

Baldwin, M.E., Roufail, S., Halford, M.M., Alitalo, K., Stacker, S.A., and Achen, M.G. (2001). Multiple Forms of Mouse Vascular Endothelial Growth Factor-D Are Generated by RNA Splicing and Proteolysis. J. Biol. Chem. *276*, 44307–44314.

Baldwin, M.E., Halford, M.M., Roufail, S., Williams, R.A., Hibbs, M.L., Grail, D., Kubo, H., Stacker, S.A., and Achen, M.G. (2005). Vascular endothelial growth factor D is dispensable for development of the lymphatic system. Mol. Cell. Biol. *25*, 2441–2449.

Banjo, T., Grajcarek, J., Yoshino, D., Osada, H., Miyasaka, K.Y., Kida, Y.S., Ueki, Y., Nagayama, K., Kawakami, K., Matsumoto, T., et al. (2013). Haemodynamically dependent valvulogenesis of zebrafish heart is mediated by flow-dependent expression of miR-21. Nat. Commun. *4*, 1–11.

Baratchi, S., Khoshmanesh, K., Woodman, O.L., Potocnik, S., Peter, K., McIntyre, P., Woodman, L., Potocnik, S., Peter, K., and McIntyre, P. (2017). Molecular Sensors of Blood Flow in Endothelial Cells. Trends Mol. Med. *23*, 850–868.

Bartman, T., Walsh, E.C., Wen, K.K., McKane, M., Ren, J., Alexander, J., Rubenstein, P.A., and Stainier, D.Y.R. (2004). Early myocardial function affects endocardial cushion development in zebrafish. PLoS Biol. *2*.

Bazigou, E., and Makinen, T. (2013). Flow control in our vessels: Vascular valves make sure there is no way back. Cell. Mol. Life Sci. *70*, 1055–1066.

Behrndt, M., Salbreux, G., Campinho, P., Hauschild, R., Oswald, F., Roensch, J., Grill, S.W., and Heisenberg, C.P. (2012). Forces driving epithelial spreading in zebrafish gastrulation. Science (80-.). *338*, 257–260.

Beis, D., Bartman, T., Jin, S.-W.W., Scott, I.C., D'Amico, L.A., Ober, E.A., Verkade, H., Frantsve, J., Field, H.A., Wehman, A., et al. (2005). Genetic and cellular analyses of zebrafish atrioventricular cushion and valve development. Development *132*, 4193–4204.

Benedito, R., Roca, C., Sörensen, I., Adams, S., Gossler, A., Fruttiger, M., and Adams, R.H. (2009). The notch ligands Dll4 and Jagged1 have opposing effects on angiogenesis. Cell *137*, 1124–1135.

Benedito, R., Rocha, S.F., Woeste, M., Zamykal, M., Radtke, F., Casanovas, O., Duarte, A., Pytowski, B., and Adams, R.H. (2012). Notch-dependent VEGFR3 upregulation allows angiogenesis without VEGF–VEGFR2 signalling. Nature *484*, 110–114.

Van Den Berg, G., Abu-Issa, R., De Boer, B.A., Hutson, M.R., De Boer, P.A.J., Soufan, A.T., Ruijter, J.M., Kirby, M.L., Van Den Hoff, M.J.B., and Moorman, A.F.M. (2009). A caudal proliferating growth center contributes to both poles of the forming heart tube. Circ. Res. *104*, 179–188.

Blum, Y., Belting, H.-G., Ellertsdottir, E., Herwig, L., Lüders, F., and Affolter, M. (2008). Complex cell rearrangements during intersegmental vessel sprouting and vessel fusion in the zebrafish embryo. Dev. Biol. *316*, 312–322.

de Boer, B.A., van den Berg, G., de Boer, P.A.J., Moorman, A.F.M., and Ruijter, J.M. (2012). Growth of the developing mouse heart: An interactive qualitative and quantitative 3D atlas. Dev. Biol. *368*, 203–213.

Bornhorst, D., Xia, P., Nakajima, H., Dingare, C., Herzog, W., Lecaudey, V., Mochizuki, N., Heisenberg, C.P., Yelon, D., and Abdelilah-Seyfried, S. (2019). Biomechanical signaling within the developing zebrafish heart attunes endocardial growth to myocardial chamber dimensions. Nat. Commun. *10*, 1–10.

Boselli, F., Freund, J.B., and Vermot, J. (2015). Blood flow mechanics in cardiovascular development. Cell. Mol. Life Sci. *72*, 2545–2559.

Boselli, F., Steed, E., Freund, J.B., and Vermot, J. (2017). Anisotropic shear stress patterns predict the orientation of convergent tissue movements in the embryonic heart. Development *144*, 4322–4327.

Bower, N.I., Vogrin, A.J., Le Guen, L., Chen, H., Stacker, S.A., Achen, M.G., and Hogan, B.M. (2017). Vegfd modulates both angiogenesis and lymphangiogenesis during zebrafish embryonic development. Dev. *144*, 507–518.

Briot, A., Civelek, M., Seki, A., Hoi, K., Mack, J.J., Lee, S.D., Kim, J., Hong, C., Yu, J., Fishbein, G.A., et al. (2015). Endothelial NOTCH1 is suppressed by circulating lipids and antagonizes inflammation during atherosclerosis. J. Exp. Med. *212*, 2147–2163.

Brown, D., Samsa, L., Qian, L., and Liu, J. (2016). Advances in the Study of Heart Development and Disease Using Zebrafish. J. Cardiovasc. Dev. Dis. *3*, 13.

Brutsaert, D.L., and Andries, L.J. (1992). The endocardial endothelium. Am. J. Physiol. - Hear. Circ. Physiol. *263*.

Burkhard, S.B., and Bakkers, J. (2018). Spatially resolved RNA-sequencing of the embryonic heart identifies a role for Wnt/β-catenin signaling in autonomic control of heart rate. Elife *7*, 1–19.

Cai, C.L., Liang, X., Shi, Y., Chu, P.H., Pfaff, S.L., Chen, J., and Evans, S. (2003). Isl1 identifies a cardiac progenitor population that proliferates prior to differentiation and contributes a majority of cells to the heart. Dev. Cell *5*, 877–889.

Cai, X., Nomura-Kitabayashi, A., Cai, W., Yan, J., Christoffelsb, V.M., and Cai, C.-L. (2012). Myocardial Tbx20 regulates early atrioventricular canal formation and endocardial epithelial-mesenchymal transition via Bmp2. Dev Biol *360*, 381–390.

Camenisch, T.D., Spicer, A.P., Brehm-Gibson, T., Biesterfeldt, J., Augustine, M. Lou, Calabro, A., Kubalak, S., Klewer, S.E., and McDonald, J.A. (2000). Disruption of hyaluronan synthase-2 abrogates normal cardiac morphogenesis and hyaluronan-mediated transformation of epithelium to mesenchyme. J. Clin. Invest. *106*, 349–360.

Chakraborty, S., Wirrig, E.E., Hinton, R.B., Merrill, W.H., Spicer, D.B., and Yutzey, K.E. (2010). Twist1 promotes heart valve cell proliferation and extracellular matrix gene expression during development in vivo and is expressed in human diseased aortic valves. Dev. Biol. *347*, 167–179.

Chen, Y.H., Ishii, M., Sucov, H.M., and Maxson, R.E. (2008). Msx1 and Msx2 are required for endothelial-mesenchymal transformation of the atrioventricular cushions and patterning of the atrioventricular myocardium. BMC Dev. Biol. *8*, 75.

Chiplunkar, A.R., Lung, T.K., Alhashem, Y., Koppenhaver, B.A., Salloum, F.N., Kukreja, R.C., Haar, J.L., and Lloyd, J.A. (2013). Krüppel-Like Factor 2 Is Required for Normal Mouse Kru Cardiac Development. *8*.

Christoffels, V.M., Hoogaars, W.M.H., Tessari, A., Clout, D.E.W., Moorman, A.F.M., and Campione, M. (2004). T-Box Transcription Factor Tbx2 Represses Differentiation and Formation of the Cardiac Chambers. Dev. Dyn. *229*, 763–770.

Combs, M.D., and Yutzey, K.E. (2009). Heart valve development: Regulatory networks in development and disease. Circ. Res. *105*, 408–421.

Conway, D.E., Breckenridge, M.T., Hinde, E., Gratton, E., Chen, C.S., and Schwartz, M.A. (2013). Fluid shear stress on endothelial cells modulates mechanical tension across VE-cadherin and PECAM-1. Curr. Biol. *23*, 1024–1030.

Coon, B.G., Baeyens, N., Han, J., Budatha, M., Ross, T.D., Fang, J.S., Yun, S., Thomas, J.L., and Schwartz, M.A. (2015). Intramembrane binding of VE-cadherin to VEGFR2 and VEGFR3 assembles the endothelial mechanosensory complex. J. Cell Biol. *208*, 975–986.

Covassin, L.D., Villefranc, J. a, Kacergis, M.C., Weinstein, B.M., and Lawson, N.D. (2006). Distinct genetic interactions between multiple Vegf receptors are required for development of different blood vessel types in zebrafish. Proc. Natl. Acad. Sci. *103*, 6554–6559.

Davis, R.L., and Turner, D.L. (2001). Vertebrate hairy and Enhancer of split related proteins: Transcriptional repressors regulating cellular differentiation and embryonic patterning. Oncogene *20*, 8342–8357.

Dekker, R.J., Van Soest, S., Fontijn, R.D., Salamanca, S., De Groot, P.G., VanBavel, E., Pannekoek, H., and Horrevoets, A.J.G. (2002). Prolonged fluid shear stress induces a distinct set of endothelial cell genes, most specifically lung Krüppel-like factor (KLF2). Blood *100*, 1689–1698.

DeRuiter, M.C., Poelmann, R.E., VanderPlas-de Vries, I., Mentink, M.M.T., and Gittenberger-de Groot, A.C. (1992). The development of the myocardium and endocardium in mouse embryos - Fusion of two heart tubes? Anat. Embryol. (Berl). *185*, 461–473.

Diaz de la Loza, M.C., and Thompson, B.J. (2017). Forces shaping the Drosophila wing. Mech. Dev. *144*, 23–32.

Dietrich, A.-C., Lombardo, V.A., Veerkamp, J., Priller, F., and Abdelilah-Seyfried, S. (2014). Blood Flow and Bmp Signaling Control Endocardial Chamber Morphogenesis. Dev. Cell *30*, 367–377.

Ten Dijke, P., Egorova, A.D., Goumans, M.J.T.H., Poelmann, R.E., and Hierck, B.P. (2012). TGF-β signaling in endothelial-to-mesenchymal transition: The role of shear stress and primary cilia. In

Science Signaling, (Sci Signal), p.

Dixon, J.B., Greiner, S.T., Gashev, A.A., Cote, G.L., Moore, J.E., and Zawieja, D.C. (2006). Lymph flow, shear stress, and lymphocyte velocity in rat mesenteric prenodal lymphatics. Microcirculation *13*, 597–610.

Dobin, A., Davis, C.A., Schlesinger, F., Drenkow, J., Zaleski, C., Jha, S., Batut, P., Chaisson, M., and Gingeras, T.R. (2013). STAR: ultrafast universal RNA-seq aligner. Bioinformatics *29*, 15–21.

Donat, S., Lourenço, M., Paolini, A., Otten, C., Renz, M., and Abdelilah-Seyfried, S. (2018). Heg1 and Ccm1/2 proteins control endocardial mechanosensitivity during zebrafish valvulogenesis. Elife *7*, 1–22.

Duchemin, A.L., Vignes, H., and Vermot, J. (2019). Mechanically activated Piezo channels modulate outflow tract valve development through the yap1 and KLF2-notch signaling axis. Elife *8*.

Dumont, D.J., Jussila, L., Taipale, J., Lymboussaki, A., Mustonen, T., Pajusola, K., Breitman, M., and Alitalo, K. (1998). Cardiovascular failure in mouse embryos deficient in VEGF receptor-3. Science (80-.). *282*, 946–949.

Egorova, A.D., Khedoe, P.P.S.J., Goumans, M.J.T.H., Yoder, B.K., Nauli, S.M., Ten Dijke, P., Poelmann, R.E., and Hierck, B.P. (2011). Lack of primary cilia primes shear-induced endothelial-to-mesenchymal transition. Circ. Res. *108*, 1093–1101.

Eisenberg, L.M., and Markwald, R.R. (1995). Molecular regulation of atrioventricular valvuloseptal morphogenesis. Circ. Res. *77*, 1–6.

El-Brolosy, M.A., Kontarakis, Z., Rossi, A., Kuenne, C., Günther, S., Fukuda, N., Kikhi, K., Boezio, G.L.M., Takacs, C.M., Lai, S.L., et al. (2019). Genetic compensation triggered by mutant mRNA degradation. Nature *568*, 193–197.

Epstein, J.A., Aghajanian, H., and Singh, M.K. (2015). Semaphorin Signaling in Cardiovascular Development. Cell Metab. *21*, 163–173.

Faucherre, A., Moha ou Maati, H., Nasr, N., Pinard, A., Theron, A., Odelin, G., Desvignes, J.P., Salgado, D., Collod-béroud, G., Avierinos, J.F., et al. (2020). Piezo1 is required for outflow tract and aortic valve development. J. Mol. Cell. Cardiol. *143*, 51–62.

Fong, G.H., Rossant, J., Gertsenstein, M., and Breitman, M.L. (1995). Role of the Flt-1 receptor tyrosine kinase in regulating the assembly of vascular endothelium. Nature *376*, 66–70.

Fontana, F., Haack, T., Reichenbach, M., Knaus, P., Puceat, M., and Abdelilah-Seyfried, S. (2020). Antagonistic Activities of Vegfr3/Flt4 and Notch1b Fine-tune Mechanosensitive Signaling during

Zebrafish Cardiac Valvulogenesis. Cell Rep. *32*, 107883.

Gagnon, J.A., Valen, E., Thyme, S.B., Huang, P., Ahkmetova, L., Pauli, A., Montague, T.G., Zimmerman, S., Richter, C., and Schier, A.F. (2014). Efficient Mutagenesis by Cas9 Protein-Mediated Oligonucleotide Insertion and Large-Scale Assessment of Single-Guide RNAs. PLoS One *9*, e98186.

Galvagni, F., Pennacchini, S., Salameh, A., Rocchigiani, M., Neri, F., Orlandini, M., Petraglia, F., Gotta, S., Sardone, G.L., Matteucci, G., et al. (2010). Endothelial cell adhesion to the extracellular matrix induces c-Src-dependent VEGFR-3 phosphorylation without the activation of the receptor intrinsic kinase activity. Circ. Res. *106*, 1839–1848.

Garg, V., Muth, A.N., Ransom, J.F., Schluterman, M.K., Barnes, R., King, I.N., Grossfeld, P.D., and Srivastava, D. (2005). Mutations in NOTCH1 cause aortic valve disease. Nature *437*, 1–5.

Geng, X., Cha, B., Mahamud, M.R., Lim, K.C., Silasi-Mansat, R., Uddin, M.K.M., Miura, N., Xia, L., Simon, A.M., Engel, J.D., et al. (2016). Multiple mouse models of primary lymphedema exhibit distinct defects in lymphovenous valve development. Dev. Biol. *409*, 218–233.

Geng, X., Cha, B., Mahamud, M.R., and Srinivasan, R.S. (2017). Intraluminal valves: development, function and disease. Dis. Model. Mech. *10*, 1273–1287.

Givens, C., and Tzima, E. (2016). Endothelial Mechanosignaling: Does One Sensor Fit All? Antioxidants Redox Signal. *25*, 373–388.

Goddard, L.M., Duchemin, A.-L.L., Ramalingan, H., Wu, B., Chen, M., Bamezai, S., Yang, J., Li, L., Morley, M.P., Wang, T., et al. (2017). Hemodynamic Forces Sculpt Developing Heart Valves through a KLF2-WNT9B Paracrine Signaling Axis. Dev. Cell *0*, 1–16.

Goetz, J.G., Steed, E., Ferreira, R.R., Roth, S., Ramspacher, C., Boselli, F., Charvin, G., Liebling, M., Wyart, C., Schwab, Y., et al. (2014). Endothelial Cilia Mediate Low Flow Sensing during Zebrafish Vascular Development. Celrep *6*, 799–808.

Grego-Bessa, J., Luna-Zurita, L., del Monte, G., Bolós, V., Melgar, P., Arandilla, A., Garratt, A.N., Zang, H., Mukouyama, Y., Chen, H., et al. (2007). Notch Signaling Is Essential for Ventricular Chamber Development. Dev. Cell *12*, 415–429.

Groenendijk, B.C.W., Hierck, B.P., Vrolijk, J., Baiker, M., Pourquie, M.J.B.M., Gittenberger-De Groot, A.C., and Poelmann, R.E. (2005). Changes in shear stress-related gene expression after experimentally altered venous return in the chicken embryo. Circ. Res. *96*, 1291–1298.

Le Guen, L., Karpanen, T., Schulte, D., Harris, N.C., Koltowska, K., Roukens, G., Bower, N.I., van Impel, A., Stacker, S. a, Achen, M.G., et al. (2014). Ccbe1 regulates Vegfc-mediated induction of Vegfr3 signaling during embryonic lymphangiogenesis. Development *141*, 1239–1249.

Gunawan, F., Gentile, A., Fukuda, R., Tsedeke, A.T., Jiménez-Amilburu, V., Ramadass, R., Iida, A., Sehara-Fujisawa, A., and Stainier, D.Y.R. (2019). Focal adhesions are essential to drive zebrafish heart valve morphogenesis. J. Cell Biol. *218*, 1039–1054.

Gunawan, F., Gentile, A., Gauvrit, S., Stainier, D.Y.R.R., and Bensimon-Brito, A. (2020). Nfatc1 Promotes Interstitial Cell Formation During Cardiac Valve Development in Zebrafish. Circ. Res. *126*, 968–984.

Haack, T., and Abdelilah-Seyfried, S. (2016). The force within: Endocardial development, mechanotransduction and signalling during cardiac morphogenesis. Dev. *143*, 373–386.

Haga, J.H., Li, Y.S.J., and Chien, S. (2007). Molecular basis of the effects of mechanical stretch on vascular smooth muscle cells. J. Biomech. *40*, 947–960.

Hägerling, R., Pollmann, C., Andreas, M., Schmidt, C., Nurmi, H., Adams, R.H., Alitalo, K., Andresen, V., Schulte-Merker, S., and Kiefer, F. (2013). A novel multistep mechanism for initial lymphangiogenesis in mouse embryos based on ultramicroscopy. EMBO J. *32*, 629–644.

Hahn, C., and Schwartz, M.A. (2009). Mechanotransduction in vascular physiology and atherogenesis. Nat. Rev. Mol. Cell Biol. *10*, 53–62.

Haiko, P., Makinen, T., Keskitalo, S., Taipale, J., Karkkainen, M.J., Baldwin, M.E., Stacker, S.A., Achen, M.G., and Alitalo, K. (2008). Deletion of Vascular Endothelial Growth Factor C (VEGF-C) and VEGF-D Is Not Equivalent to VEGF Receptor 3 Deletion in Mouse Embryos. Mol. Cell. Biol. *28*, 4843–4850.

Hajdu, Z., Romeo, S.J., Fleming, P.A., Markwald, R.R., Visconti, R.P., and Drake, C.J. (2011). Recruitment of bone marrow-derived valve interstitial cells is a normal homeostatic process. J. Mol. Cell. Cardiol. *51*, 955–965.

Heckel, E., Boselli, F., Roth, S., Krudewig, A., Belting, H.G., Charvin, G., Vermot, J., Krudewig, A., and Belting, H.G. (2015). Oscillatory flow modulates mechanosensitive klf2a expression through trpv4 and trpp2 during heart valve development. Curr. Biol. *25*, 1354–1361.

Heinolainen, K., Karaman, S., D'Amico, G., Tammela, T., Sormunen, R., Eklund, L., Alitalo, K., and Zarkada, G. (2017). VEGFR3 Modulates Vascular Permeability by Controlling VEGF/VEGFR2 Signaling. Circ. Res. *120*, 1414–1425.

Helker, C.S.M., Schuermann, A., Karpanen, T., Zeuschner, D., Belting, H.G., Affolter, M., Schulte-Merker, S., and Herzog, W. (2013). The zebrafish common cardinal veins develop by a novel mechanism: Lumen ensheathment. Dev. *140*, 2776–2786.

Hellström, M., Phng, L.K., Hofmann, J.J., Wallgard, E., Coultas, L., Lindblom, P., Alva, J., Nilsson,

A.K., Karlsson, L., Gaiano, N., et al. (2007). Dll4 signalling through Notch1 regulates formation of tip cells during angiogenesis. Nature *445*, 776–780.

Herwig, L., Blum, Y., Krudewig, A., Ellertsdottir, E., Lenard, A., Belting, H.-G., and Affolter, M. (2011). Distinct Cellular Mechanisms of Blood Vessel Fusion in the Zebrafish Embryo. Curr. Biol. *21*, 1942–1948.

Hierck, B.P., Van Der Heiden, K., Poelma, C., Westerweel, J., and Poelmann, R.E. (2008a). Fluid shear stress and inner curvature remodeling of the embryonic heart. Choosing the right lane! Sci. World J. *8*, 212–222.

Hierck, B.P., Van Der Heiden, K., Alkemade, F.E., Van De Pas, S., Van Thienen, J. V., Groenendijk, B.C.W., Bax, W.H., Van Der Laarse, A., DeRuiter, M.C., Horrevoets, A.J.G., et al. (2008b). Primary cilia sensitize endothelial cells for fluid shear stress. Dev. Dyn. *237*, 725–735.

High, F.A., Jain, R., Stoller, J.Z., Antonucci, N.B., Min, M.L., Loomes, K.M., Kaestner, K.H., Pear, W.S., and Epstein, J.A. (2009). Murine Jagged1/Notch signaling in the second heart field orchestrates Fgf8 expression and tissue-tissue interactions during outflow tract development. J. Clin. Invest. *119*, 1986–1996.

Hinton, R.B., and Yutzey, K.E. (2011). Heart Valve Structure and Function in Development and Disease. Annu. Rev. Physiol. *73*, 29–46.

Hofmann, J.J., and Iruela-Arispe, M.L. (2007). Notch signaling in blood vessels: Who is talking to whom about what? Circ. Res. *100*, 1556–1568.

Hogan, B.M., Bos, F.L., Bussmann, J., Witte, M., Chi, N.C., Duckers, H.J., and Schulte-Merker, S. (2009a). Ccbe1 is required for embryonic lymphangiogenesis and venous sprouting. Nat. Genet. *41*, 396–398.

Hogan, B.M., Herpers, R., Witte, M., Heloterä, H., Alitalo, K., Duckers, H.J., and Schulte-Merker, S. (2009b). Vegfc/Flt4 signalling is suppressed by Dll4 in developing zebrafish intersegmental arteries. Development *136*, 4001–4009.

Hove, J.R., Köster, R.W., Forouhar, A.S., Acevedo-Bolton, G., Fraser, S.E., and Gharib, M. (2003). Intracardiac fluid forces are an essential epigenetic factor for embryonic cardiogenesis. Nature *421*, 172–177.

Huang, D.W., Sherman, B.T., and Lempicki, R.A. (2009). Systematic and integrative analysis of large gene lists using DAVID bioinformatics resources. Nat. Protoc. *4*, 44–57.

Hurlstone, A.F.L., Haramis, A.P.G., Wienholds, E., Begthel, H., Korving, J., Van Eeden, F., Cuppen, E., Zivkovic, D., Plasterk, R.H.A., and Clevers, H. (2003). The Wnt/β-catenin pathway regulates

cardiac valve formation. Nature *425*, 633–637.

Huynh, C., Poliseno, L., Segura, M.F., Medicherla, R., Haimovic, A., Menendez, S., Shang, S., Pavlick, A., Shao, Y., Darvishian, F., et al. (2011). The Novel Gamma Secretase Inhibitor RO4929097 Reduces the Tumor Initiating Potential of Melanoma. PLoS One *6*, e25264.

van Impel, A., Zhao, Z., Hermkens, D.M.A., Roukens, M.G., Fischer, J.C., Peterson-Maduro, J., Duckers, H., Ober, E. a, Ingham, P.W., and Schulte-Merker, S. (2014). Divergence of zebrafish and mouse lymphatic cell fate specification pathways. Dev. *141*, 1228–1238.

Iomini, C., Tejada, K., Mo, W., Vaananen, H., and Piperno, G. (2004). Primary cilia of human endothelial cells disassemble under laminar shear stress. J. Cell Biol. *164*, 811–817.

Jakobsson, L., Franco, C.A., Bentley, K., Collins, R.T., Ponsioen, B., Aspalter, I.M., Rosewell, I., Busse, M., Thurston, G., Medvinsky, A., et al. (2010). Endothelial cells dynamically compete for the tip cell position during angiogenic sprouting. Nat. Cell Biol. *12*, 943–953.

Jarrell, Lennon, and Jacot (2019). Epigenetics and Mechanobiology in Heart Development and Congenital Heart Disease. Diseases *7*, 52.

Jeltsch, M., Kaipainen, A., Joukov, V., Meng, X., Lakso, M., Rauvala, H., Swartz, M., Fukumura, D., Jain, R.K., and Alitalo, K. (1997). Hyperplasia of Lymphatic Vessels in VEGF-C Transgenic Mice. Science (80-.). *276*, 1423–1425.

Jin, S.-W., Beis, D., Mitchell, T., Chen, J.-N., and Stainier, D.Y.R. (2005). Cellular and molecular analyses of vascular tube and lumen formation in zebrafish. Development *132*, 5199–5209.

Jin, S.C., Homsy, J., Zaidi, S., Lu, Q., Morton, S., Depalma, S.R., Zeng, X., Qi, H., Chang, W., Sierant, M.C., et al. (2017). Contribution of rare inherited and de novo variants in 2,871 congenital heart disease probands. Nat. Genet. *49*, 1593–1601.

Jin, Z.G., Ueba, H., Tanimoto, T., Lungu, A.O., Frame, M.D., and Berk, B.C. (2003). Ligand-independent activation of vascular endothelial growth factor receptor 2 by fluid shear stress regulates activation of endothelial nitric oxide synthase. Circ. Res. *93*, 354–363.

Joukov, V., Pajusola, K., Kaipainen, A., Chilov, D., Lahtinen, I., Kukk, E., Saksela, O., Kalkkinen, N., and Alitalo, K. (1996). A novel vascular endothelial growth factor, VEGF-C, is a ligand for the Flt4 (VEGFR-3) and KDR (VEGFR-2) receptor tyrosine kinases. EMBO J. *15*, 290–298.

Joukov, V., Sorsa, T., Kumar, V., Jeltsch, M., Claesson-Welsh, L., Cao, Y., Saksela, O., Kalkkinen, N., and Alitalo, K. (1997). Proteolytic processing regulates receptor specificity and activity of VEGF-C. EMBO J. *16*, 3898–3911.

Just, S., Berger, I.M., Meder, B., Backs, J., Keller, A., Marquart, S., Frese, K., Patzel, E., Rauch, G.J., Katus, H.A., et al. (2011). Protein kinase D2 controls cardiac valve formation in zebrafish by regulating histone deacetylase 5 activity. Circulation *124*, 324–334.

Kaipainen, A., Korhonen, J., Mustonen, T., van Hinsbergh, V.W., Fang, G.H., Dumont, D., Breitman, M., and Alitalo, K. (1995). Expression of the fms-like tyrosine kinase 4 gene becomes restricted to lymphatic endothelium during development. Proc. Natl. Acad. Sci. U. S. A. *92*, 3566–3570.

Kalogirou, S., Malissovas, N., Moro, E., Argenton, F., Stainier, D.Y.R., and Beis, D. (2014). Intracardiac flow dynamics regulate atrioventricular valve morphogenesis. Cardiovasc. Res. *104*, 49–60.

Karaman, S., Leppänen, V.M., and Alitalo, K. (2018). Vascular endothelial growth factor signaling in development and disease. Dev. *145*, 1–8.

Karkkainen, M.J., Haiko, P., Sainio, K., Partanen, J., Taipale, J., Petrova, T. V, Jeltsch, M., Jackson, D.G., Talikka, M., Rauvala, H., et al. (2004). Vascular endothelial growth factor C is required for sprouting of the first lymphatic vessels from embryonic veins. Nat. Immunol. *5*, 74–80.

Kasey, J.T., Jinah, B., Calvo, C., Nurmi, H., Eichmann, A.C., Alitalo, K., Thomas, J.L., Baker, K., Han, J., Calvo, C., et al. (2013). Interactions between VEGFR and Notch signaling pathways in endothelial and neural cells. Cell. Mol. Life Sci. *70*, 1779–1792.

Keegan, B.R., Feldman, J.L., Begemann, G., Ingham, P.W., and Yelon, D. (2005). Retinoic acid signaling restricts the cardiac progenitor pool. Science (80-.). *307*, 247–249.

Kelly, R.G., Brown, N.A., and Buckingham, M.E. (2001). The Arterial Pole of the Mouse Heart Forms from Fgf10-Expressing Cells in Pharyngeal Mesoderm. Dev. Cell *1*, 435–440.

Koefoed, K., Veland, I.R., Pedersen, L.B., Larsen, L.A., and Christensen, S.T. (2014). Cilia and coordination of signaling networks during heart development. Organogenesis *10*, 108–125.

Kok, F.O.O., Shin, M., Ni, C.-W.W., Gupta, A., Grosse, A.S.S., van Impel, A., Kirchmaier, B.C.C., Peterson-Maduro, J., Kourkoulis, G., Male, I., et al. (2014). Reverse Genetic Screening Reveals Poor Correlation between Morpholino-Induced and Mutant Phenotypes in Zebrafish. Dev. Cell *32*, 97–108.

Kovacic, J., Dimmeler, S., Harvey, R., Finkel, T., Aikawa, E., Krenning, G., and Baker, A.H. (2019). Endothelial to Mesenchymal Transition in Cardiovascular Disease. J. Am. Coll. Cardiol. *73*.

Küchler, A.M., Gjini, E., Peterson-Maduro, J., Cancilla, B., Wolburg, H., and Schulte-Merker, S. (2006). Development of the Zebrafish Lymphatic System Requires Vegfc Signaling. Curr. Biol. *16*, 1244–1248.

Kumai, M., Nishii, K., Nakamura, K.I., Takeda, N., Suzuki, M., and Shibata, Y. (2000). Loss of connexin45 causes a cushion defect in early cardiogenesis. Development *127*, 3501–3512.

Kwon, C., Qian, L., Cheng, P., Nigam, V., Arnold, J., and Srivastava, D. (2009). A regulatory pathway involving Notch1/β-catenin/Isl1 determines cardiac progenitor cell fate. Nat. Cell Biol. *11*, 951–957.

Kwon, H.B., Wang, S., Helker, C.S., Rasouli, S.J., Maischein, H.M., Offermanns, S., Herzog, W., and Stainier, D.Y. (2016). In vivo modulation of endothelial polarization by Apelin receptor signalling. Nat Commun *7*, 11805.

Lagendijk, A.K., Goumans, M.J., Burkhard, S.B., and Bakkers, J. (2011). MicroRNA-23 restricts cardiac valve formation by inhibiting has2 and extracellular hyaluronic acid production. Circ. Res. *109*, 649–657.

Lai, J.K.H., Gagalova, K.K., Kuenne, C., El-Brolosy, M.A., and Stainier, D.Y.R. (2019). Induction of interferon-stimulated genes and cellular stress pathways by morpholinos in zebrafish. Dev. Biol. *454*, 21–28.

Lawson, N.D., Scheer, N., Pham, V.N., Kim, C.H., Chitnis, A.B., Campos-Ortega, J.A., and Weinstein, B.M. (2001). Notch signaling is required for arterial-venous differentiation during embryonic vascular development. Development *128*, 3675–3683.

Lee, J.S., Yu, Q., Shin, J.T., Sebzda, E., Bertozzi, C., Chen, M., Mericko, P., Stadtfeld, M., Zhou, D., Cheng, L., et al. (2006). Klf2 Is an Essential Regulator of Vascular Hemodynamic Forces In Vivo. Dev. Cell *11*, 845–857.

Leung, D.W., Cachianes, G., Kuang, W.J., Goeddel, D. V., and Ferrara, N. (1989). Vascular endothelial growth factor is a secreted angiogenic mitogen. Science (80-.). *246*, 1306–1309.

Levesque, M.J., and Nerem, R.M. (1985). The elongation and orientation of cultured endothelial cells in response to shear stress. J. Biomech. Eng. *107*, 341–347.

Lewis, J. (1998). Notch signalling and the control of cell fate choices in vertebrates. Semin. Cell Dev. Biol. *9*, 583–589.

Li, J., Hou, B., Tumova, S., Muraki, K., Bruns, A., Ludlow, M.J., Sedo, A., Hyman, A.J., McKeown, L., Young, R.S., et al. (2014). Piezo1 integration of vascular architecture with physiological force. Nature *515*, 279–282.

Li, X., Zhao, X., Fang, Y., Jiang, X., Duong, T., Fan, C., Huang, C.C., and Kain, S.R. (1998). Generation of destabilized green fluorescent protein as a transcription reporter. J. Biol. Chem. *273*, 34970–34975.

Lin, C.-J., Lin, C.-Y., Chen, C.-H., Zhou, B., and Chang, C.-P. (2012a). Partitioning the heart: mechanisms of cardiac septation and valve development. Development *139*, 3277–3299.

Lin, Y.F., Swinburne, I., and Yelon, D. (2012b). Multiple influences of blood flow on cardiomyocyte hypertrophy in the embryonic zebrafish heart. Dev. Biol. *362*, 242–253.

Lindsey, S.E., and Butcher, J.T. (2011). The cycle of form and function in cardiac valvulogenesis. Aswan Hear. Cent. Sci. Pract. Ser. *2011*, 10.

Lipowsky, H.H., Kovalcheck, S., and Zweifach, B.W. (1978). The distribution of blood rheological parameters in the microvasculature of cat mesentery. Circ. Res. *43*, 738–749.

Liu, J., Bressan, M., Hassel, D., Huisken, J., Staudt, D., Kikuchi, K., Poss, K.D., Mikawa, T., and Stainier, D.Y.R. (2010). A dual role for ErbB2 signaling in cardiac trabeculation. Development *137*, 3867–3875.

Liu, X., Pasula, S., Song, H., Tessneer, K.L., Dong, Y., Hahn, S., Yago, T., Brophy, M., Chang, B., Cai, X., et al. (2014). Temporal and Spatial Regulation of Epsin Abundance and VEGFR3 Signaling are Required for Lymphatic Valve Formation and Function. Sci Signal *7*.

Livak, K.J., and Schmittgen, T.D. (2001). Analysis of Relative Gene Expression Data Using Real-Time Quantitative PCR and the 2−ΔΔCT Method. Methods *25*, 402–408.

Lobov, I.B., Renard, R.A., Papadopoulos, N., Gale, N.W., Thurston, G., Yancopoulos, G.D., and Wiegand, S.J. (2007). Delta-like ligand 4 (DII4) is induced by VEGF as a negative regulator of angiogenic sprouting. Proc. Natl. Acad. Sci. U. S. A. *104*, 3219–3224.

Lockhart, M., Wirrig, E., Phelps, A., and Wessels, A. (2011). Extracellular matrix and heart development. Birth Defects Res. A. Clin. Mol. Teratol. *91*, 535–550.

Lombardo, V.A., Otten, C., and Abdelilah-Seyfried, S. (2015). Large-scale Zebrafish Embryonic Heart Dissection for Transcriptional Analysis. J. Vis. Exp. *95*, 52087.

Ma, L., Lu, M.-F., Schwartz, R.J., and Martin, J.F. (2005). Bmp2 is essential for cardiac cushion epithelial-mesenchymal transition and myocardial patterning. Development *132*, 5601–5611.

Macgrogan, D., Luxán, G., Driessen-Mol, A., Bouten, C., Baaijens, F., and De La Pompa, J.L. (2014). How to make a heart valve: From embryonic development to bioengineering of living valve substitutes. Cold Spring Harb. Perspect. Med. *4*.

MacGrogan, D., D'Amato, G., Travisano, S., Martinez-Poveda, B., Luxán, G., Del Monte-Nieto, G., Papoutsi, T., Sbroggio, M., Bou, V., Gomez-Del Arco, P., et al. (2016). Sequential Ligand-Dependent Notch Signaling Activation Regulates Valve Primordium Formation and Morphogenesis. Circ. Res.

118, 1480–1497.

MacGrogan, D., Münch, J., and de la Pompa, J.L. (2018). Notch and interacting signalling pathways in cardiac development, disease, and regeneration. Nat. Rev. Cardiol. *15*, 685–704.

Mack, J.J., and Iruela-Arispe, M.L. (2018). NOTCH regulation of the endothelial cell phenotype. Curr. Opin. Hematol. *25*, 212–218.

Mack, J.J., Mosqueiro, T.S., Archer, B.J., Jones, W.M., Sunshine, H., Faas, G.C., Briot, A., Aragón, R.L., Su, T., Romay, M.C., et al. (2017). NOTCH1 is a mechanosensor in adult arteries. Nat. Commun. *8*, 1620.

Maglione, D., Guerriero, V., Viglietto, G., Delli-Bovi, P., and Persico, M.G. (1991). Isolation of a human placenta cDNA coding for a protein related to the vascular permeability factor. Proc. Natl. Acad. Sci. U. S. A. *88*, 9267–9271.

Mahler, G.J., Frendl, C.M., Cao, Q., and Butcher, J.T. (2014). Effects of shear stress pattern and magnitude on mesenchymal transformation and invasion of aortic valve endothelial cells. Biotechnol. Bioeng. *111*, 2326–2337.

Mahmoud, M.M., Serbanovic-Canic, J., Feng, S., Souilhol, C., Xing, R., Hsiao, S., Mammoto, A., Chen, J., Ariaans, M., Francis, S.E., et al. (2017). Shear stress induces endothelial-to-mesenchymal transition via the transcription factor Snail. Sci. Rep. *7*, 3375.

Martin, R.T., and Bartman, T. (2009). Analysis of heart valve development in larval zebrafish. Dev. Dyn. *238*, 1796–1802.

Matthews, W., Jordan, C.T., Wiegand, G.W., Pardoll, D., and Lemischka, I.R. (1991). A receptor tyrosine kinase specific to hematopoietic stem and progenitor cell-enriched populations. Cell *65*, 1143–1152.

McColl, B.K., Baldwin, M.E., Roufail, S., Freeman, C., Moritz, R.L., Simpson, P.J., Alitalo, K., Stacker, S.A., and Achen, M.G. (2003). Plasmin activates the lymphangiogenic growth factors VEGF-C and VEGF-D. J. Exp. Med. *198*, 863–868.

McColl, B.K., Paavonen, K., Karnezis, T., Harris, N.C., Davydova, N., Rothacker, J., Nice, E.C., Harder, K.W., Roufail, S., Hibbs, M.L., et al. (2007). Proprotein convertases promote processing of VEGF-D, a critical step for binding the angiogenic receptor VEGFR-2. FASEB J. *21*, 1088–1098.

Mehta, V., Pang, K.L., Rozbesky, D., Nather, K., Keen, A., Lachowski, D., Kong, Y., Karia, D., Ameismeier, M., Huang, J., et al. (2020). The guidance receptor plexin D1 is a mechanosensor in endothelial cells. Nature *578*, 290–295.

Mickoleit, M., Schmid, B., Weber, M., Fahrbach, F.O., Hombach, S., Reischauer, S., and Huisken, J. (2014). High-resolution reconstruction of the beating zebrafish heart. Nat. Methods *11*, 919–922.

Moorman, A.F.M., and Christoffels, V.M. (2003). Cardiac chamber formation: Development, genes, and evolution. Physiol. Rev. *83*, 1223–1267.

Moro, E., Ozhan-Kizil, G., Mongera, A., Beis, D., Wierzbicki, C., Young, R.M., Bournele, D., Domenichini, A., Valdivia, L.E., Lum, L., et al. (2012). In vivo Wnt signaling tracing through a transgenic biosensor fish reveals novel activity domains. Dev. Biol. *366*, 327–340.

Munch, J., Gonzalez-Rajal, A., and de la Pompa, J.L. (2013). Notch regulates blastema proliferation and prevents differentiation during adult zebrafish fin regeneration. Development *140*, 1402–1411.

Münch, J., Grivas, D., González-Rajal, Á., Torregrosa-Carrión, R., and de la Pompa, J.L. (2017). Notch signalling restricts inflammation and serpine1 expression in the dynamic endocardium of the regenerating zebrafish heart. Development *144*, 1425–1440.

Nakamura, T., Colbert, M.C., and Robbins, J. (2006). Neural Crest Cells Retain Multipotential Characteristics in the Developing Valves and Label the Cardiac Conduction System. Circ. Res. *98*, 1547–1554.

Nicoli, S., Standley, C., Walker, P., Hurlstone, A., Fogarty, K.E., and Lawson, N.D. (2010). MicroRNA-mediated integration of haemodynamics and Vegf signalling during angiogenesis. Nature *464*, 1196–1200.

Niessen, K., and Karsan, A. (2007). Notch signaling in the developing cardiovascular system. Am. J. Physiol. Physiol. *293*, C1–C11.

Niessen, K., and Karsan, A. (2008). Notch signaling in cardiac development. Circ. Res. *102*, 1169–1181.

Ninov, N., Borius, M., and Stainier, D.Y.R. (2012). Different levels of Notch signaling regulate quiescence , renewal and differentiation in pancreatic endocrine progenitors. *1567*, 1557–1567.

le Noble, F., Klein, C., Tintu, A., Pries, A., and Buschmann, I. (2008). Neural guidance molecules, tip cells, and mechanical factors in vascular development. Cardiovasc. Res. *78*, 232–241.

Noria, S., Cowan, D.B., Gotlieb, A.I., and Langille, B.L. (1999). Transient and steady-state effects of shear stress on endothelial cell adherens junctions. Circ. Res. *85*, 504–514.

Norrmén, C., Ivanov, K.I., Cheng, J., Zangger, N., Delorenzi, M., Jaquet, M., Miura, N., Puolakkainen, P., Horsley, V., Hu, J., et al. (2009). FOXC2 controls formation and maturation of lymphatic collecting vessels through cooperation with NFATc1. J. Cell Biol. *185*, 439–457.

Novodvorsky, P., and Chico, T.J.A. (2014). The role of the transcription factor KLF2 in vascular development and disease. In Progress in Molecular Biology and Translational Science, (Elsevier Inc.), pp. 155–188.

Novodvorsky, P., Watson, O., Gray, C., Wilkinson, R.N., Reeve, S., Smythe, C., Beniston, R., Plant, K., Maguire, R., M. K. Rothman, A., et al. (2015). klf2ash317 Mutant Zebrafish Do Not Recapitulate Morpholino-Induced Vascular and Haematopoietic Phenotypes. PLoS One *10*, e0141611.

Oates, A.C., Pratt, S.J., Vail, B., Yan, Y., Ho, R.K., Johnson, S.L., Postlethwait, J.H., and Zon, L.I. (2001). The zebrafish klf gene family. *98*, 1792–1801.

Ober, E.A., Olofsson, B., Makinen, T., Jin, S., Shoji, W., Koh, G.Y., Alitalo, K., and Stainier, D.Y.R. (2004). Vegfc is required for vascular development and endoderm morphogenesis in zebrafish. EMBO Rep. *5*.

Ohnesorge, N., Viemann, D., Schmidt, N., Czymai, T., Spiering, D., Schmolke, M., Ludwig, S., Roth, J., Goebeler, M., and Schmidt, M. (2010). Erk5 Activation Elicits a Vasoprotective Endothelial Phenotype via Induction of Krüppel-like Factor 4 (KLF4). J. Biol. Chem. *285*, 26199–26210.

Olofsson, B., Pajusola, K., Kaipainen, A., von Euler, G., Joukov, V., Saksela, O., Orpana, A., Pettersson, R.F., Alitalo, K., and Eriksson, U. (1996). Vascular endothelial growth factor B, a novel growth factor for endothelial cells. Proc. Natl. Acad. Sci. U. S. A. *93*, 2576–2581.

Olsson, A.K., Dimberg, A., Kreuger, J., and Claesson-Welsh, L. (2006). VEGF receptor signalling - In control of vascular function. Nat. Rev. Mol. Cell Biol. *7*, 359–371.

Otten, C., Knox, J., Boulday, G., Eymery, M., Haniszewski, M., Neuenschwander, M., Radetzki, S., Vogt, I., Hähn, K., De Luca, C., et al. (2018). Systematic pharmacological screens uncover novel pathways involved in cerebral cavernous malformations. EMBO Mol. Med. *10*, 1–17.

Paolini, A., and Abdelilah-Seyfried, S. (2018). The mechanobiology of zebrafish cardiac valve leaflet formation. Curr. Opin. Cell Biol. *55*, 52–58.

Paquet-Fifield, S., Levy, S.M., Sato, T., Shayan, R., Karnezis, T., Davydova, N., Nowell, C.J., Roufail, S., Ma, G.Z.M., Zhang, Y.F., et al. (2013). Vascular endothelial growth factor-d modulates caliber and function of initial lymphatics in the dermis. J. Invest. Dermatol. *133*, 2074–2084.

Park, J.E., Chen, H.H., Winer, J., Houck, K.A., and Ferrara, N. (1994). Placenta growth factor. Potentiation of vascular endothelial growth factor bioactivity, in vitro and in vivo, and high affinity binding to Flt-1 but not to Flk-1/KDR. J. Biol. Chem. *269*, 25646–25654.

Park, Y.G., Choi, J., Jung, H.K., Song, I.K.N.K.Y.U.N.K.Y.U.N.K.Y.U., Shin, Y., Park, S.Y., and Seol, J.W. (2017). Fluid shear stress regulates vascular remodeling via VEGFR-3 activation, although

independently of its ligand, VEGF-C, in the uterus during pregnancy. Int. J. Mol. Med. *40*, 1210–1216.

Parmar, K.M., Larman, H.B., Dai, G., Zhang, Y., Wang, E.T., Moorthy, S.N., Kratz, J.R., Lin, Z., Jain, M.K., Gimbrone, M.A., et al. (2006). Integration of flow-dependent endothelial phenotypes by Kruppel-like factor 2. J. Clin. Invest. *116*, 49–58.

Paz, N.G., Walshe, T.E., Leach, L.L., Saint-geniez, M., Amore, P.A.D., dela Paz, N.G., Walshe, T.E., Leach, L.L., Saint-geniez, M., D'Amore, P.A., et al. (2012). Role of shear-stress-induced VEGF expression in endothelial cell survival. J. Cell Sci. *125*, 831–843.

dela Paz, N.G., Melchior, B., and Frangos, J.A. (2013). Early VEGFR2 activation in response to flow is VEGF-dependent and mediated by MMP activity. Biochem. Biophys. Res. Commun. *434*, 641–646.

Pestel, J., Ramadass, R., Gauvrit, S., Helker, C., Herzog, W., and Stainier, D.Y.R. (2016). Real-time 3D visualization of cellular rearrangements during cardiac valve formation. Development *143*, 2217–2227.

Planas-Paz, L., Strilić, B., Goedecke, A., Breier, G., Fässler, R., and Lammert, E. (2012). Mechanoinduction of lymph vessel expansion. EMBO J. *31*, 788–804.

Polacheck, W.J., Kutys, M.L., Yang, J., Eyckmans, J., Wu, Y., Vasavada, H., Hirschi, K.K., and Chen, C.S. (2017). A non-canonical Notch complex regulates adherens junctions and vascular barrier function. Nature *552*, 258–262.

Pompa, L. De, D'Amato, G., Luxán, G., and de la Pompa, J.L. (2016). Notch signalling in ventricular chamber development and cardiomyopathy. FEBS J.

Ranade, S.S., Qiu, Z., Woo, S.-H., Hur, S.S., Murthy, S.E., Cahalan, S.M., Xu, J., Mathur, J., Bandell, M., Coste, B., et al. (2014). Piezo1, a mechanically activated ion channel, is required for vascular development in mice. Proc. Natl. Acad. Sci. *111*, 10347–10352.

Rasouli, S.J., El-Brolosy, M., Tsedeke, A.T., Bensimon-Brito, A., Ghanbari, P., Maischein, H.-M.M., Kuenne, C., and Stainier, D.Y. (2018). The flow responsive transcription factor Klf2 is required for myocardial wall integrity by modulating Fgf signaling. Elife *7*, 1–70.

Raya, A., Koth, C.M., Büscher, D., Kawakami, Y., Itoh, T., Raya, R.M., Sternik, G., Tsai, H.-J., Rodríguez-Esteban, C., and Izpisúa-Belmonte, J.C. (2003). Activation of Notch signaling pathway precedes heart regeneration in zebrafish. Proc. Natl. Acad. Sci. U. S. A. *100 Suppl*, 11889–11895.

Renshaw, M.W., Price, L.S., and Schwartz, M.A. (1999). Focal adhesion kinase mediates the integrin signaling requirement for growth factor activation of MAP kinase. J. Cell Biol. *147*, 611–618.

Renz, M., Otten, C., Faurobert, E., Rudolph, F., Zhu, Y., Boulday, G., Duchene, J., Mickoleit, M., Dietrich, A.-C., Ramspacher, C., et al. (2015). Regulation of β1 Integrin-Klf2-Mediated Angiogenesis by CCM Proteins. Dev. Cell *32*, 181–190.

Reuter, M.S., Jobling, R., Chaturvedi, R.R., Manshaei, R., Costain, G., Heung, T., Curtis, M., Hosseini, S.M., Liston, E., Lowther, C., et al. (2018). Haploinsufficiency of vascular endothelial growth factor related signaling genes is associated with tetralogy of Fallot. Genet. Med. *0*.

Roca, C., and Adams, R.H. (2007). Regulation of vascular morphogenesis by Notch signaling. Genes Dev. *21*, 2511–2524.

Rohr, S., Otten, C., and Abdelilah-Seyfried, S. (2008). Asymmetric Involution of the Myocardial Field Drives Heart Tube Formation in Zebrafish. Circ. Res. *102*, e12-9.

Roman, B.L., Pham, V.N., Lawson, N.D., Kulik, M., Childs, S., Lekven, A.C., Garrity, D.M., Moon, R.T., Fishman, M.C., Lechleider, R.J., et al. (2002). Disruption of acvrl1 increases endothelial cell number in zebrafish cranial vessels. Development *129*, 3009–3019.

Rossi, A., Kontarakis, Z., Gerri, C., Nolte, H., Hölper, S., Krüger, M., and Stainier, D.Y.R. (2015). Genetic compensation induced by deleterious mutations but not gene knockdowns. Nature.

Rutenberg, J.B., Fischer, A., Jia, H., Gessler, M., Zhong, T.P., and Mercola, M. (2006). Developmental patterning of the cardiac atrioventricular canal by Notch and Hairy-related transcription factors. Development *133*, 4381–4390.

Saad, S., Stanners, S.R., Yong, R., Tang, O., and Pollock, C.A. (2010). Notch mediated epithelial to mesenchymal transformation is associated with increased expression of the Snail transcription factor. Int. J. Biochem. Cell Biol. *42*, 1115–1122.

Sabine, A., Agalarov, Y., Maby-ElHajjami, H., Jaquet, M., Hägerling, R., Pollmann, C., Bebber, D., Pfenniger, A., Miura, N., Dormond, O., et al. (2012). Mechanotransduction, PROX1, and FOXC2 Cooperate to Control Connexin37 and Calcineurin during Lymphatic-Valve Formation. Dev. Cell *22*, 430–445.

Samsa, L.A., Yang, B., and Liu, J. (2013). Embryonic cardiac chamber maturation: Trabeculation, conduction, and cardiomyocyte proliferation. Am. J. Med. Genet. Part C Semin. Med. Genet. *163*, 157–168.

Samsa, L.A., Givens, C., Tzima, E., Stainier, D.Y.R., Qian, L., and Liu, J. (2015). Cardiac contraction activates endocardial Notch signaling to modulate chamber maturation in zebrafish. Development *142*, 4080–4091.

Scheer, N., and Campos-Ortega, J.A. (1999). Use of the Gal4-UAS technique for targeted gene

expression in the zebrafish. Mech. Dev. *80*, 153–158.

Scherz, P.J., Huisken, J., Sahai-Hernandez, P., and Stainier, D.Y.R. (2008). High-speed imaging of developing heart valves reveals interplay of morphogenesis and function. Development *135*, 1179–1187.

Schindelin, J., Arganda-Carreras, I., Frise, E., Kaynig, V., Longair, M., Pietzsch, T., Preibisch, S., Rueden, C., Saalfeld, S., Schmid, B., et al. (2012). Fiji: an open-source platform for biological-image analysis. Nat. Methods *9*, 676–682.

Schoenebeck, J.J., Keegan, B.R., and Yelon, D. (2007). Vessel and blood specification override cardiac potential in anterior mesoderm. Dev. Cell *13*, 254–267.

Sedmera, D., Pexieder, T., Rychterova, V., Hu, N., and Clark, E.B. (1999). Remodeling of chick embryonic ventricular myoarchitecture under experimentally changed loading conditions. Anat. Rec. *254*, 238–252.

Seebach, J., Donnert, G., Kronstein, R., Werth, S., Wojciak-Stothard, B., Falzarano, D., Mrowietz, C., Hell, S.W., and Schnittler, H.J. (2007). Regulation of endothelial barrier function during flow-induced conversion to an arterial phenotype. Cardiovasc. Res. *75*, 596–607.

Sehnert, A., Hug, A., Weinstein, B., Walker, C., Fishman, M., and Stainier, D. (2002). Cardiac troponin T is essential in sarcomere assembly and cardiac contractility. Nat. Genet. *31*, 106–110.

Selvaraj, D., Gangadharan, V., Michalski, C.W., Kurejova, M., Stösser, S., Srivastava, K., Schweizerhof, M., Waltenberger, J., Ferrara, N., Heppenstall, P., et al. (2015). A Functional Role for VEGFR1 Expressed in Peripheral Sensory Neurons in Cancer Pain. Cancer Cell *27*, 780–796.

Shelton, E.L., and Yutzey, K.E. (2007). Tbx20 regulation of endocardial cushion cell proliferation and extracellular matrix gene expression. Dev. Biol. *302*, 376–388.

Shelton, E.L., and Yutzey, K.E. (2008). Twist1 function in endocardial cushion cell proliferation , migration , and differentiation during heart valve development. Dev. Biol. *317*, 282–295.

Shibuya, M. (2013). VEGFR and type-V RTK activation and signaling. Cold Spring Harb. Perspect. Biol. *5*, a009092–a009092.

Shibuya, M., Yamaguchi, S., Yamane, A., Ikeda, T., Tojo, A., Matsushime, H., and Sato, M. (1990). Nucleotide sequence and expression of a novel human receptor-type tyrosine kinase gene (flt) closely relatd to the fms family. Oncogene *5*, 519–524.

Sidhwani, P., and Yelon, D. (2019). Fluid forces shape the embryonic heart: Insights from zebrafish. Curr. Top. Dev. Biol. *132*, 395–416.

Siegfried, G., Basak, A., Cromlish, J.A., Benjannet, S., Marcinkiewicz, J., Chrétien, M., Seidah, N.G., and Khatib, A.-M. (2003). The secretory proprotein convertases furin, PC5, and PC7 activate VEGF-C to induce tumorigenesis. J. Clin. Invest. *111*, 1723–1732.

Siekmann, A.F., and Lawson, N.D. (2007). Notch signalling limits angiogenic cell behaviour in developing zebrafish arteries. *445*, 781–784.

Simons, M., Gordon, E., and Claesson-Welsh, L. (2016). Mechanisms and regulation of endothelial VEGF receptor signalling. Nat. Rev. Mol. Cell Biol. *17*, 611–625.

Singleman, C., and Holtzman, N.G. (2012). Analysis of postembryonic heart development and maturation in the zebrafish, *Danio rerio*. Dev. Dyn. *241*, 1993–2004.

Sizarov, A., Ya, J., De Boer, B.A., Lamers, W.H., Christoffels, V.M., and Moorman, A.F.M. (2011). Formation of the building plan of the human heart: Morphogenesis, growth, and differentiation. Circulation *123*, 1125–1135.

Slough, J., Cooney, L., and Brueckner, M. (2008). Monocilia in the embryonic mouse heart suggest a direct role for cilia in cardiac morphogenesis. Dev. Dyn. *237*, 2304–2314.

Soufan, A.T., Van Den Berg, G., Ruijter, J.M., De Boer, P.A.J., Van Den Hoff, M.J.B., and Moorman, A.F.M. (2006). Regionalized sequence of myocardial cell growth and proliferation characterizes early chamber formation. Circ. Res. *99*, 545–552.

Stacker, S.A., Stenvers, K., Caesar, C., Vitali, A., Domagala, T., Nice, E., Roufail, S., Simpson, R.J., Moritz, R., Karpanen, T., et al. (1999). Biosynthesis of vascular endothelial growth factor-D involves proteolytic processing which generates non-covalent homodimers. J. Biol. Chem. *274*, 32127–32136.

Stainier, D.Y.R., Lee, R.K., and Fishman, M.C. (1993). Cardiovascular development in the zebrafish: I. Myocardial fate map and heart tube formation. Development *119*, 31–40.

Steed, E., Boselli, F., and Vermot, J. (2016a). Hemodynamics driven cardiac valve morphogenesis. Biochim. Biophys. Acta - Mol. Cell Res. *1863*, 1760–1766.

Steed, E., Faggianelli, N., Roth, S., Ramspacher, C., Concordet, J.-P., and Vermot, J. (2016b). Klf2a Couples Mechanotransduction and Zebrafish Valve Morphogenesis Through Fibronectin Synthesis. Nat. Commun. *7*, 11646.

Suchting, S., Freitas, C., Le Noble, F., Benedito, R., Bréant, C., Duarte, A., and Eichmann, A. (2007). The Notch ligand Delta-like 4 negatively regulates endothelial tip cell formation and vessel branching. Proc. Natl. Acad. Sci. U. S. A. *104*, 3225–3230.

Sugden, W.W., Meissner, R., Aegerter-Wilmsen, T., Tsaryk, R., Leonard, E. V., Bussmann, J., Hamm,

M.J., Herzog, W., Jin, Y., Jakobsson, L., et al. (2017). Endoglin controls blood vessel diameter through endothelial cell shape changes in response to haemodynamic cues. Nat. Cell Biol. *19*, 653–665.

Sugi, Y., Ito, N., Szebenyi, G., Myers, K., Fallon, J.F., Mikawa, T., and Markwald, R.R. (2003). Fibroblast growth factor (FGF)-4 can induce proliferation of cardiac cushion mesenchymal cells during early valve leaflet formation. Dev. Biol. *258*, 252–263.

Tammela, T., Zarkada, G., Wallgard, E., Murtomäki, A., Suchting, S., Wirzenius, M., Waltari, M., Hellström, M., Schomber, T., Peltonen, R., et al. (2008). Blocking VEGFR-3 suppresses angiogenic sprouting and vascular network formation. Nature *454*, 656–660.

Tammela, T., Zarkada, G., Nurmi, H., Jakobsson, L., Heinolainen, K., Tvorogov, D., Zheng, W., Franco, C.A., Murtomäki, A., Aranda, E., et al. (2011). VEGFR-3 controls tip to stalk conversion at vessel fusion sites by reinforcing Notch signalling. Nat. Cell Biol. *13*, 1202–1213.

Tan, H., Junor, L., Price, R.L., Norris, R.A., Potts, J.D., and Goodwin, R.L. (2011). Expression and deposition of fibrous extracellular matrix proteins in cardiac valves during chick development. Microsc. Microanal. *17*, 91–100.

Tao, G., Levay, A.K., Gridley, T., and Lincoln, J. (2011). Mmp15 is a direct target of Snai1 during endothelial to mesenchymal transformation and endocardial cushion development. Dev. Biol. *359*, 209–221.

Taylor, J.S., Braasch, I., Frickey, T., Meyer, A., and Van de Peer, Y. (2003). Genome duplication, a trait shared by 22,000 species of ray-finned fish. Genome Res. *13*, 382–390.

Terman, B.I., Carrion, M.E., Kovacs, E., Rasmussen, B.A., Eddy, R.L., and Shows, T.B. (1991). Identification of a new endothelial cell growth factor receptor tyrosine kinase. Oncogene *6*, 1677–1683.

Theodoris, C. V., Li, M., White, M.P., Liu, L., He, D., Pollard, K.S., Bruneau, B.G., and Srivastava, D. (2015). Human disease modeling reveals integrated transcriptional and epigenetic mechanisms of NOTCH1 haploinsufficiency. Cell *160*, 1072–1086.

Timmerman, L.A., Grego-Bessa, J., Raya, A., Bertrán, E., Pérez-Pomares, J.M., Díez, J., Aranda, S., Palomo, S., McCormick, F., Izpisúa-Belmonte, J.C., et al. (2004). Notch promotes epithelial-mesenchymal transition during cardiac development and oncogenic transformation. Genes Dev. *18*, 99–115.

Trapnell, C., Roberts, A., Goff, L., Pertea, G., Kim, D., Kelley, D.R., Pimentel, H., Salzberg, S.L., Rinn, J.L., and Pachter, L. (2012). Differential gene and transcript expression analysis of RNA-seq

experiments with TopHat and Cufflinks. Nat. Protoc. *7*, 562–578.

Tzima, E. (2006). Role of Small GTPases in Endothelial Cytoskeletal Dynamics and the Shear Stress Response. Circ. Res. *98*, 176–185.

Tzima, E., Irani-Tehrani, M., Kiosses, W.B., Dejana, E., Schultz, D.A., Engelhardt, B., Cao, G., DeLisser, H., and Schwartz, M.A. (2005). A mechanosensory complex that mediates the endothelial cell response to fluid shear stress. Nature *437*, 426–431.

Urner, S., Planas-Paz, L., Hilger, L.S., Henning, C., Branopolski, A., Kelly-Goss, M., Stanczuk, L., Pitter, B., Montanez, E., Peirce, S.M., et al. (2019). Identification of ILK as a critical regulator of VEGFR3 signalling and lymphatic vascular growth. EMBO J. *38*, 1–21.

VanDusen, N.J., Casanovas, J., Vincentz, J.W., Firulli, B.A., Osterwalder, M., Lopez-Rios, J., Zeller, R., Zhou, B., Grego-Bessa, J., DeLaPompa, J., et al. (2014). Hand2 Is an Essential Regulator for Two Notch-Dependent Functions within the Embryonic Endocardium. Cell Rep. *9*, 2071–2083.

Veerkamp, J., Rudolph, F., Cseresnyes, Z., Priller, F., Otten, C., Renz, M., Schaefer, L., and Abdelilah-Seyfried, S. (2013). Unilateral Dampening of Bmp Activity by Nodal Generates Cardiac Left-Right Asymmetry. Dev. Cell *24*, 660–667.

Verhoeven, M.C., Haase, C., Christoffels, V.M., and Weidinger, G. (2011). Wnt Signaling Regulates Atrioventricular Canal Formation Upstream of BMP and Tbx2. *440*.

Vermot, J., Forouhar, A.S., Liebling, M., Wu, D., Plummer, D., Gharib, M., and Fraser, S.E. (2009). Reversing blood flows act through klf2a to ensure normal valvulogenesis in the developing heart. PLoS Biol. *7*, 12–14.

Visconti, R.P., Ebihara, Y., LaRue, A.C., Fleming, P.A., McQuinn, T.C., Masuya, M., Minamiguchi, H., Markwald, R.R., Ogawa, M., and Drake, C.J. (2006). An In Vivo Analysis of Hematopoietic Stem Cell Potential. Circ. Res. *98*, 690–696.

de Vlaming, A., Sauls, K., Hajdu, Z., Visconti, R.P., Mehesz, A.N., Levine, R.A., Slaugenhaupt, S.A., Hagège, A., Chester, A.H., Markwald, R.R., et al. (2012). Atrioventricular valve development: New perspectives on an old theme. Differentiation *84*, 103–116.

Vogrin, A.J., Bower, N.I., Gunzburg, M.J., Roufail, S., Okuda, K.S., Paterson, S., Headey, S.J., Stacker, S.A., Hogan, B.M., and Achen, M.G. (2019). Evolutionary Differences in the Vegf/Vegfr Code Reveal Organotypic Roles for the Endothelial Cell Receptor Kdr in Developmental Lymphangiogenesis. Cell Rep. *28*, 2023-2036.e4.

Walsh, E.C., and Stainier, D.Y.R. (2001). UDP-glucose dehydrogenase required for cardiac valve formation in zebrafish. Science (80-.). *293*, 1670–1673.

Wang, J.F., Zhang, X.F., and Groopman, J.E. (2001). Stimulation of β1 Integrin Induces Tyrosine Phosphorylation of Vascular Endothelial Growth Factor Receptor-3 and Modulates Cell Migration. J. Biol. Chem. *276*, 41950–41957.

Wang, L., Zhang, P., Wei, Y., Gao, Y., Patient, R., and Liu, F. (2011). A blood flow–dependent klf2a-NO signaling cascade is required for stabilization of hematopoietic stem cell programming in zebrafish embryos. Blood *118*, 4102–4110.

Wang, Y., Wu, B., Chamberlain, A.A., Lui, W., Koirala, P., Susztak, K., Klein, D., Taylor, V., and Zhou, B. (2013). Endocardial to Myocardial Notch-Wnt-Bmp Axis Regulates Early Heart Valve Development. PLoS One *8*.

Wani, M.A., Means, R.T., and Lingrel, J.B. (1998). Loss of LKLF function results in embryonic lethality in mice. Transgenic Res. *7*, 229–238.

Warboys, C.M., de Luca, A., Amini, N., Luong, L., Duckles, H., Hsiao, S., White, A., Biswas, S., Khamis, R., Chong, C.K., et al. (2014). Disturbed Flow Promotes Endothelial Senescence via a p53-Dependent Pathway. Arterioscler. Thromb. Vasc. Biol. *34*, 985–995.

Welch-Reardon, K.M., Wu, N., and Hughes, C.C.W. (2015). A role for partial endothelial-mesenchymal transitions in angiogenesis? Arterioscler. Thromb. Vasc. Biol. *35*, 303–308.

Wessels, A., van den Hoff, M.J.B., Adamo, R.F., Phelps, A.L., Lockhart, M.M., Sauls, K., Briggs, L.E., Norris, R.A., van Wijk, B., Perez-Pomares, J.M., et al. (2012). Epicardially derived fibroblasts preferentially contribute to the parietal leaflets of the atrioventricular valves in the murine heart. Dev. Biol. *366*, 111–124.

Westerfield, M., Doerry, E., Kirkpatrick, A.E., Driever, W., and Douglas, S.A. (1997). An on-line database for zebrafish development and genetics research. Semin. Cell Dev. Biol. *8*, 477–488.

Wild, R., Klems, A., Takamiya, M., Hayashi, Y., Strähle, U., Ando, K., Mochizuki, N., Van Impel, A., Schulte-Merker, S., Krueger, J., et al. (2017). Neuronal sFlt1 and Vegfaa determine venous sprouting and spinal cord vascularization. Nat. Commun. *8*.

Xiao, H., Qin, X., Ping, D., and Zuo, K. (2013). Inhibition of Rho and Rac Geranylgeranylation by Atorvastatin Is Critical for Preservation of Endothelial Junction Integrity. PLoS One *8*, e59233.

Yalcin, H.C., Shekhar, A., McQuinn, T.C., and Butcher, J.T. (2011). Hemodynamic patterning of the avian atrioventricular valve. Dev. Dyn. *240*, 23–35.

Yang, B., Radel, C., Hughes, D., Kelemen, S., and Rizzo, V. (2011). P190 RhoGTPase-activating protein links the β1 integrin/caveolin-1 mechanosignaling complex to RhoA and actin remodeling. Arterioscler. Thromb. Vasc. Biol. *31*, 376–383.

Yaniv, K., Isogai, S., Castranova, D., Dye, L., Hitomi, J., and Weinstein, B.M. (2006). Live imaging of lymphatic development in the zebrafish. Nat. Med. *12*, 711–716.

Yelon, D., Horne, S.A., and Stainier, D.Y.R. (1999). Restricted Expression of Cardiac Myosin Genes Reveals Regulated Aspects of Heart Tube Assembly in Zebrafish. Dev. Biol. *214*, 23–37.

Zaffran, S., Kelly, R.G., Meilhac, S.M., Buckingham, M.E., and Brown, N.A. (2004). Right ventricular myocardium derives from the anterior heart field. Circ. Res. *95*, 261–268.

Zhang, L., Zhou, F., Han, W., Shen, B., Luo, J., Shibuya, M., and He, Y. (2010). VEGFR-3 ligand-binding and kinase activity are required for lymphangiogenesis but not for angiogenesis. Cell Res. *20*, 1319–1331.

Zhao, J.H., Reiske, H., and Guan, J.L. (1998). Regulation of the cell cycle by focal adhesion kinase. J. Cell Biol. *143*, 1997–2008.

Zhao, L., Borikova, A.L., Ben-Yair, R., Guner-Ataman, B., MacRae, C.A., Lee, R.T., Geoffrey Burns, C., and Burns, C.E. (2014). Notch signaling regulates cardiomyocyte proliferation during zebrafish heart regeneration. Proc. Natl. Acad. Sci. U. S. A. *111*, 1403–1408.

Zhong, A., and Simmons, C.A. (2016). Heart Valve Mechanobiology in Development and Disease. 255–276.

Zhou, B., von Gise, A., Ma, Q., Hu, Y.W., and Pu, W.T. (2010). Genetic fate mapping demonstrates contribution of epicardium-derived cells to the annulus fibrosis of the mammalian heart. Dev. Biol. *338*, 251–261.

Zhou, Y., Cashman, T.J., Nevis, K.R., Obregon, P., Carney, S.A., Liu, Y., Gu, A., Mosimann, C., Sondalle, S., Peterson, R.E., et al. (2011). Latent TGF-βbinding protein 3 identifies a second heart field in zebrafish. Nature *474*, 645–648.

6. Appendix

6.1. Abbreviations

A	atrium
Alcam	activated leukocyte cell adhesion molecule
ALPM	anterior lateral plate mesoderm
AV	atrio-ventricular
AVC	atrio-ventricular canal
BAC	Bacterial artificial chromosome
Bmp	Bone morphogenetic protein
bp	base pair
BSA	Bovine Serum Albumin
Cas	CRISPR-associated system
CCM	cerebral cavernous malformation
Cdh5	Cadherin-5 /Vascular endothelial Cadherin
cDNA	complementary DNA
CRISPR	Clustered regularly interspaced short palindromic repeat
Ct	Cycle threshold
ctrl	control
DAPI	4',6-diamidino-2-phenylindole
ddH2O	double destilled water
DMSO	dimethyl sulfoxide
DNA	deoxyribonucleic acid
dpf	Days post fertilization
E	embryonic day (mice)
e.g.	*exempli gratia*
EC	Endothelial cell
ECM	extra-cellular matrix
EdC	Endocardial cell
EGFP	Enhanced Green Fluorescent Protein
endoMT	Endothelial-to-mesenchymal transition
eNOS	endothelial nitric oxide synthase
EtOH	ethanol
FA	Focal adhesion
FAK	focal adhesion kinase
FHF	first heart field
Fli1a	Fli-1 proto oncogene
Flt	Fms-related tyrosine kinase
Fw	forward
HEG1	Heart development protein with EGF-like domains 1

hpf	hours post-fertilization
HUVEC	Human umbilical vein endothelial cell
i. e.	*id est*
IFT	inflow tract
IHC	immunohistochemistry
ISV	intersegmental vessel
kDa	kilodalton
Kdr	kinase insert domain receptor
Kdrl	kinase insert domain receptor like
Klf	Krüppel-like factor
LPM	lateral plate mesoderm
LSM	laser scanning microscope
miRNA	microRNA
ml	milliliter
mM	millimolar
MO	morpolino antisense oligonucleotide/morphant
mRNA	messenger RNA
NaCl	natrium chloride
NFATc1	nuclear factor of activated T-cells 1
NGS	normal goat serum
NICD	Notch intracellular domain
NO	nitric oxide
O/N	overnight
OFT	outflow tract
PBDT	PBS + DMSO + Tween-20
PBS	phosphate buffered saline
PBT	PBS + Tween-20
PCR	polymerase chain reaction
PECAM-1	platelet endothelial cell adhesion molecule-1
PFA	paraformaldehyde
pH	potential of hydrogen
PTU	N-phenylthiourea
qRT-PCR	quantitative real-time polymerase chain reaction
RNA	ribonucleic acid
RNAseq	RNA sequencing
RT	room temperature
Rv	reverse
s	somite
SD	standard deviation
SEM	standard error mean
SHF	second heart field
Src	Sarcoma protein kinase
TCF	T-cell factor

Tg	transgene
Tgfβ	Transformaing growth factor β
Tnnt2a	troponin 2a
TP1	Epstein Barr Virus terminal protein 1
Trpv4	Transient receptor potential cation channel 4
UAS	Upstream activator sequence
UV	ultra violet
V	ventricle
Vegf	vascular endothelial growth factor
Vegfr	vascular endothelial growth factor receptor
Wnt	Wingless-related integration site molecule
WT	wild type
Yap1	Yes-associated protein 1
µl	microliter
µm	micrometer
µM	micromolar

6.2. List of Figures

7. Publications and manuscripts

Fontana F., Haack T., Reichenbach M., Knaus P., Puceat M., Abdelilah-Seyfried S. Antagonistic activities of Vegfr3/Flt4 and Notch1b fine-tune mechanosensitive signaling during cardiac valvulogenesis. *Cell Reports* (2020).

Yang Z.*, Wu S.*, **Fontana F.***, Li Y., Xiao W., Gao Z., Stephan A., Affolter M., Belting H.G., Abdelilah-Seyfried S., Zhang J. The tight junctions protein Claudin-5 limits endothelial cell motility. *Journal of Cell Science* (2020).

Jatzlau J., Sesver A., **Fontana F.**, Mendez P., Ertürk G.R., Reichenbach M., Abdelilah-Seyfried S., Stricker S., Hiepen C., Knaus P. Fluid shear stress and BMP upregulate UNC5B, an arterial BMP co-receptor, which balances ALK1/ALK5 SMAD signaling. Manuscript in revision (2020).

Paolini A., **Fontana F.**, Rödel C.J., Abdelilah-Seyfried S. Mechanosensitive Notch and Klf2 pathway signaling intersects in guiding valvulogenesis in zebrafish. Manuscript in revision (2020).

* Authors contributed equally

Acknowledgements

First of all, I would like to thank my supervisor Prof. Dr. Seyfried, for giving me the chance to join his lab and work on this exciting project. Thanks for all the guidance, motivation, scientific input and inspiring discussions. Thank you also for the opportunity to open fruitful collaborations and attend amazing scientific conferences. I also would like to thank Prof. Dr. Petra Knaus for her support as my second supervisor.

I am deeply grateful for all the help I received from each of the former and current lab members. In particular, thanks to Dr. Claudia Rödel, Dr. Juliane Münch and Dr. Cécile Otten for their endless support and all their advices. You have been a great model to me. A special thanks to Juliane also for her help with my Zusammenfassung. My deepest thanks to Dr. Alessio Paolini, who has been since my first day in the lab an invaluable source of support, scientifically and personally. Thanks also to my former officemate and current friend Dr. Stefan Donat, for his shared knowledge and his constant help with the German Verwaltung. Thanks to Carla Igual for her friendship and interest in my PhD life. Many thanks also to Dr. Timm Haack, who contributed a lot to this work and hosted me several times in Hannover after long lab days. Thanks also to Dr. Dorothee Bornhorst, her contagious enthusiasm and motivation have been precious. For technical assistance and fish husbandry, thanks to Martina Kneisler, Angela Hubig, Bärbel Wuntke and Laura Gresch. Thanks to Prof. Dr. Otto Baumann for his constant availability and his valuable help with microscopy. Thanks to my collaborators, Dr. Michel Puceat, Dr. Maria Reichenbach, Prof. Dr. Petra Knaus, and Dr. Oliver Dittrich-Breiholz, for their help and input to this project.

For all the support I received outside of the lab, I would like to thank my friends, the ones who adopted me in Germany and the ones who have been with me from Italy. In particular, thanks to my flatmate Solveig, who has been on my side through the entire writing of this work, sharing&caring. Finally, I am eternally thankful to my parents, my brother and family, for their infinite patience and love. Grazie di cuore.